THE GIANT MASCOT ULTRAMAFITE AND ITS RELATED ORES

by

JAMES ALBERT McLEOD
B.A.Sc., University of British Columbia, 1969

A THESIS SUBMITTED IN PARTIAL FULFILMENT OF
THE REQUIREMENTS FOR THE DEGREE OF
MASTERS OF APPLIED SCIENCE

in the Department

of

GEOLOGICAL SCIENCES

We accept this thesis as conforming to the required standard

THE UNIVERSITY OF BRITISH COLUMBIA

July, 1975

In presenting this thesis in partial fulfilment of the requirements for an advanced degree at the University of British Columbia, I agree that the Library shall make it freely available for reference and study. I further agree that permission for extensive copying of this thesis for scholarly purposes may be granted by the Head of my Department or by his representatives. It is understood that copying or publication of this thesis for financial gain shall not be allowed without my written permission.

Department of Geological Sciences

The University of British Columbia
2075 Wesbrook Place
Vancouver, Canada
V6T 1W5

Date July 29/75

ABSTRACT

The Giant Mascot Ultramafite is on the southeastern flank of the Coast Crystalline Belt 100 miles east of Vancouver, B.C. It is roughly elliptical (1 x 2 mi.), crudely zoned ranging from peridotite through pyroxenite and hornblende-pyroxenite to marginal hornblendite. It is enclosed in dioritic rocks of the Spuzzum Intrusions. Twenty-eight pipe-like orebodies within the ultramafite have been mined for their massive Ni-Cu ores.

Studies on the 3050 level cross-cut show that silicates and sulfides in pyroxenites differ in composition from those in peridotites. Furthermore, pentlandite from orebodies differs in composition from accessory pentlandite in ultrabasic rocks.

K-Ar dating yields minimum ages for orebodies and ultramafite ranging from 104 m.y. to 119 m.y. Hornblendite dykes, the youngest rocks in the mine are dated at 95 m.y. K-Ar ages of Spuzzum Diorite near the mine and several miles to the south are 89 m.y. Tonalite, a border phase of the Spuzzum Intrusions, yields a hornblende age of 85 m.y. and a biotite age of 79 m.y., consistent with earlier investigations.

Temperatures calculated from 15 coexisting clino- and orthopyroxene pairs from the 3050 level cross-cut average 990°C for equilibration of these silicates. Distribution coefficients (mean K_D=0.738) for these silicates suggest a magmatic origin.

The Climax and Chinaman orebodies on the 3050 level cross-cut are steeply plunging pipe-like bodies with higher grade sections concentrated in the trough or footwall. They are found at peridotite-pyroxenite contacts and appear spatially related to norite.

It is concluded that the Giant Mascot Ultramafite originated by diapiric re-emplacement of crudely stratiform crystal mushes and sulfide melts from a

differentiating sub-volcanic magma chamber, possibly an early phase of Spuzzum magmatic activity. This material was subsequently engulfed by rising Spuzzum dioritic magmas which superimposed a hornblendite rim on the ultramafite.

TABLE OF CONTENTS

page

page

FIGURES

page

page

TABLES

ACKNOWLEDGEMENTS

This thesis was done under the kind supervision of Dr. K.C. McTaggart to whom the author is very indebted.

Giant Mascot Mines Ltd., is thanked for their financial assistance and for providing full access to the Giant Mascot Mine. In addition, Mr. F. Holland (mine general manager), Mr. L. DeRoux (chief mine geologist) and Mr. R. Gonzales (exploration geologist) are thanked for their help and hospitality.

Mr. D.P. Moore's invaluable assistance in underground mapping and sampling and his astute observations are gratefully appreciated. His physical support made this work possible.

Dr. T.H. Brown is thanked for his help and advice in connection with the departments microprobe. Mr. A. Lacis of the Department of Metallurgy is thanked for his help in the operation of that departments microprobe. Also, Mr. J. Harakal's help in K-Ar age determinations is appreciated.

Dr. P. Christopher of the B.C. Department of Mines and Petroleum Resources was of assistance in supplying some data about the Giant Mascot Mine.

Appreciation is extended to the technical staff of the department for their generous "behind the scenes" help and to Ann Carr for typing this manuscript.

The author wishes to extend his gratitude to all those friends and colleagues whose moral support proved invaluable and, in particular, to his wife Joanne.

INTRODUCTION

Location

Giant Mascot Mine lies 7 miles northwest of the town of Hope, B.C. and 90 miles east of Vancouver, (latitude 49° 28' W., and longitude 121° 30' W). Access from Hope is by paved highway for 7 miles and then 5 miles of gravel road which winds westward into the rugged Coast Range mountains.

General Statement

The subject of this study is the geology and mineralization along the 3050 cross-cut, which give access to the two most recently worked orebodies of Giant Mascot mine, - the Climax and the Chinaman. The writer and a colleague spent approximately three weeks during the spring of 1973 mapping and sampling the cross-cut and assembling mine records of the area of interest. Additional sampling and specimen collection were made later during several brief visits to the mine.

Thin-sections and polished sections were studied under the microscope and by electron microprobe, and K-Ar ages were determined for ultrabasic rocks which contain the ore deposits and for the surrounding plutonic rocks.

History

The showings of the Giant Mascot property were discovered in 1923. Exploration work was carried on between 1923 and 1937 and

again between 1951 and 1954. The property was brought into production in 1958 and operated continually until shut down in September 1974.

Previous Investigations

Early investigators include Cairnes (1924), Cockfield and Walker (1933), and Horwood (1937). Their conclusions are in considerable conflict with regard to the origin of the ultrabasic rocks and contained mineralization and the relationship of ultramafites to the surrounding diorites. Aho (1956) provides the most detailed and comprehensive account of the ultramafite, the orebodies, and their genesis. Recently, Muir (1971) studied the 4600 orebody at Giant Mascot. The Department of Mines and Petroleum Resources has started a new investiagion of the mine.

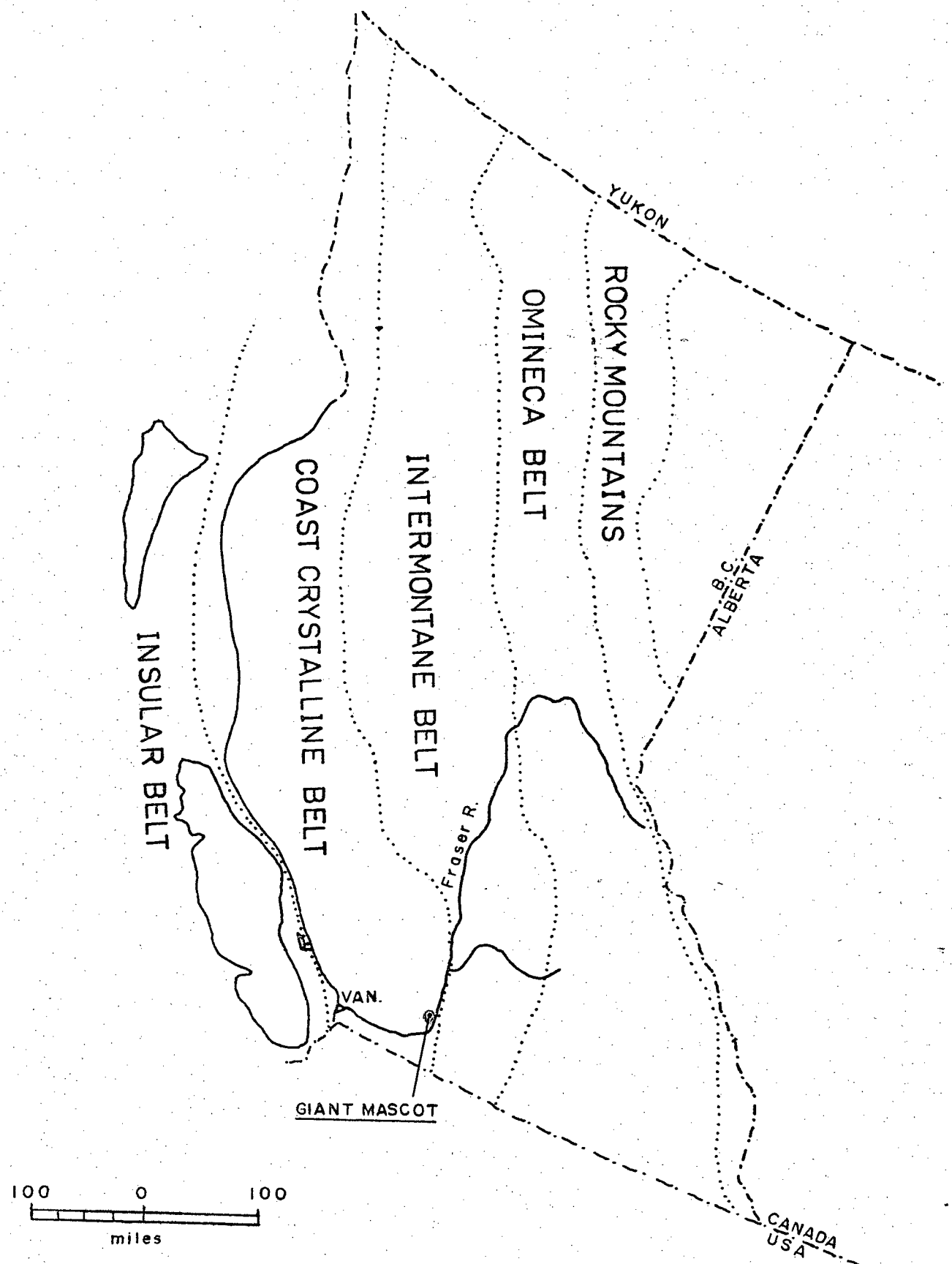

LOCATION AND TECTONIC MAP - BRITISH COLUMBIA

FIGURE 1

REGIONAL GEOLOGY

Regional Setting

The ultrabasic complex at Giant Mascot mine lies at the south-eastern flank of the Coast Crystalline Belt, near the junction of the Coast and Cascade mountain systems (Fig. 1). The Coast Crystalline Belt is one of uniform stratigraphy, structure and metallogeny as defined by Sutherland-Brown et. al., (1971). A map (Fig. 2) illustrates the various rock units present in the region and these rock units are described below.

Stratified Rocks

Hozameen Group

This well stratified group flanks the batholitic rocks on the east side. The Group consists of pelitic rocks, chert, basic volcanic rocks and limestone that have been regionally metamorphosed in general to a low grade but locally to high grade. Most early writers believed the rocks to be late Paleozoic, but Monger (1970) suggests that they may be as young as Triassic.

Chilliwack Group

The lithology of the Chilliwack Group is more clastic than that of the Hozameen Group. Stratigraphic units are mostly pelites, sandstones, and siltstones with lesser volcanic rock. This group lies to the immediate west of batholitic rocks described and is believed to be Pennsylvanian and Permian in age. Metamorphism is mostly low grade regional, but high grades are encountered in the north.

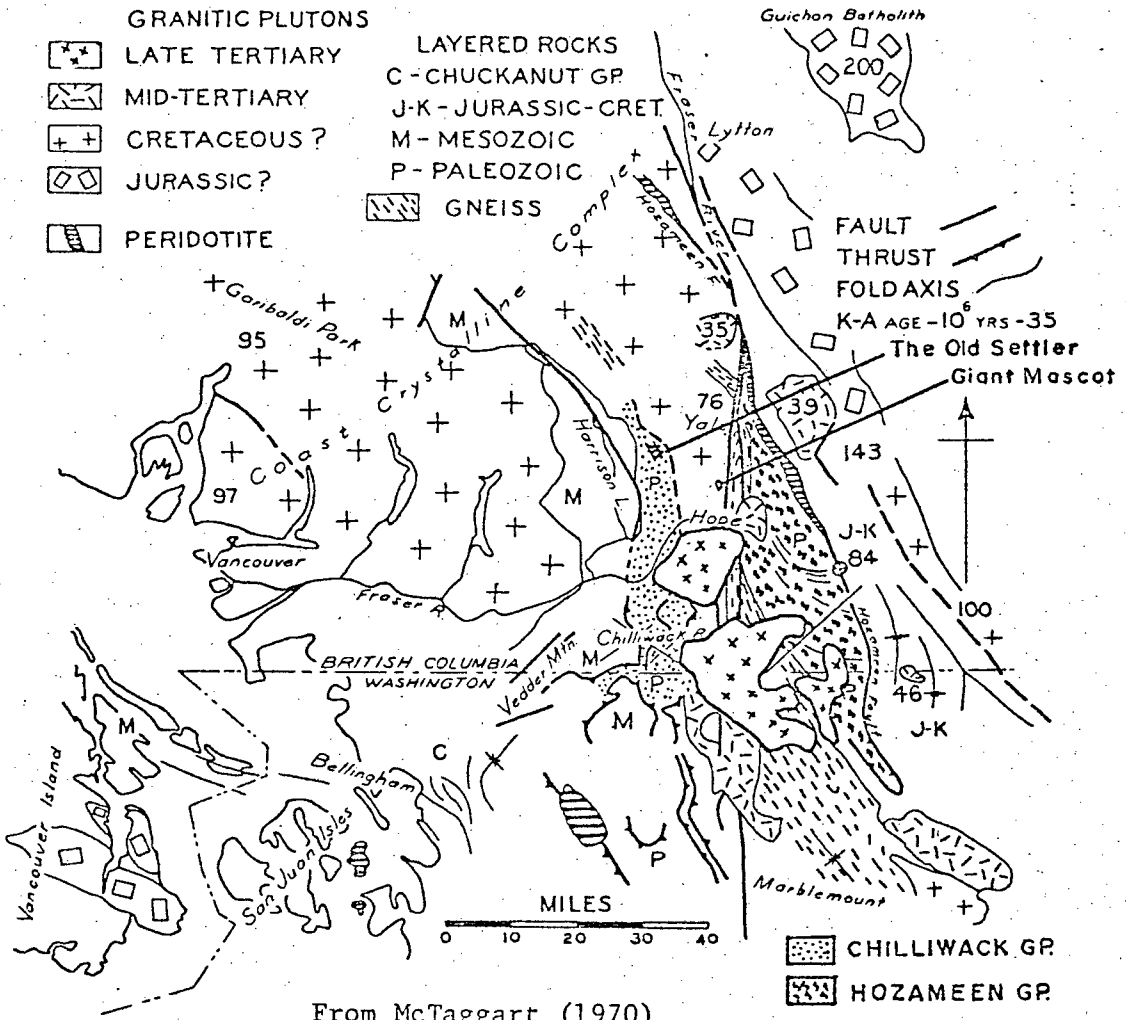

From McTaggart (1970)

Figue 2 : Generalized geology of the Northern Cascades Region.

Metasedimentary and Metavolcanic Rocks

North of the Fraser River near Hope, pelitic schist, phyllite and amphibolite of high grade Barrovian style metamorphism adjoin the Scuzzy and Spuzzum plutons. The age of these rocks is uncertain, but on the basis of composition they are probably formed from the Upper Paleozoic Hozameen Group. The age of metamorphism is thought to be roughly contemporaneous with Late Cretaceous plutonism (McTaggart and Thompson, 1967). Read (1960) suggested that metamorphism preceded plutonism, as staurolite and sillimanite isograds do not parallel the contact of the Spuzzum Pluton.

Gneiss

In the Hope area the Custer Gneiss lies between metasedimentary, metavolcanic, and batholitic rocks to the west and the Hozameen Group and diminishes to the north in a wedge-like fashion. This rock consists of layered amphibolite, leucocratic gneiss, augen gneiss, minor marble and trondhjemite pegmatite. The age of the gneiss is uncertain. Zircons dated by Mattinson (1970) yield Precambrian ages and he suggests an episode of metamorphism and migmatization in the Upper Cretaceous.

Granitoid Rocks

The Spuzzum and Scuzzy Pluton in the north and the Chilliwack Pluton in the south form a north-trending heterogeneous belt of granitic rocks passing just west of Hope and Yale. The Spuzzum Pluton, which consists of diorite and tonalite is considered Late Cretaceous (Richards, 1971) and has been classified as catazonal to mesozonal. The contiguous Scuzzy Pluton to the north is described (Roddick and Hutchison, 1969) as a granodiorite, but has definite trondhjemite trend. The age of this pluton is Late Cretaceous (Hutchison, 1970). Richards (1971) describes the late Cenozoic Chilliwack Pluton as having up to nine phases, but consisting mainly of quartz diorite to granodiorite. Structural and textural features and its age (26-29 my), suggest that it was emplaced in the epizone.

Ultramafites

Ultramafic rocks lie to the east and west of the Spuzzum Batholith. The eastern body, the Coquihalla Serpentine Belt (Cairnes, 1930)

is of the alpine type and forms the eastern contact of the Hozameen Group. This belt runs from 16 miles south-east of Hope to Boston Bar a distance of 40 miles and consists of serpentine, serepentinized peridotite, pyroxenite and gabbro. The ultramafite and the Hozameen rocks to the west form a typical ophiolite succession and may have been emplaced as an obducted slice.

To the west, a less well defined belt composed of small bodies of pyroxenite, peridotite, hornblendite, dunite and gabbroic rocks appears fault controlled. North of the Fraser River this fault, the Shuksan Thrust, marks the eastern boundary of the Chilliwack Group. This belt extends from the border to The Old Settler mountain, then swings abruptly north-west. Much of the ultramafic rock is serpentinized and classed as alpine type.

A crudely zoned body ranging from hornblendite through pyroxenite to peridotite lies on the very eastern edge, but within the Spuzzum diorite. This body, the Giant Mascot Ultramafite, is described in greater detail in the following section.

Exploration by Giant Mascot Mines in the vicinity of The Old Settler mountain has revealed ultrabasic rocks that are texturally and lithologically similar to the Giant Mascot Ultramafite. These rocks are coarse-grained, fresh hornblende pyroxenites and peridotites. The contact relationships of these ultramafic rocks with the dioritic rocks tends to be ambiguous and conflicting (K.C. McTaggart, pers. comm.).

Structures

The overall structural trend of the area is roughly northerly. Major fault systems including the Shuksan thrust on the west, the

Hope and Yale faults on the immediate eastern flank of the batholith and the Hozameen fault in the east all trend northerly or northwest. These fault systems in turn separate and delineate major lithological northerly trending belts. Folding tends to be along northwest trending axes. According to Read (pers. comm.) metamorphism increases from both east and west towards the batholithic rocks of the northern Cascades and south eastern Coast mountains.

LOCAL GEOLOGY

Introduction

The present description of the geology around the Giant Mascot mine draws on the field work of several authors, but mainly on the detailed work of Aho (1956).

The Giant Mascot Ultramafite is approximately 2 miles long in the east-west direction and 1 mile wide in a north-south direction. In plan the body appears very irregular with many salients and re-entrants with surrounding diorite. In the southeast corner the complex is in contact with, or very close to, high grade metamorphic rocks. A simplified geological plan is shown in (Fig. 3) after Aho (1956).

Metamorphic Rocks

Metamorphic rocks form inclusions within the ultramafite and the diorite and may abut the complex on the southeast corner. These rocks are mica schists, locally with garnet, kyanite or staurolite. They probably are high grade equivalents of the Upper Paleozoic Hozameen Group which they resemble in composition (Monger, 1970). The rocks belong to the staurolite-almandine subfacies of the almandine-amphibolite facies of Barrovian metamorphism. Contact metamorphism by the ultramafite has produced orthopyroxene subfacies rock of the orthoclase-cordierite-hornfels facies (Aho, 1956), believed to indicate temperatures of at least 600^{o}C. This would indicate a solidus temperature of at least 1000^{o}C for the ultramafite (Winkler, 1967, pp.79-83).

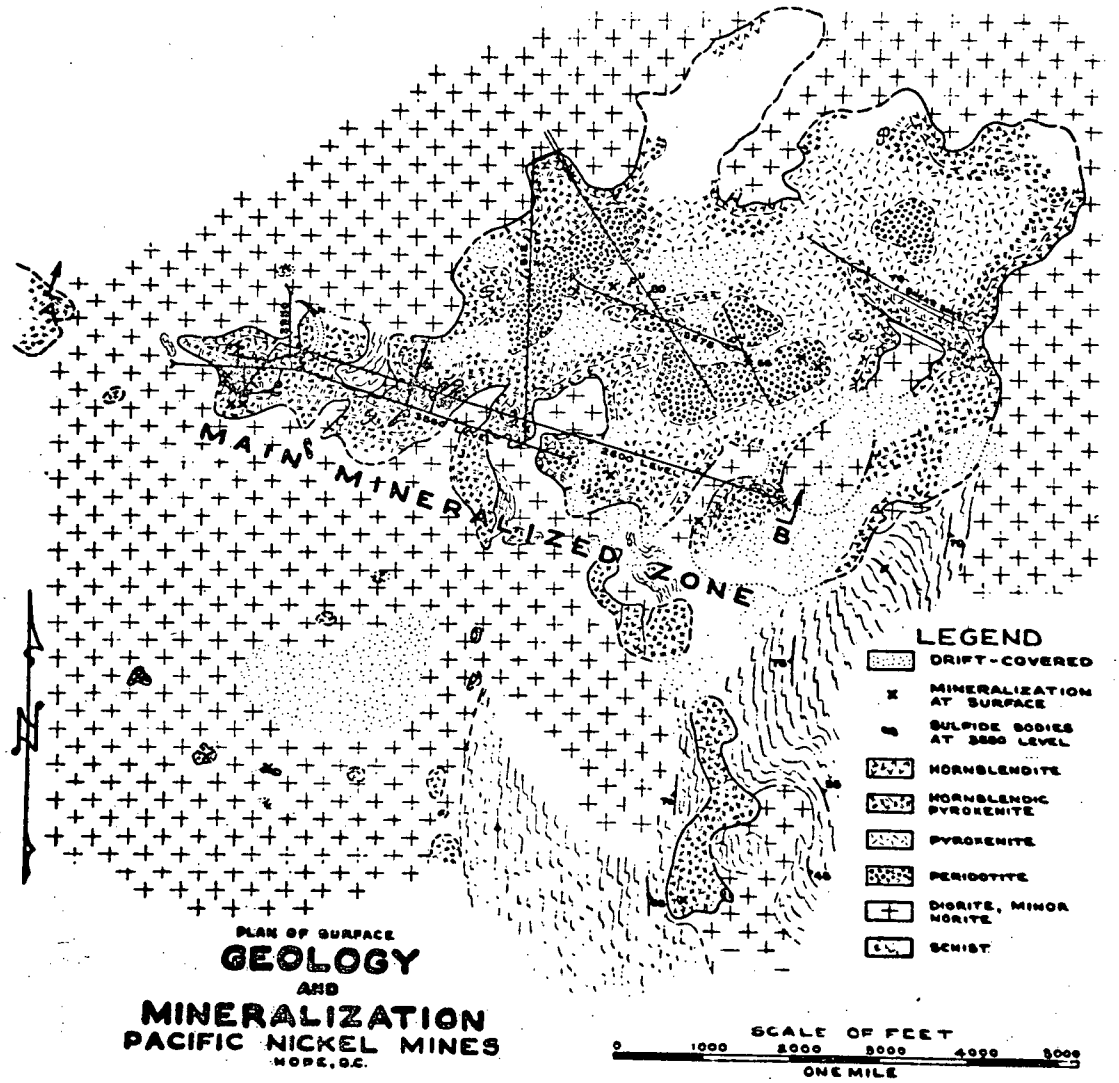

from Aho (1956) Fig.3

Ultrabasic Rocks

Aho (1956) was the first to point out a crude zonation of the ultrabasic complex which consists essentially of pyroxenite with cores of peridotite. The pyroxenite becomes increasingly hornblendic outwards and a remarkable margin, up to 100 yards wide, of coarse-grained hornblendite is present at the diorite-ultrabasic contact.

The relative age of the diorite and the ultramafite is unresolved, several authors holding conflicting opinions. Aho (1956) found that in a large part the ultrabasic rocks appear to cut the diorites as had been observed by Cairnes (1924). Aho does concede that the reverse relation is seen in some places and distinguishes several different dioritic rocks. Cockfield and Walker (1933) concluded that the ultrabasics were intruded by surrounding diorite. Most authors stress that there is a strong genetic relationship between ultrabasic and the surrounding feldspathic rocks.

Feldspathic Rocks

The principal country rock around the ultramafite consists of diorite, norite and tonalite. These rocks generally contain plagioclase of andesine to labradorite composition, hypersthene, diopsidic augite, lesser hornblende and biotite and a varying amount of quartz. These rocks have been grouped together as part of the complexly differentiated Spuzzum Pluton of Upper Cretaceous age. Large intrusions or xenoliths of diorite and norite are present within the ultramafite, but their relation to the Spuzzum pluton is not certain.

Orebodies

More than 28 orebodies have been located within the ultramafite. They occur as steeply plunging, pipe-like ore zones and have been classified as either zoned or massive, (Aho, 1956).

The zoned orebodies are circular or elliptical in plan, pipe-like in section, with mineralization concentrically distributed around

an olivine-rich core of peridotite or within the core itself. The periodite gives way to an olivine pyroxenite and outward to orthopyroxenite. Mineralization is gradational to barren rock. This type of ore was believed to be of replacement origin.

The massive orebodies occur as more irregular pipe-like structures and appear to be unzoned. The ore is present as a uniform groundmass of sulfide surrounding silicate grains at lithologic contacts between various ultramafic rock types. These ores generally have sharp contacts with wall rock but may grade into disseminated ores. Commonly these orebodies show marginal "flow lines", banding, and "drag folding" suggestive of magmatic injection, (Aho, 1956). Aho states that these two categories may be end members of a continuum, as some ore zones have features of both categories.

PETROLOGY OF THE 3050 LEVEL CROSS-CUT

General Statement

The 3050 level (Fig. 37) cross-cut was washed and sampled from 6400N to 8600N and mapped at 1" = 20'. Sample locations and a geologic map of the Climax area are appended. Representative rock samples were chosen for thin sectioning for detailed petrological study.

Mineralogical determinations of silicate compositions were made by universal stage and electron probe.

Classification of Rock Types

The following rock classification (Fig. 4) after Streckeisen (1967) was used by the author, with slight modifications.

Felsic Rocks:

Diorite. . . . . mainly adesine or oligoclase, hornblende major mafic.

Norite . . . . . mainly bytownite or labradorite, orthopyroxene major mafic.

Hornblendite:

. . . . . hornblende, 80 - 100%, plagioclase, 0-20%.

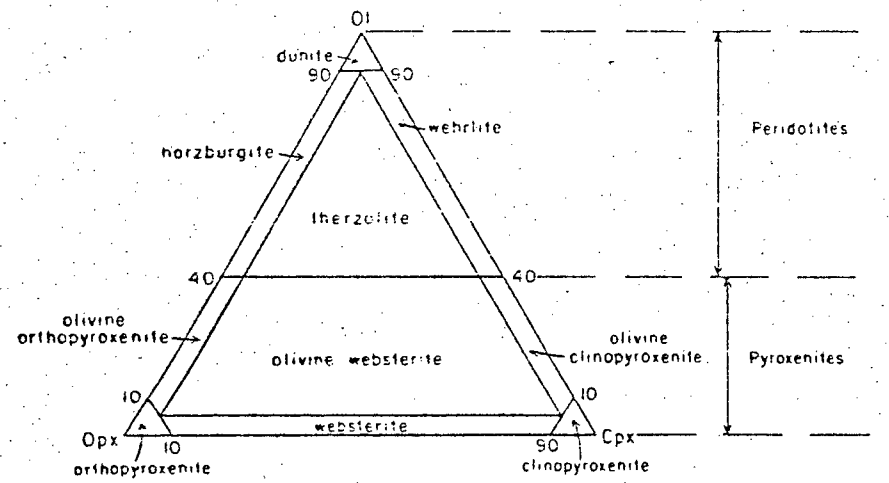

Ultramafic rocks composed of olivine, orthopyroxene, and clinopyroxene.

Ultramafic rocks that contain hornblende.

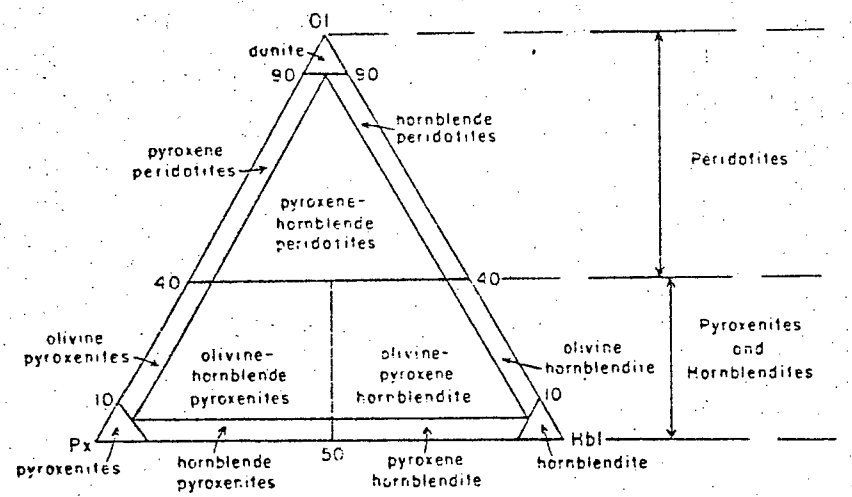

Classification and nomenclature of ultramafic rocks. Ol + Opx + Cpx + Hbl (+ Bi + Gar + Sp) ≧ 95; opaque minerals ≦ 5.

Fig. 4

Description of Rock Types

Norite

Norite occurs along the 3050 level cross-cut as inclusions, host and fragments in breccia and as apophyses into more basic material. The rock is medium grained, light coloured, and shows a strong alignment of mafic minerals.

Norite is composed of interlocking subhedral plagioclase laths with mafic content usually less than 40%. Plagioclase is as calcic as An90 in some inclusions and as sodic as An65 in apophyses. Normal zoning is accentuated by dust inclusions which lend them a pinkish tint. These are probably hematite produced by metamorphism. Very little interstitial quartz is present in these rocks.

Hypersthene, mostly subhedral, the dominant pyroxene, contains "schiller" inclusions and patches of clinopyroxene exsolution lamellae. Many of the grains are corroded or rimmed by a pale green, actinolite amphibole or rimmed or replaced by green-brown hornblende. Subordinate anhedral augite forms clots around orthopyroxene and showsvarious stages of replacement from the core to rim by hornblende.

Brown to green hornblende is ubiquitous, rimming or replacing pyroxenes or forming poikilitic grains enclosing pyroxenes and plagioclase. Magnetite is present as primary euhedral grains and as a product of alteration of pyroxenes. Sulfidesare present in various amounts, usually as wormy, interstitial aggregates or blebs.

A norite inclusion encountered about 150' south of the Climax ore zone, a few feet across is fresh norite in the center becoming increasingly finer grained toward the margin, and is a hornfels at the margin, which intertongues with pyroxenite. The mineralogy is plagioclase and orthopyroxene and suggests high temperature (700^{o}C) contact metamorphism. From 8000N. to 8350N. many inclusions of norite form sharp (Fig. 5) to gradational contact with ultrabasic rock and in places actually incorporate ultrabasic material. These inclusions and apophyses are usually accompanied by many hornblende-rich clots and dykes. Figure 6, demonstrates

the complex and uncertain age relations of the norite with ultrabasic rock.

Ultrabasic Rocks

(1) Mineralogy

The ultrabasic rocks encountered in the 3050 cross-cut contain fresh orthopyroxenes and clinopyroxenes, olivines and hornblende. Feldspars are scarce. All minerals except olivine occur as poikilitic grains and all minerals except hornblende show some deformation (Fig. 7). Cumulus-like textures are common especially with olivine and pyroxene-rich rocks (Figs. 8 and 9). Grain size of these rocks range from fine to coarse but are generally medium, that is 1-5 mm. Grains range from euhedral to anhedral. Pyroxenes grains are subhedral, olivines tend to occur as corroded or wormy subhedral grains and hornblende is present as anhedral poikilitic, interstitial, or replacement grains.

Cumulus-like textures are suggestive of magmatic origin. The formation of large poikilitic grains of hornblende appear to be by late stage replacement of ortho-and clinopyroxenes.

Olivine in all rocks has a range of composition from Fo80 to Fo86 with the majority ranging from Fo84-86, ($2V_x=89\pm2^o$).* The more Mg-rich olivine is found in the more olivine-rich peridotites. Olivine is cut by serpentine-magnetite veinlets and shows typical "church-window" texture. Boundaries between olivines and orthopyroxenes are regular, especially when olivine is enclosed in bronzite. Some diopside-olivine boundaries are ragged and show extensive corrosion or alteration as do hornblende-olivine boundaries.

* 2V determined on the universal stage, compositions from probe and universal stage.

Fig. 5. Sharp contact of norite with pyroxenite, norite at top.

Fig. 6. Complex age relationship of norite to ultrabasic rocks. Note hornblende pyroxenite inclusion in norite at hammer. Also top center and center shows pyroxenite fragments in hornblende pyroxenite.

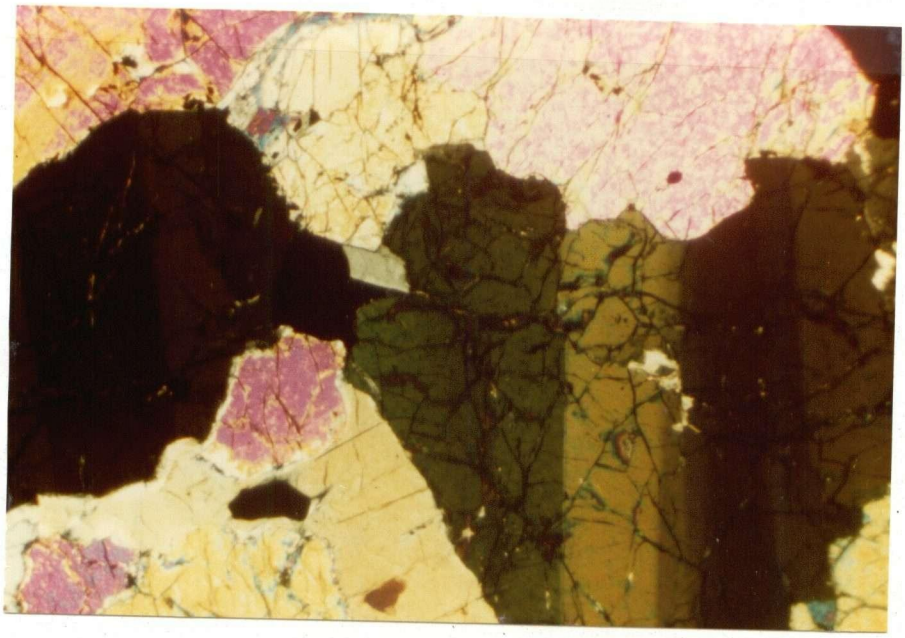

1mm.

Fig. 7. Strained olivine grains . X10, X-nicols.

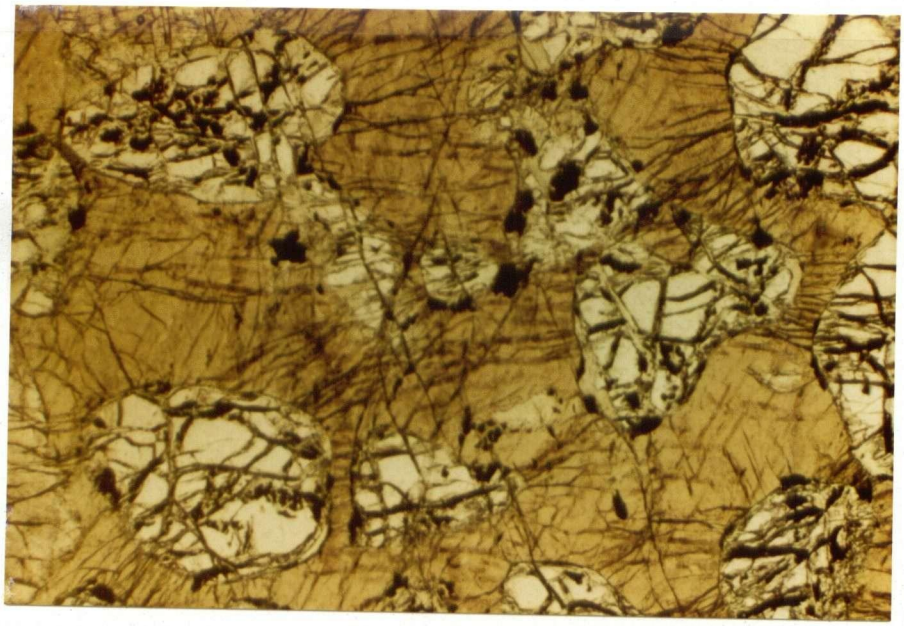

1mm.

Fig. 8. Cumulus-like olivines in poikilitic grain of hornblende . X10, plain light.

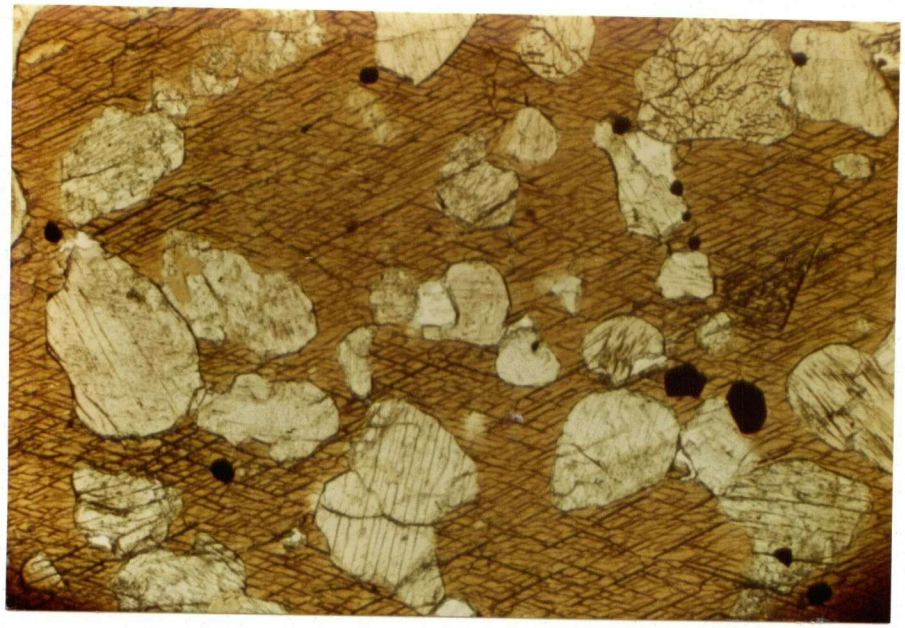

Fig. 9. Cumulus-like orthopyroxenes in poikilitic hornblende. X10, plain light.

Orthopyroxene (En75 - 85)* is the main constituent of the pyroxenites and the principal pyroxene in this area of the ultramafite. Many grains show schiller structure with exsolved lamellae and patches of clinopyroxene along cleavage traces. Many grains show a zoning illustrated by a slight variation in 2V from rim to core. Occasionally, clinopyroxene or hornblende form jackets around orthopyroxenes. Orthopyroxene, although much of it is a interlocking mosaic of grains, may poikilitically enclose olivine and may be enclosed by all other minerals.

Clinopyroxene, mostly diopside (determined by microprobe) has a wide range of composition from Mg (44-53), Ca (40-48), and Fe (6-11), (Fig. 32), and is present in most pyroxenite and some peridotite. Most diopside is mottled by hornblende and shows a great degree of replacement

* Composition determined by probe and universal stage.

by it. Clinopyroxene is anhedral and intergranular but much of it poikilitically encloses bronzite and, in a few rocks, olivine.

Common hornblende in the ultrabasic rocks is brown to olive green. Texturally it ranges from mottled replacement patches, interstitial to large poikilitic grains enclosing all types of primary silicates including rare plagioclase grains.

Plagioclase in the ultrabasic rocks and the hornblendites has a composition of An80-90, (bytownite). These grains, generally interstitial, are found in a few pyroxenites and most hornblendites but never in olivine-bearing rocks.

Accessory minerals are chromite and magnetite which both occur as euhedral primary grains within silicates. Alteration products common in the ultramafic rocks are phlogopite after hornblende, chlorite, talc, actinolite-tremolite, serpentine, magnetite, anthophyllite, and carbonates.

(11) Pyroxenite

The most common pyroxenite is a websterite, a medium grained, dark brown rock composed of two pyroxenes, bronzite and diopside. Although the orthorhombic pyroxene is the more abundant, some rocks contain a greater proportion of clinopyroxene. Websterites predominate from about 6400N. in the cross-cut to the south side (footwall) of the Climax ore zone (Fig. 37 and App. 1). In this area hornblende is present up to 5% in all the pyroxenites. Plagioclase is very rare but may reach 2-3% in some rocks.

Websterites north of 7560N. and particularly those north of 8000N., which occur as bodies too small to be shown properly on a map tend to be rich in hornblende. As the southeast edge of the Chinaman ore zone is approached hornblende websterites become deficient in clinopyroxene to the point where they are classed as orthopyroxenites.

Pyroxenite grades to peridotite as the proportion of olivine increases. Minor olivine is present in pyroxenites for a distance of about 50' on the south (footwall) side of the Climax orebody. At the orebody the olivine content in the rocks increases and the rock is an olivine pyroxenite. Near the north edge of the Climax ore zone the rock becomes periodotitic. In some places the olivine content changes abruptly, producing sharp contacts as at 7260N., (Fig. 10) where the rock changes from a websterite to an olivine pyroxenite. In most instances in the more northerly sections of the 3050 cross-cut, olivine pyroxenites are modified by abundant hornblende, frequently poikilitic.

(111) Peridotite

Peridotite shows a wide range of appearance depending upon the minerals present and the degree of alteration. Fresh harzburgites such as those on the hanging wall of the Climax orebody are dense, hard, black rocks containing orthopyroxene and olivine. Poikilitic, flashy, black, dense rocks found in the northern part of the cross-cut are hornblende-peridotites containing orthopyroxene, minor clino-pyroxene, hornblende and olivine. Just north of the Climax orebody for a distance of perhaps 300 feet the rock is green, soft and altered and crumbles in the hand.

In such rocks, many of the pyroxenes have been altered to hornblende and large plates of phlogopite have formed around olivine grains (Fig. 11). In these rocks olivine shows some serpentinization with abundant magnetite trains but is still remarkably fresh. Uralitization of pyroxene is common and chlorite forms on the ragged edges and boundaries of phlogopite.

(1V) Hornblendite

Hornblendite occurs as dykes or veins and as large clots or pegmatitic zones especially in the northern Chinaman area of the crosscut. Fine-grained, dense, black dykes or veins from a few mm. to 5-10 cm. cut all rock units and ore zones on the 3050 level. They have very sharp contacts. They are composed of aligned prismatic hornblende with interstitial plagioclase up to 10% (bytownite in composition), (Fig. 12). Larger, coarser grained, very irregular, discontinuous hornblende dykes occur mainly in protoclastic zones (which are described later) south of the Chinaman orebody, some showing a reaction margin (Fig. 13). They appear to incorporate or form the host for breccia fragments of ultrabasic and norite and diorite rocks; they also traverse such inclusions and appear as inclusions themselves.

East of the Chinaman zone large clots of coarse-grained hornblende-plagioclase pegmatitic material is present. Hornblende crystals several inches long are cemented by interstitial plagioclase and minor quartz. This zone is a possible reaction margin between the pyroxenites on the east edge of the Chinaman orebody and an adjacent norite revealed by drilling to the immediate east.

Fig. 10. Sharp contact at 7260N. between websterite on left and olivine-rich pyroxenite.

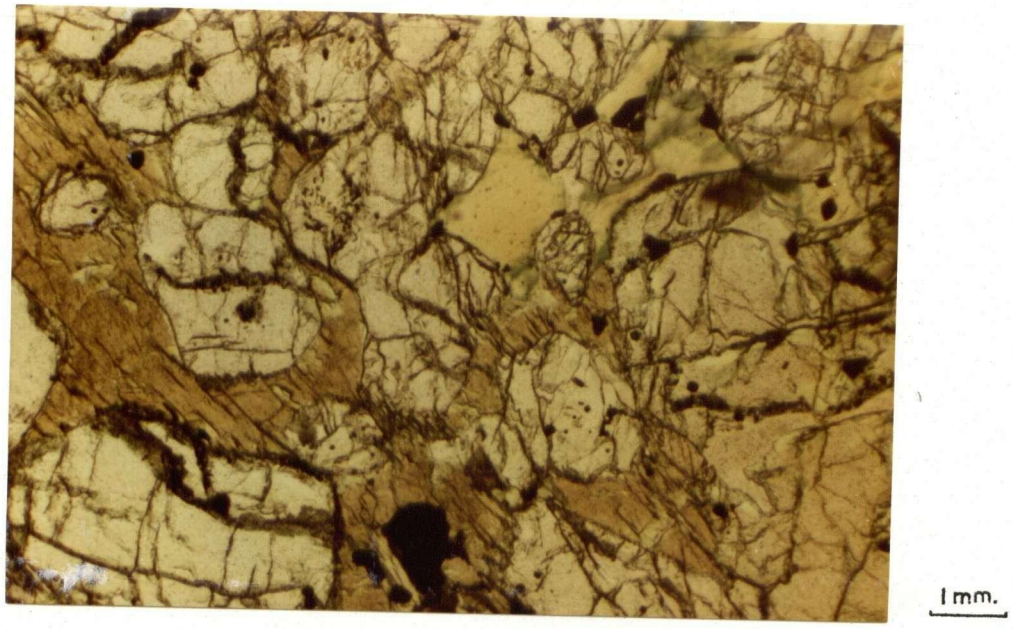

Fig. 11. Olivine grains in hornblende. Top right center, phlogopite after hornblende with incipient chlorite alteration. Right side Orthopyroxene unaltered. 10X, plain light.

Fig. 12. A fine grained hornblendite dyke cutting another hornblendite dyke and host ultrabasic rocks

Fig. 13. One foot wide hornblendite dyke with reaction margin. Protoclastic area on south side of Chinaman ore zone.

MINERALIZATION AND OREBODIES

Introduction

Sulfide minerals on the 3050 level cross-cut occur as disseminated grains, as veinlets and schlieren, and as massive clots all exclusively in ultrabasic rocks. The mineralogy is simple, consisting of pyrrhotite, pentlandite, chalcopyrite, magnetite and very minor pyrite. Early investigators tentantively identified other Ni-bearing sulfides but none was seen in this area of the mine. Some secondary or supergene minerals, chalcocite, covellite and limonite, coat surfaces on exposed, weathered, sulfide-bearing rocks but are lost during preparation of polished sections.

Disseminated Sulfides

All ultrabasic rock units within this area of the mine contain the three principal sulfides as singular or composite, xenomorphic blebs and interstitial fillings between fresh euhedral to subhedral grains of olivine, orthopyroxene and in some places clinopyroxene (Fig. 14). In many specimens these sulfides occupy positions similar to those occupied in other specimens by interstitial hornblende, and may be replaced by hornblende, possible as a late stage magmatic reaction. The occurrence of the sulfides in ultramafic rocks resembles that of primary crystallization from an immiscible sulfide phase. This resemblance is enhanced by the presence of rounded or vermicular blebs of the sulfide enclosed in unaltered

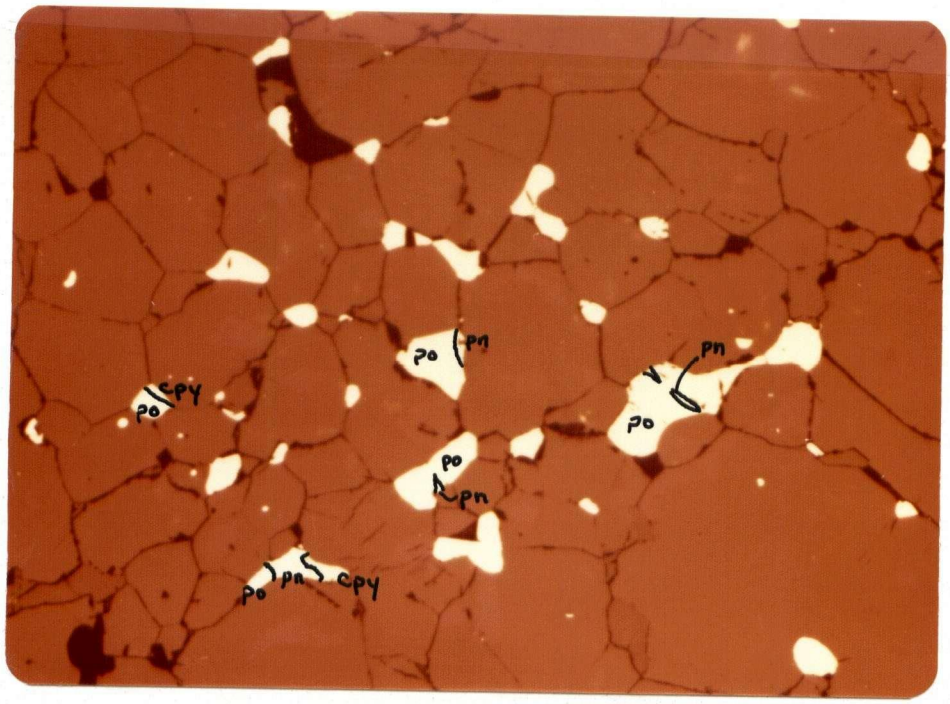

Fig. 14. Interstitial po.-pn.-cpy. grains in fresh pyroxenite. X16, plain light.

Fig. 15. Composite po.-cpy. bleb and magnetite grain enclosed in olivine. X63, plain light.

olivine and orthopyroxene grains (Fig. 15). The chemical compositions of the accessory pyrrhotite and pentlandite are variable and appear directly related to the lithological unit that contains them, as expanded upon in the following section. The sulfide component appears to undergo a bulk compositional change from Cu- and Ni-rich composite aggregates in pyroxenites to more Cu- and Ni-poor aggregates in the peridotites.

Net-Textured Sulfides

Net-texture can be considered an extension of the disseminated type where the sulfides expand to form a nearly continuous net between silicates, forming an interconnected, lacy texture. The silicates, particularly olivine and bronzite, are more euhedral than in the disseminated type, forming unaltered isolated crystals in a allotriomorphic sulfide groundmass. The sulfides here appear to occur in the same manner as the hornblende in poikilitic hornblende pyroxenites and peridotites (Fig. 16).

The net-texture is seen to occur in weakly mineralized areas of the cross-cut, mainly in pyroxenites, but are best developed and seen in the low grade sections of the Climax and Chinaman ore zones. In particular, the net texture, is well developed in the hanging wall part of the Climax orebody where olivine predominates as euhedral crystals and also in the core of the Chinaman ore zone. That these sulfidic net-textured peridotites can be mined economically is due in part to their proximity to more massive sulfides.

Massive Sulfides

Massive sulfides form most of the ore. The sulfides form a continuous anhedral groundmass commonly up to 50% of the material present (Fig. 17). Gangue minerals consist of euhedral crystals of olivine and pyroxene which appear to "float" in the sulfide groundmass. These crystals are larger and better developed than those found in less massive ores. In the Chinaman orebody, which is more hornblendic, large crystals of hornblende, apparently primary crystals, are enclosed by massive sulfides.

Some silicate crystals show corrosion, and partial to almost complete replacement. Such features as replacement along cleavages, embayments and sketetal remains may be ascribed to selective replacement, late magmatic reactions or both.

Massive ores, particularly in the Chinaman zone seem to have been modified by late stage movements of the sulfide minerals producing a protoclastic texture (Fig. 18). Fragments of disseminated and net-textured material have been incorporated into the massive sulfides. These fragments are rimmed by massive sulfide stringers and in some instances appear fractured and rehealed by sulfide stringers.

The protoclastic texture led Aho (1956) to suggest a possible hydrothermal origin for the ore minerals. On the other hand, scattered anhedral grains typical of primary accessories, euhedral silicates floating in a groundmass of sulfide and vermicular blebs of sulfides enclosed in pyroxenes, olivines and early hornblende support a magmatic origin for the ore minerals.

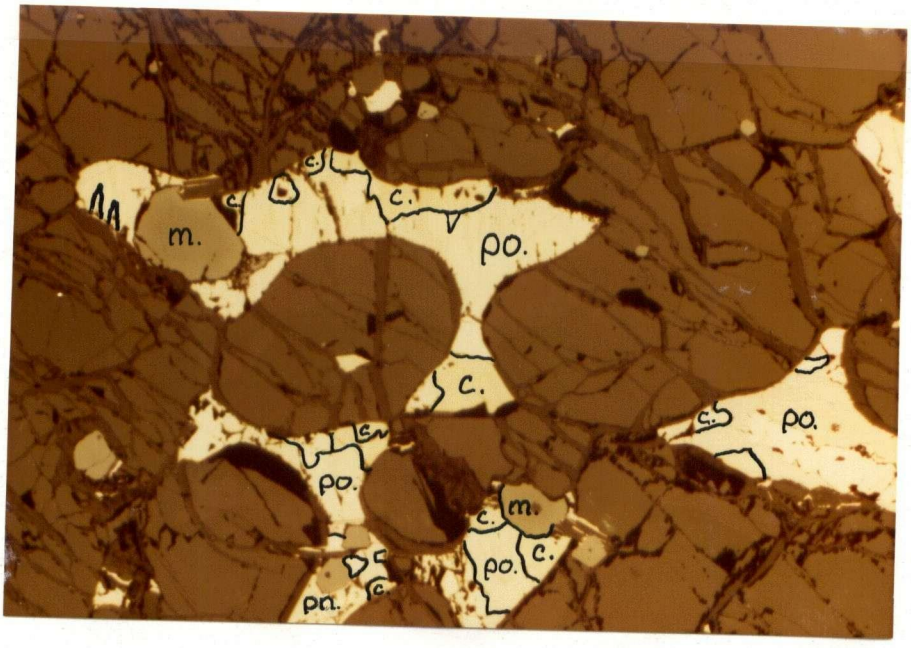

Fig. 16. Net-textured sulfides in an olivine gangue. 16X, plain light.

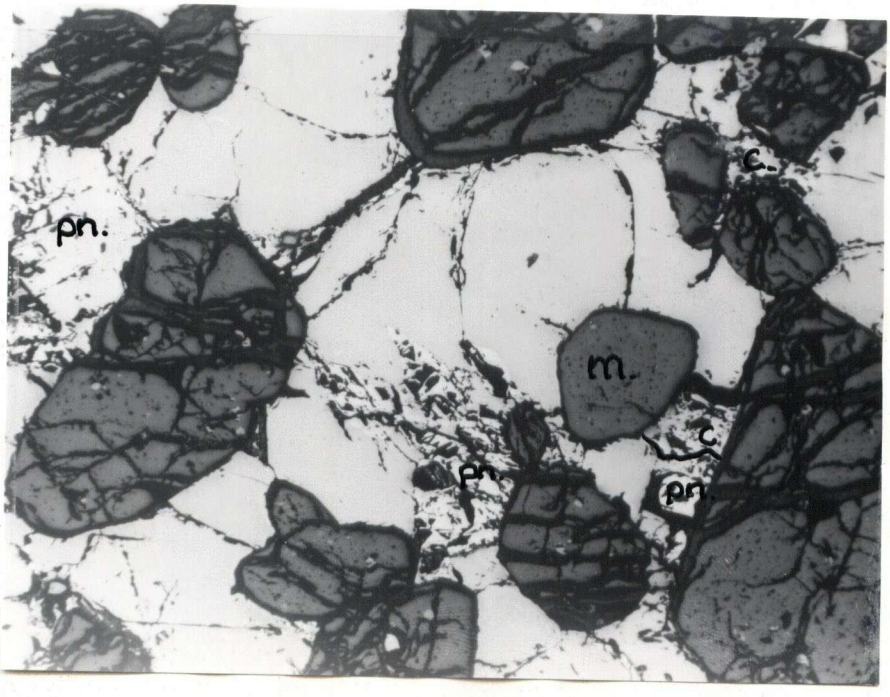

Fig. 17. Massive sulfides with euhedral silicates "floating". X60, plain light.

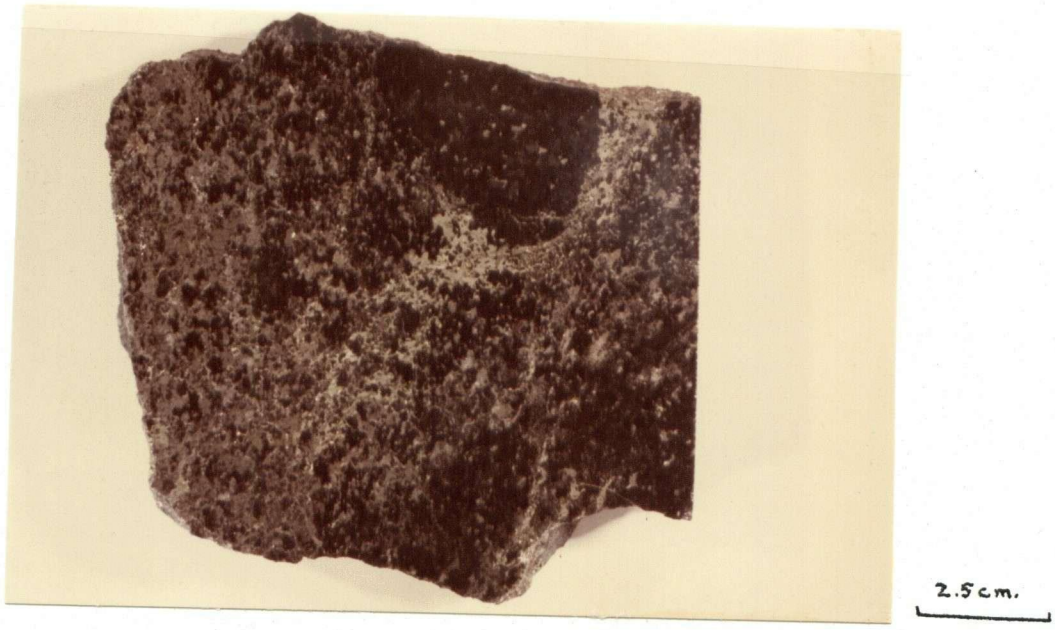

Fig. 18. Protoclastic texture of Chinaman ore, fragments of disseminated and net-textured ore with sulfide schlieren and fracture filling by sulfides.

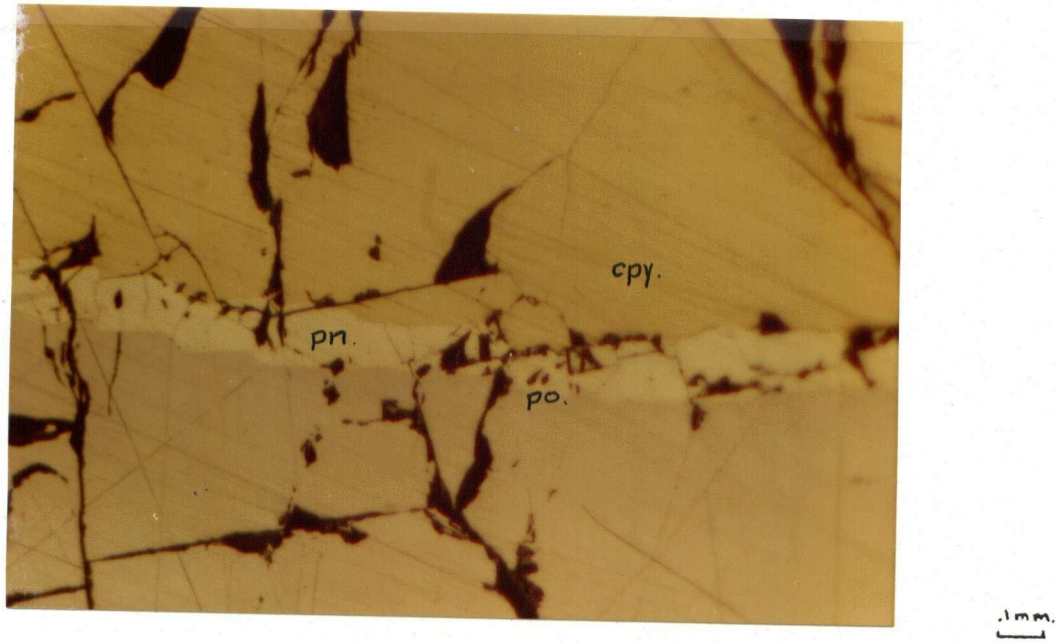

Fig. 19. Chalcopyrite on edge of composite grain separated from pyrrhotite by pentlandite. X63, plain light

Textural Relations Between the Various Sulfides

Disseminated to massive, pyrrhotite, pentlandite, and chalcopyrite are all present in ore samples and have roughly constant proportions, with pyrrhotite the most abundant and chalcopyrite the least. This proportion appears to be 70:20:10. Pyrrhotite forms an irregular, medium- to fine-grained mosaic of composite anhedral grains. Pentlandite usually occurs at pyrrhotite grain boundaries, as does chalcopyrite, as medium- to fine-grained anhedra and composite masses. In some specimens, chalcopyrite is seen to be separated from pyrrhotite by pentlandite (Fig. 19). In some instances pentlandite occurs as irregular blebs within pyrrhotite, and chalcopyrite appears as cross-cutting laths in pyrrhotite. Discontinuous aggregates of pyrrhotite may be connected by pentlandite and chalcopyrite. Chalcopyrite principally and to a lesser extent pentlandite and pyrrhotite form as cross-cutting fillings or replacements in fractured silicates, (Fig. 20), suggesting some remobilization of the sulfides (Fig. 24). Chalcopyrite is also seen to cut the other sulfides, mainly pentlandite. Pentlandite and infrequently chalcopyrite are seen to form laths, flame-like and exsolution-like textures in pyrrhotite. In the case of chalcopyrite, this texture is usually restricted to very small, isolated, composite sulfide aggregates in barren rock.

Paragenesis

The Cu-Ni-Fe-S mineral assemblage seen at Giant Mascot are those seen at most nickeliferous pyrrhotite deposits. Most orebodies

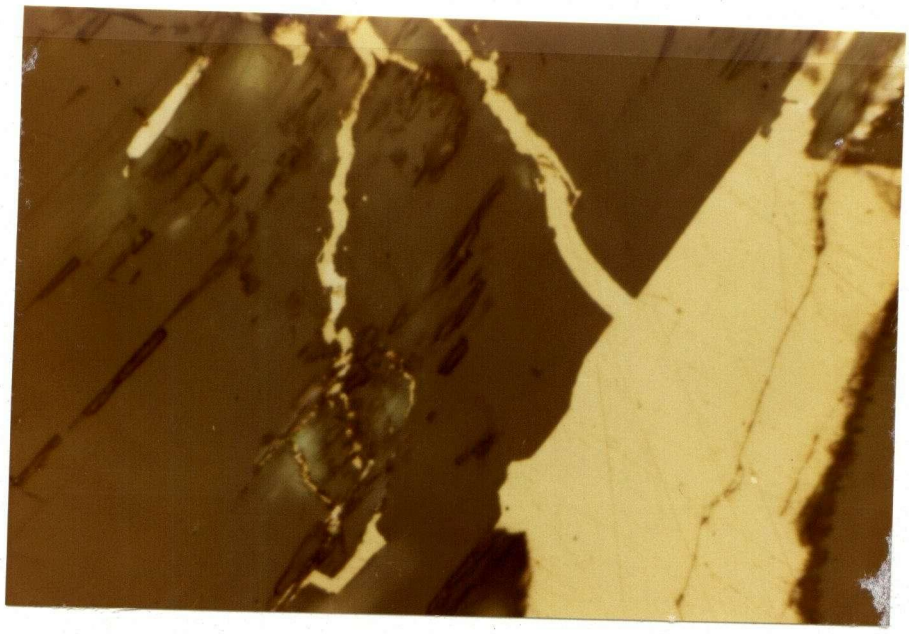

Fig. 20. Chalcopyrite replacing fractures in silicate. X160, plain light.

of this type are accepted as being magmatic in origin (Craig and Kullerud, 1969) and are formed through unmixing, exsolution and re-equilibration by slow cooling from a monosulfide solid solution. Kullerud, Yund and Moh (1969), and Craig and Kullerud (1969), have made extensive reviews of the phase relations in the various ternary systems and the quarternary system containing Cu-Ni-Fe-S and have offered several stable isothermal mineral assemblages in the temperature ranges from above 1000°C to below 550°C. The paragenetic sequence seen at the Chinaman and Climax orebodies will be interpreted in the light of these studies.

The average bulk composition of the Giant Mascot ores are believed to lie within the single phase region of the monosulfide solid solution

(Mss) at 1000°C as illustrated in figure 21. This composition was approximated by the use of sulfide analyses of Horwood (1937), Aho (1956) Muir (1971) and estimates of pyrrhotite - pentlandite - chalcopyrite proportions by the present author. As these plots are all very similar to that composition assigned to Sudbury, Hawley (1962), the Sudbury figure is plotted. Variations from the Sudbury bulk compositions will account for individual paragenetic sequences and assemblages.

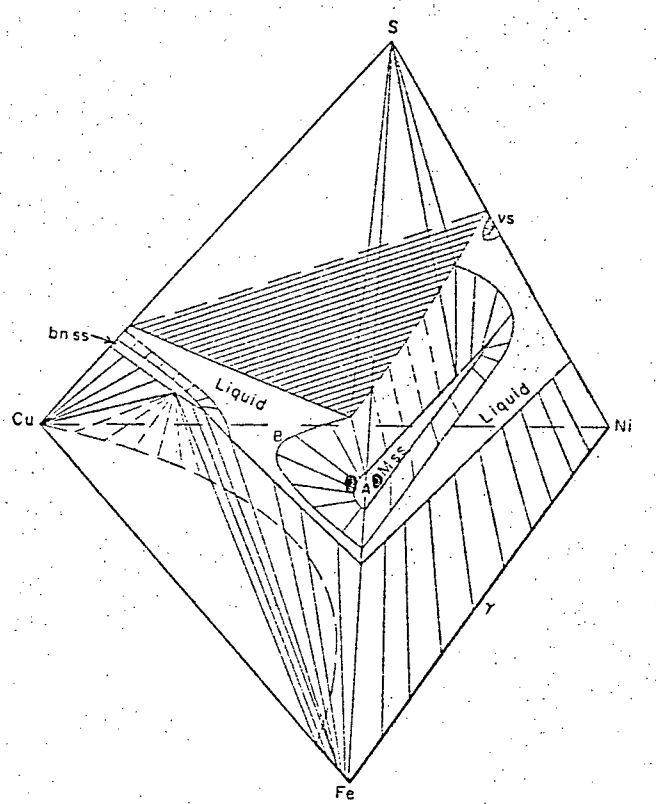

FIG. 21. Schematic 1,000° C isothermal diagram of the Cu-Fe-Ni-S system in the presence of vapor. Tie lines to S liquid are omitted for clarity. Note the wide extent of the homogeneous sulfide liquid (stippled) and the large region of liquid immiscibility (sulfur liquid and sulfide liquid). The Mss nearly spans the Fe-Ni-S face of the system. Points designated A and B are discussed in the text.

The liquidus temperature may be as low as 1000°C at which point a pyrrhotitic nickel-bearing liquid (Mss, Fig. 21) phase A coexists with a copper-rich liquid, phase B. Upon cooling at some temperature above 850°C it is possible for a copper-enriched liquid to segregate from the Mss and form two sulfide phases, a Ni-pyrrhotite solid solution and a chalcopyrite solid solution (Cpss). This mechanism may account for the chalcopyrite rich segregations and veining seen at Giant Mascot and many other Cu-Ni deposits related to ultrabasic rocks (Fig. 22).

In general the bulk compositions of Ni-Cu sulfide ores commonly lie within the quaternary Mss down to 500°C. Pyrite may form in some quaternary systems at temperatures of 743°C where tie lines are established between Cpss and pyrite. This is very sulfur dependant and a small decrease in sulfur will prevent pyrite formation. At some temperature below 600°C a chalcopyrite and/or pentlandite (ss) can exsolve from the Mss and will continue to do this as the temperature is lowered and the pyrrhotitic Mss becomes depleted in Ni and Cu. At temperatures of 500°C the Mss can only accomodate 1% Cu but may contain greater than 5% Ni. In most cases as at Giant Mascot the exsolution temperature for pentlandite is considerably lower than 600°C and pentlandite formation follows that of chalcopyrite from the Mss. At temperatures of 590°C Cpss will breakdown into two cubic phases (chalocpyrite and cubanite). The absence of cubanite and scarcity of pyrite can be explained by the fact that below 334°C this mineral pair forming in Ni-poor assemblages, reacts to form chalcopyrite and pyrrhotite. A more likely explanation of their absence is that at Giant Mascot, where 5% or more Ni is present, Cpss and nickeliferous pyrrhotite Mss can coexist and no cubanite - pyrite assemblage

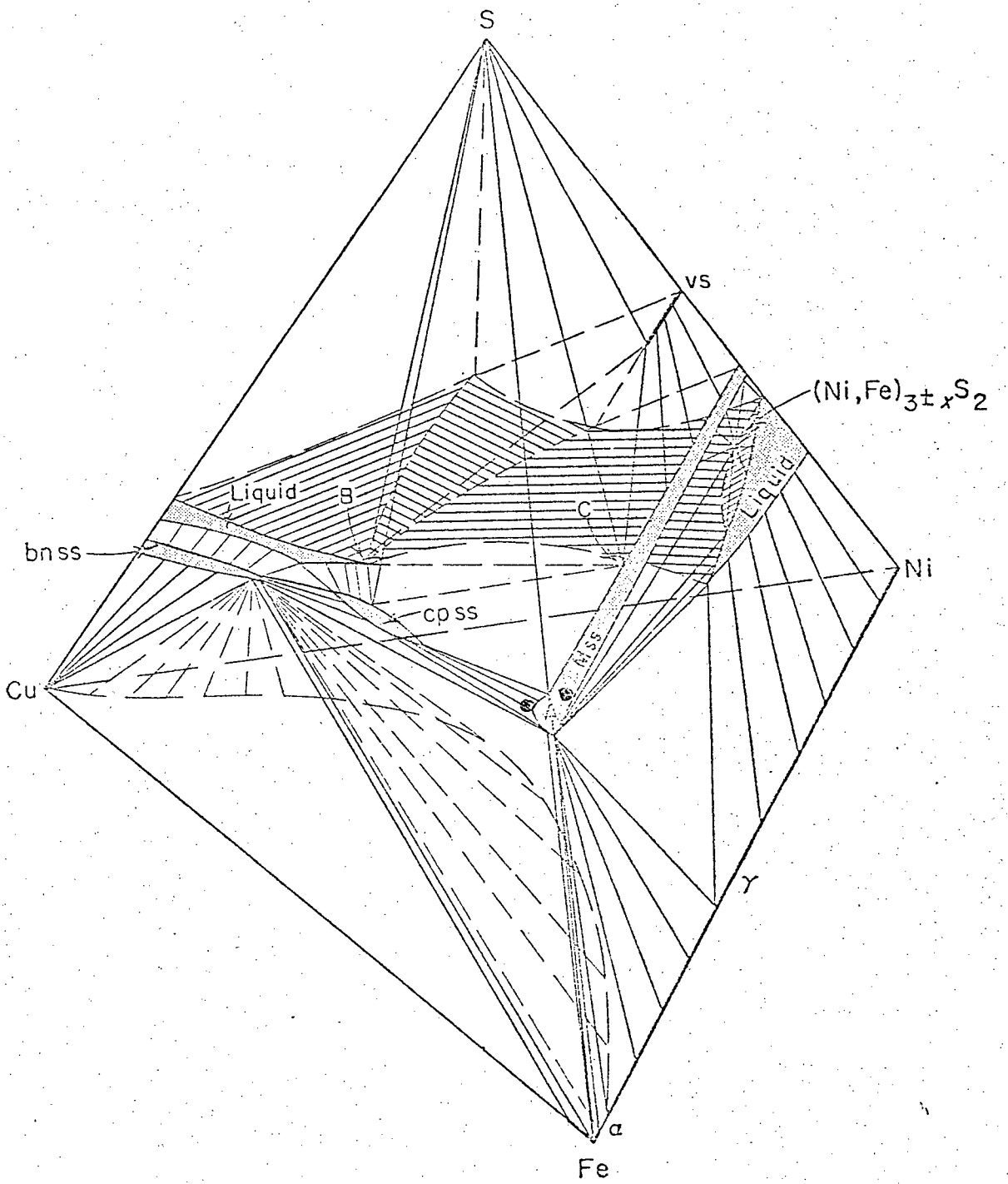

FIG. 22. Schematic 850° C isothermal diagram of the Cu-Fe-Ni-S system in the presence of vapor. Most tie lines to sulfur are omitted for clarity. Note that the region of homogeneous liquid has diminished from 1,000° C. that Mss spans the entire Fe-Ni-S face of the system, and that cp and $(Ni,Fe)_{3\pm x}S_2$ are stable phases.

is formed. At very low temperatures, considerably below 300°C, the Mss breaks down to an assemblage of pyrrhotite and pentlandite - pyrite. Relations involving the formation of pentlandite - pyrite are not clear. The minor pyrite seen at Giant Mascot appears as late stage veining or intergrowths with pentlandite. In figure 23 the common assemblages at low temperatures observed in most massive Ni-Cu ores which include those of Giant Mascot are shown.

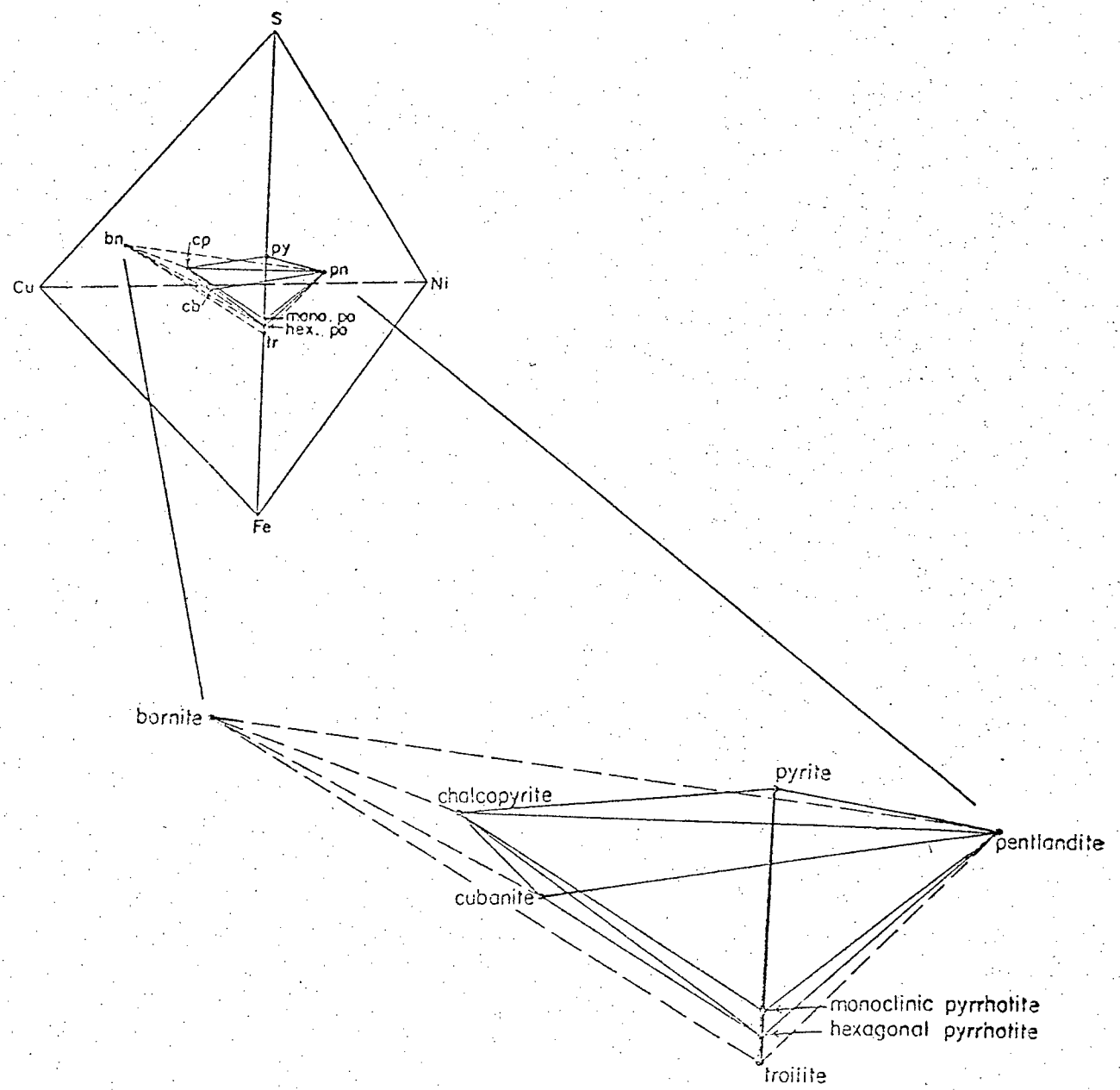

FIG. 23. Low temperature mineral assemblages in Ni-Cu ores. The most common associations are indicated by solid lines whereas those less common are indicated by dashed lines.

In summary the paragenesis and mineral assemblages noted at Giant Mascot are well documented by laboratory experimental workers. An illustration of the sequence of formation of silicates and sulfide phases at Giant Mascot is shown in figure 24.

Apparent Paragenesis Fig. 24

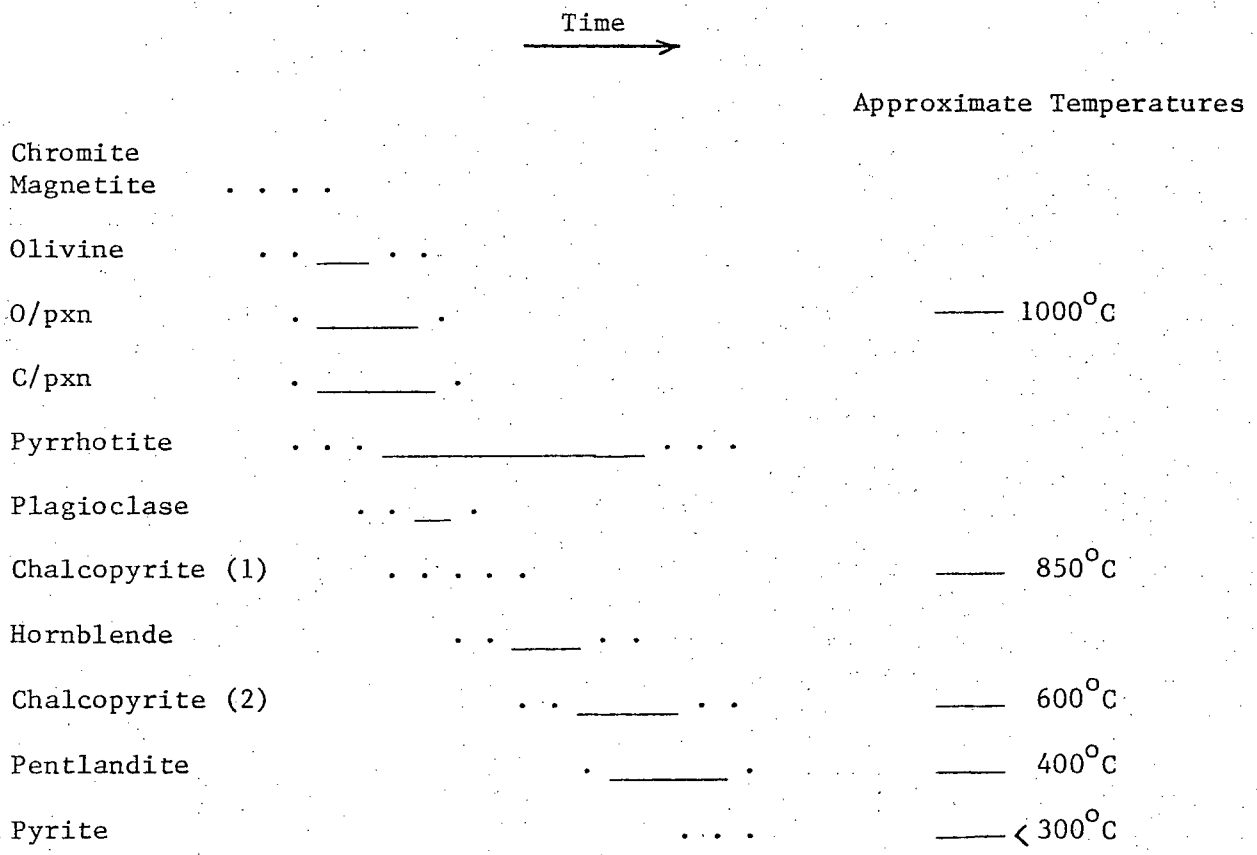

Climax Orebody

The Climax orebody, crudely cylindrical, intersected by the 3050 level cross-cut at 6900N., see map, Appendix 1, has maximum dimensions of 90 x 50 feet in plan. The mineralized zone plunges at 63^{o} in a N. 30^{o} W. direction with a vertical length of almost 600 feet, terminating at the 2700 foot level.

The ore zone occurs at the contact between peridotite (hanging wall) and pyroxenite. The pyroxenite on the south side of the ore zone is websterite with minor olivine and becomes more bronzitic and olivine rich in the high grade area. The contact between the pyroxenite and peridotite is sharp and corresponds to textural and tenor changes in the ore minerals. In general, the wall rocks of the Climax ore zone range from peridotite through pyroxenite to norite which is present on the western edge. This orebody corresponds to Aho's massive type, an ore zone at or near the contact between two rock units with no zonal distribution of lithological or ore units. See Map 1, Appendix 2, for the general geology of the Climax area.

Olivine and pyroxene in the ore zone show deformational strain as evidenced by twinning and undulatory extinction. Other features such as drag folds, banding and marginal flow lines as cited by Aho (1956) as criteria for what he called, "massive, injection origin ore", are not reported at the Climax body.

The tenor of the orebody appears to change vertically with an apparent maximum Ni and Cu content at the 3108 foot elevation accompanied by a low ratio of Ni/Cu. This is deduced from calculations of ring drilling assay tests on three levels and the overall grade and

tonnage of the orebody as illustrated in Table 1.

Table 1

Climax Ore Calculations

Elev.	Tons/vert.ft.	Ni%	Cu.%	Ni/Cu
3198	446	1.01	.38	2.66
3108	435	1.33	.66	2.00
2959	414	1.08	.43	2.51
Average of block between 3298 and and 2700	353	0.78	0.36	2.16

Total Tonnage = 211,000

On the basis of these somewhat incomplete data it can be concluded that the orebody decreases in size and Ni grade down the plunge.

Zonation of the ore minerals is illustrated remarkably well in figures 25, 26, and 27, which are computer contour plots of Ni, Cu and Cu/(Cu+Ni) respectively at the 3108 foot level. Additional level contour plots which do not show zonation as well are appended. Nickel values are seen to increase concentrically inward with the highest grade zone corresponding to the footwall or "trough" of the ore pipe. Copper values behave in a similar fashion but a high grade zone is noted on the western side of the orebody. This feature is further reflected in the Cu/(Cu+Ni) plot which shows the highest ratio on the western side of the elliptical shaped ore plan. This western bias of mineralization is noted on levels above and below the 3108. The western boundary is near a large adjacent norite implying some genetic link between mineral-

ization or localization of ore minerals and noritic phases within the ultramafite.

Chinaman Orebody

The Chinaman orebody is intersected in the 3050 level cross-cut at 8540N. It is crudely elliptical and elongate in the direction of plunge when viewed in plan. The maximum dimensions of the ore zone are 90 x 100 feet with a vertical extent of 638' terminating at the 2700 foot level. The mineralized zone plunges at 68^{o} in a N. 60^{o} W. direction. Above 3200 feet and below 2800 feet the ore zone consists of two or three discrete units which become small, low grade, and much faulted.

The relationship of ore to the geological rock units is not well known but it appears that the core of the mineralized zone is a low grade to barren peridotite. The ore zone forms a partial envelope around peridotite and vertically is discontinuous forming more than one mineral zone in hornblendic pyroxenite. This unit is surrounded by very hornblende-rich phases. The footwall, south and east side, appears to be a hornblendite, pyroxenite, and norite breccia. Further east, norite, possibly a large inclusion, has been indicated by drilling.

Although mapping is inconclusive, study of drill logs and discussion with mine personnel suggest that this orebody corresponds to Aho's zoned type which he describes as being zoned in a cylindrical fashion around or in a peridotite core with other rock units concentrically ringing the core. Specifically this orebody closely resembles the 1900 orebody which he described as "more complex, lower in grade,

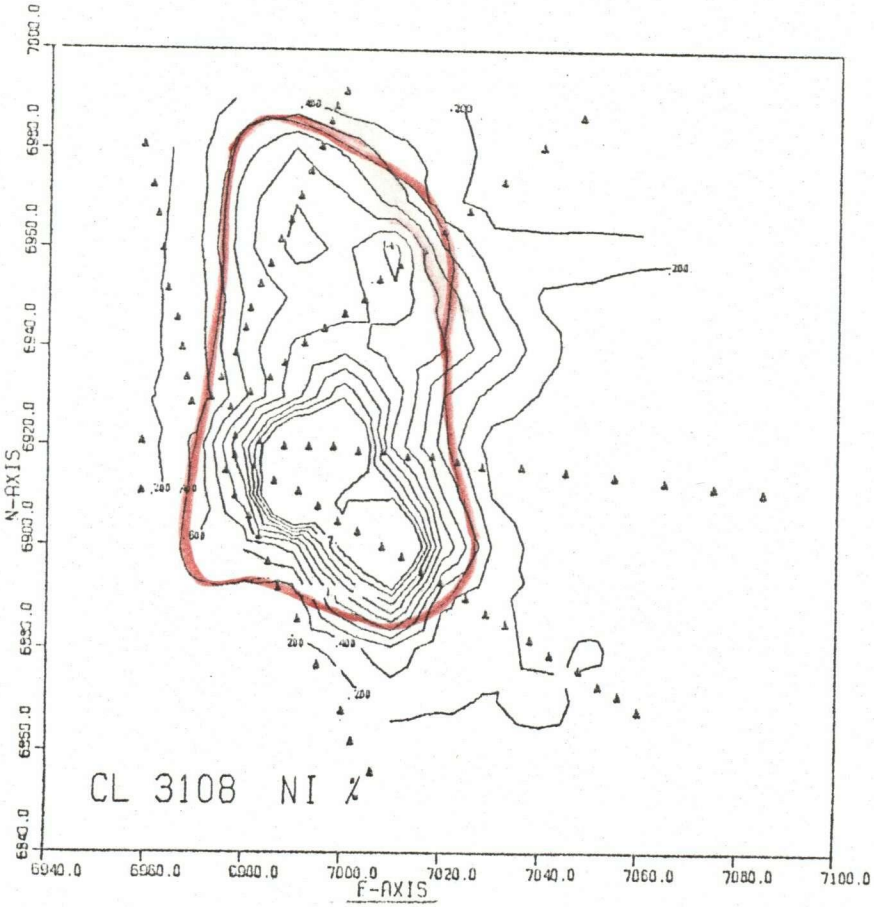

Fig. 25. Ni contour plot of Climax ore at 3108' elevation, in percent.

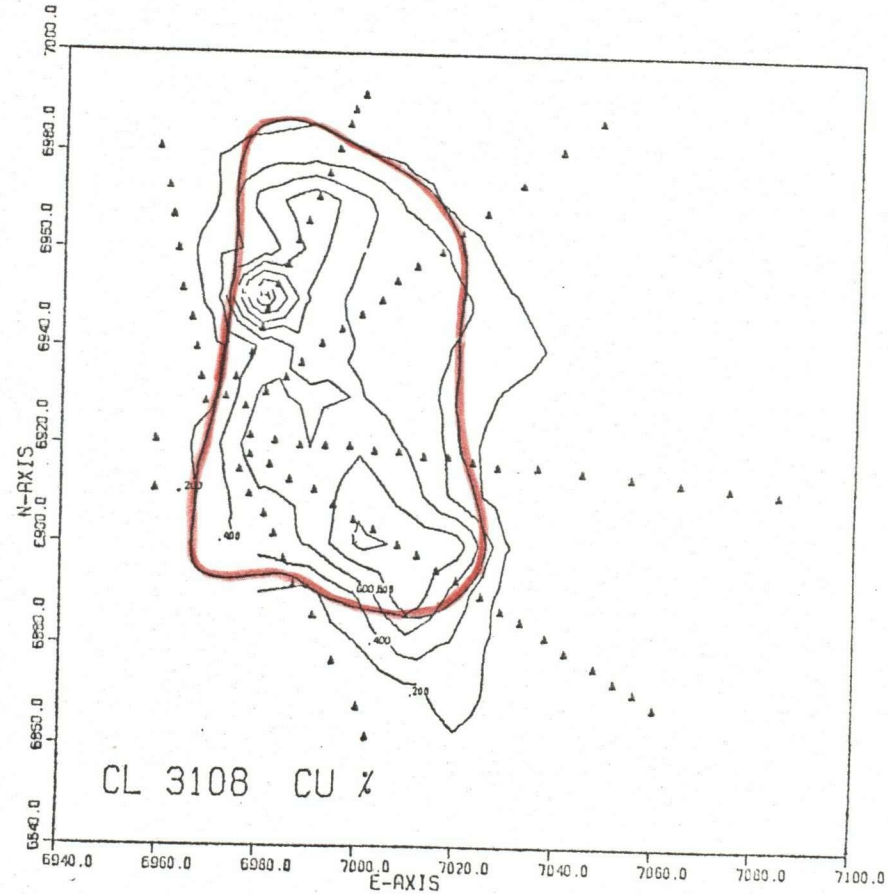

Fig. 26. Cu contour plot of Climax ore at 3018' elevation, in percent.

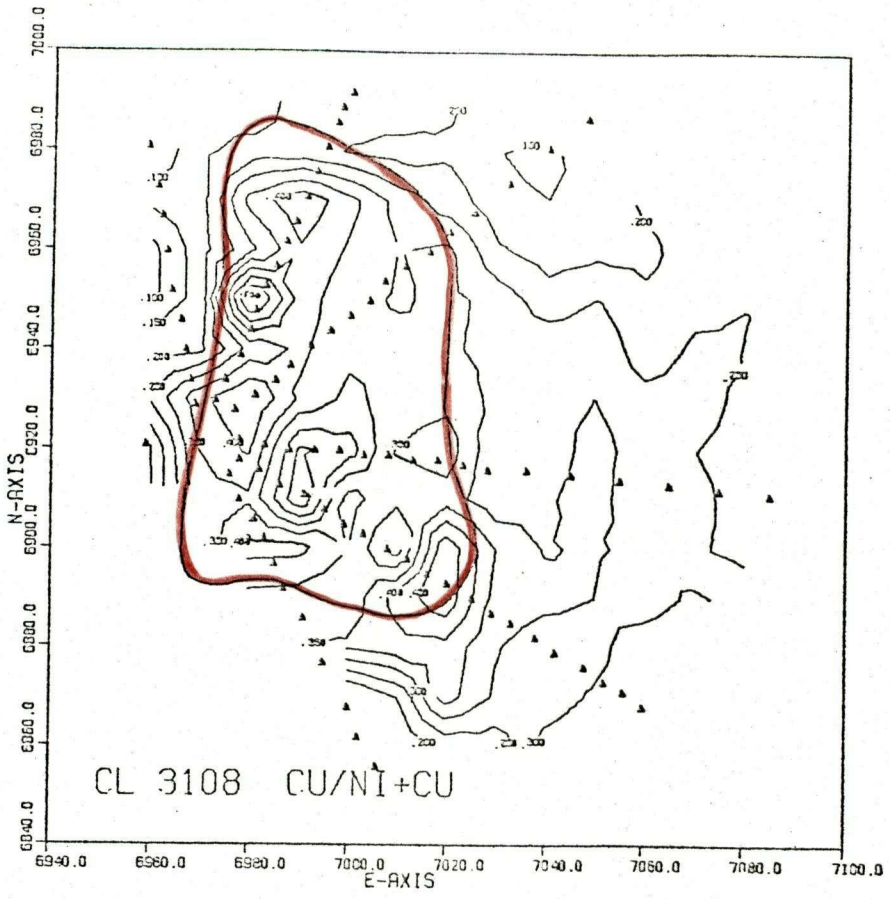

Fig. 27. Cu/(Cu+Ni) plot of Climax ore at 3108' elevation. Ratio in percent.

lower in ratio of nickel to copper and more hornblendic than the others, and is more suggestive of replacement origin."

The tenor of the Chinaman ore and the size appear to change erratically in vertical direction. This variation can be attributed to the structural nature of the ore zones at different elevations. The large low grade sections, especially on the 3207 level, are really three adjacent zones mined as one orebody, whereas three zones are distinguished on the 3292 level and the grade is higher but tonnage lower. This kind of structure does not hold true in the lower reaches of the ore zone.

Calculations from ring drilling assay results from the Chinaman orebody are illustrated in the following Table 2.

Table 2

Chinaman Ore Calculations

Elev.	Tons/vert.ft.	Ni%	Cu%	Ni/Cu
3292	613	.67	.29	2.31
3207	945	.42	.16	2.63
3160	727	.61	.37	1.65
2802	432	.50	.21	2.38
Average of block between 3338 and 2700	589	.73	.30	2.43

Total Tonnage = 376,000

Zonal features of the ore minerals by element are presented in figures 28, 29, and 30, which are computer drawn contour plots of assay information on the 3160 level of Ni., Cu., and Cu/(Cu+Ni). Additional level contour plots which do not illustrate zonation as well are appended. Both the Ni and Cu plots show the elongation in the direction of plunge with the concentrically zoned higher grade parts corresponding to the "trough" or footwall region of the ore zone. The Cu/(Cu+Ni) ratio also appears higher here but in general this plot is erratic and does not support Aho, (1956), who predicts that the copper values should be higher on the periphery and lower towards the core of the orebody. It is also worth noting that the bias of the higher grade mineralization is towards the noritic rocks to the east in much the same manner as in the Climax body.

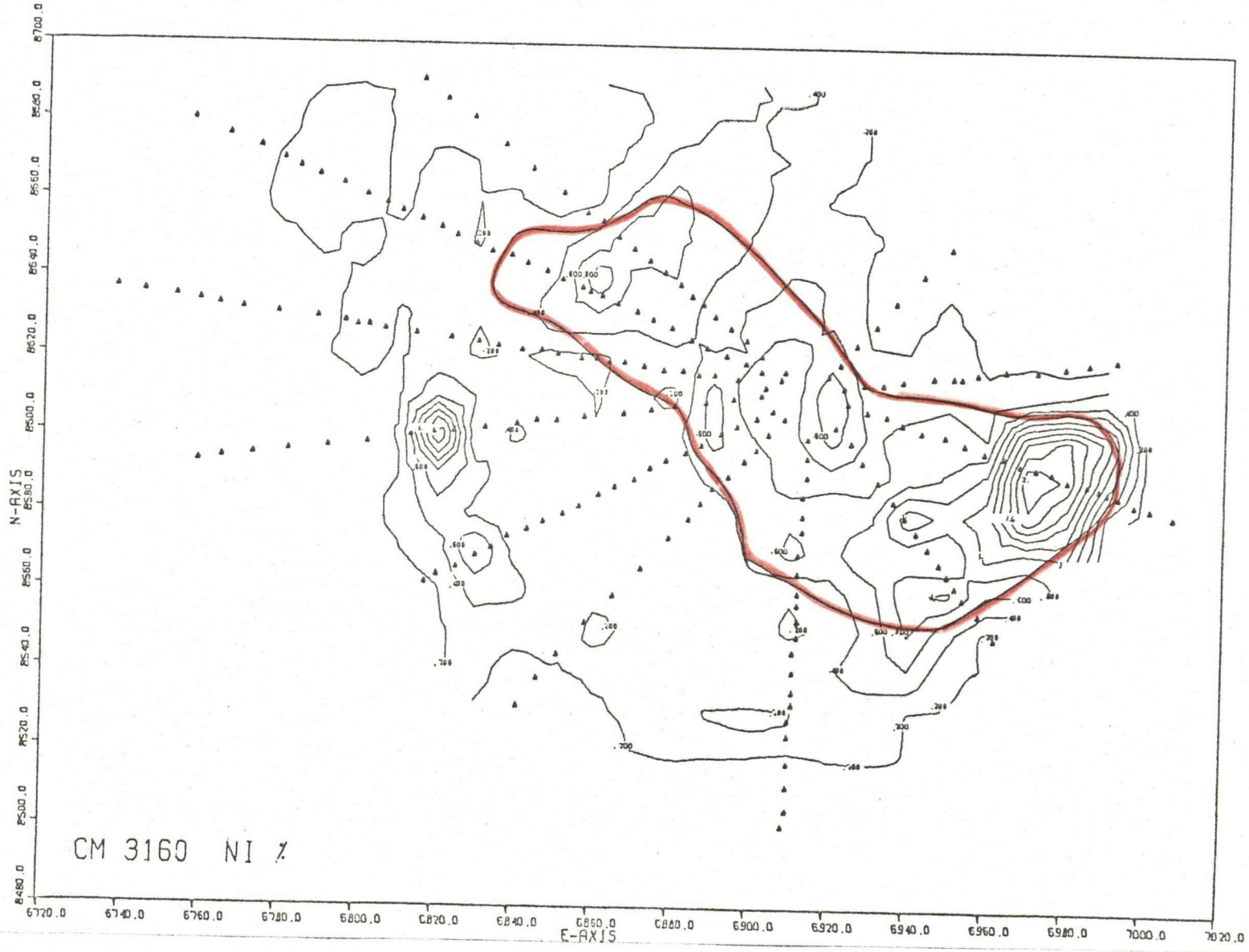

Fig. 28. Ni contour plot of Chinaman ore at 3160' elevation, in percent.

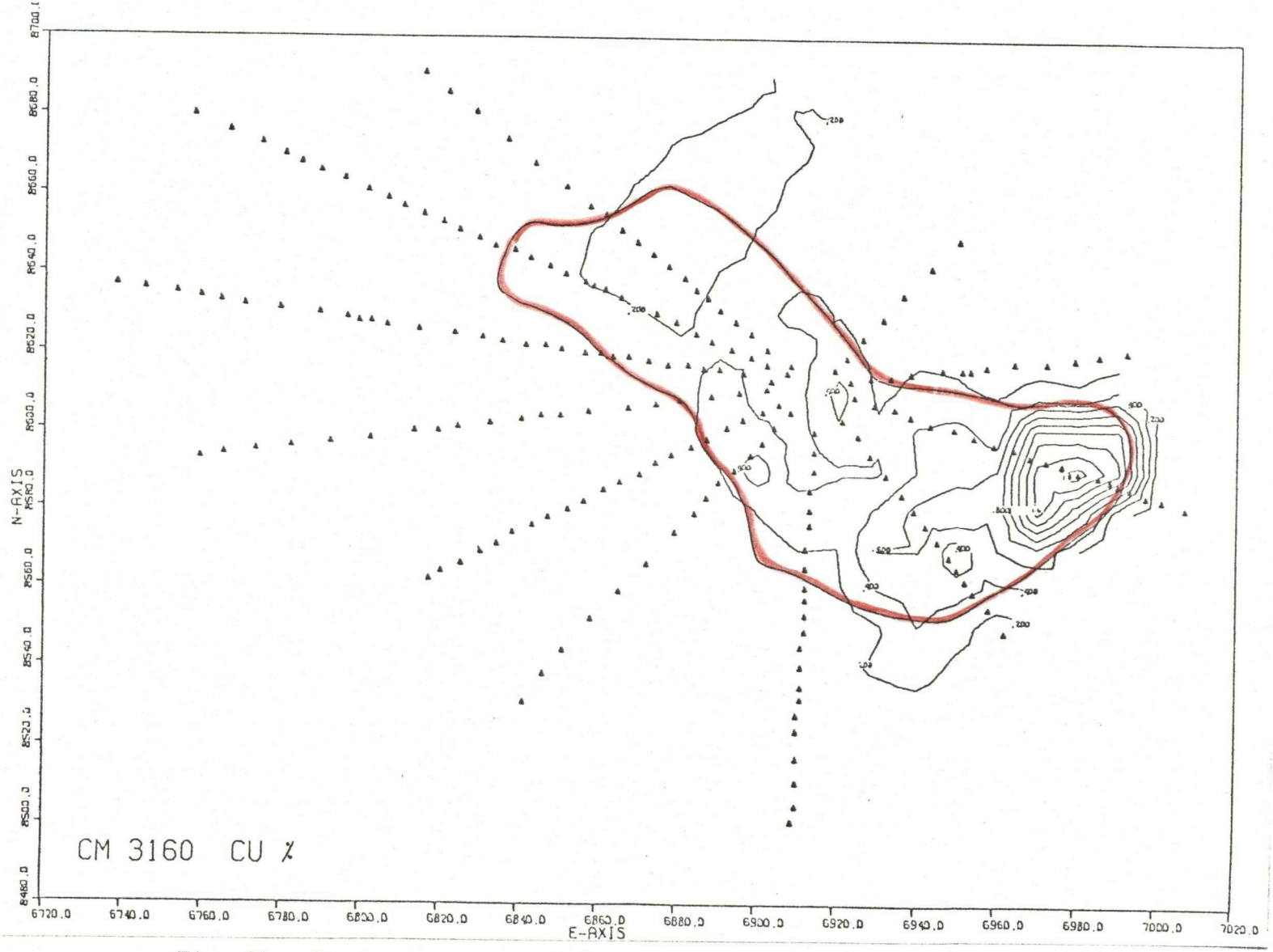

Fig. 29. Cu. contour plot of Chinaman ore at 3160' elevation, in percent.

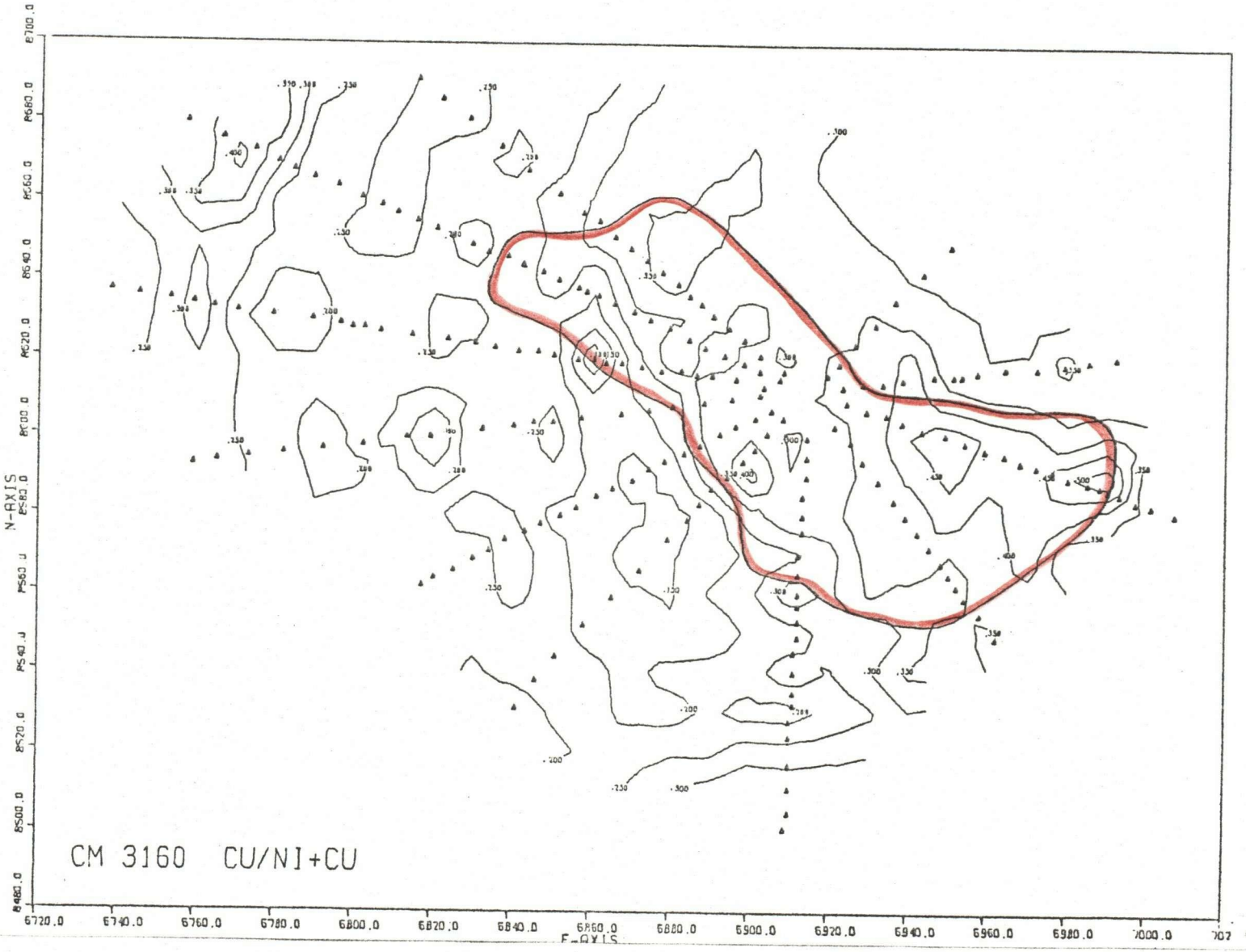

Fig. 30. Cu/(Cu+Ni) plot of Chinaman ore at 3160' elevation, ratio in percent.

These two orebodies which account for greater than 10% of the total production to the present time mined at Giant Mascot seem to correspond to Aho's, (1956), two-type classification of massive (Climax) and zoned (Chinaman). Although he ascribes a magmatic injection origin to the former and a replacement origin to the latter it is believed by the writer, and this subject will be expanded upon in more detail later, that both types of ore have magmatic injection origin with the "zoned" type being modified by later geologic events.

CHEMICAL ANALYSES OF SILICATES AND SULFIDES

Silicate Analytical Techniques

Chemical analyses of silicate minerals were made with an ARL SEMQ scanning electron microprobe. The probe was run at 15 Kev. with a specimen current of 25 to 30 n.A. Sample information was gathered in the "peak-seek" mode and output collected and refined by the on-board computer using Bence-Albee correction factors. The refined data, in weight percent, are printed out at a teletype terminal.

Grains in each rock specimen were analyzed using an incident beam approximately 10 μ. in diameter. This beam size was selected in an attempt to avoid exsolution lamallae. In most instances elemental analysis was believed good to ±1% of the amount percent, but in the case of Si and Ca the error was larger, possibly greater than ±2%.

A total of 30 rock specimens yielded 29 orthopyroxene, 17 clinopyroxene and 13 olivine compositions. In most cases the analyses were made in the centre of a grain and 8 elements were determined. Detailed work on specimens of all three minerals was carried out to determine homogeneity and to test for the presence of additional elements. A complete tabulation of all analyses in weight percent and as mole fractions is given in Appendix 4.

Silicate Analyses

Fig. 31, a part of the pyroxene quadrilateral, illustrates the chemical compositions of the pyroxenes and of coexisting pairs. Orthopyroxenes range in composition from $En_{85.65}$ to $En_{75.10}$ and, clinopyroxenes

range from $Wo_{39.45}$ to $Wo_{48.15}$, $En_{43.95}$ to $En_{52.75}$ and $Fs_{5.8}$ to $Fs_{10.8}$. Olivines, not plotted, range from $Fo_{80.0}$ to $Fo_{86.65}$.

Tie-lines in the pyroxene quadrilateral show close parallelism suggesting sound analytical technique. The shift of the tie-lines indicates bulk compositional changes. Iron-enrichment trends within a particular rock unit may define a zoning or cryptic layering.

Elemental variation plots of orthopyroxenes along the 3050 cross-cut, Fig. 32, show high Fe in pyroxenites and corresponding low Fe in peridotites. This is particularly well illustrated at 7260N. where a small pyroxenite unit shows a marked change in orthopyroxene composition when compared to the large peridotite units that surround it. Although not readily apparent in the illustration, in the Chinaman orebody and the brecciated footwall on the south, those orthopyroxenes high in Fe are from pyroxenitic rocks and those with low $Fe/_{Fe+Mg}$ ratios are found in peridotites. From the Climax orebody south, the elemental variation suggest a discrete change in bulk composition and though not detectable megascopically the change might be considered evidence of heterogeneity within the pyroxenite.

The Ca-variation appears sympathetic to Fe-variation in the pyroxenite up to the lithological boundary in the Climax zone and again in and near the Chinaman orebody. In most other places Ca content varies sympathetically with Mg.

An illustration of elemental variation in clinopyroxenes, Fig. 33, is included although paucity of data makes interpretation difficult. As in the case of orthopyroxenes Fe tends to be high when Mg is low and

QUADRILATERAL PLOT OF
PYROXENE COMPOSITIONS
3050 CROSS-CUT

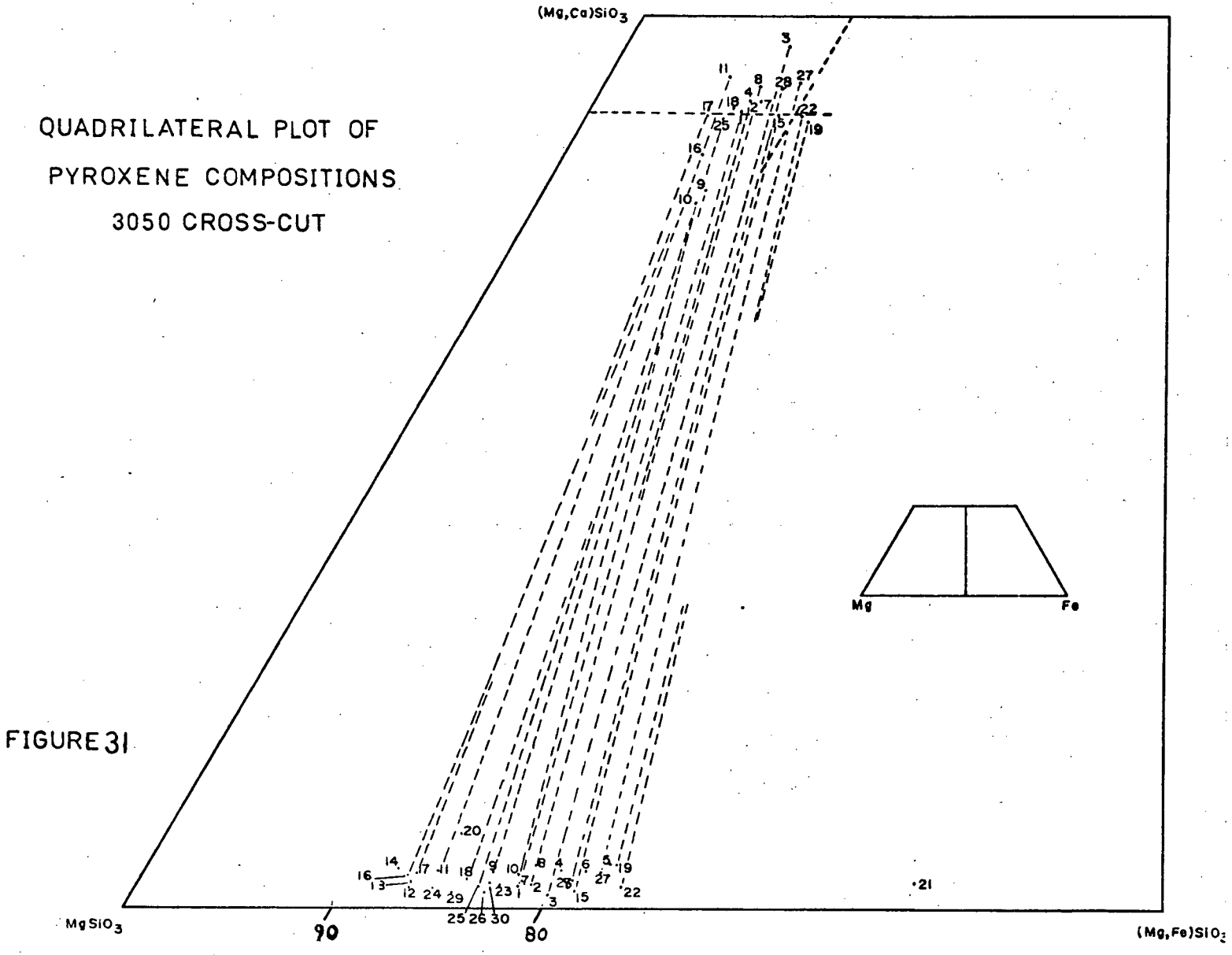

FIGURE 31

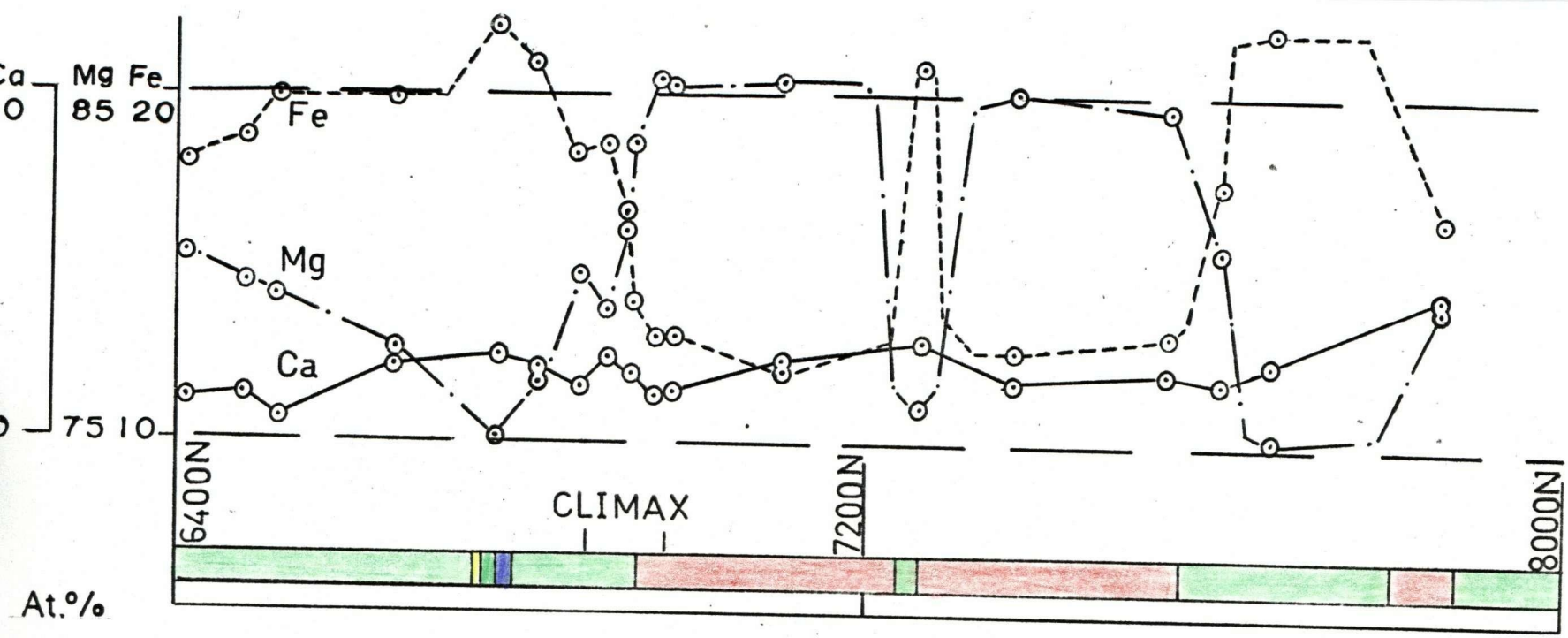

FIGURE 32

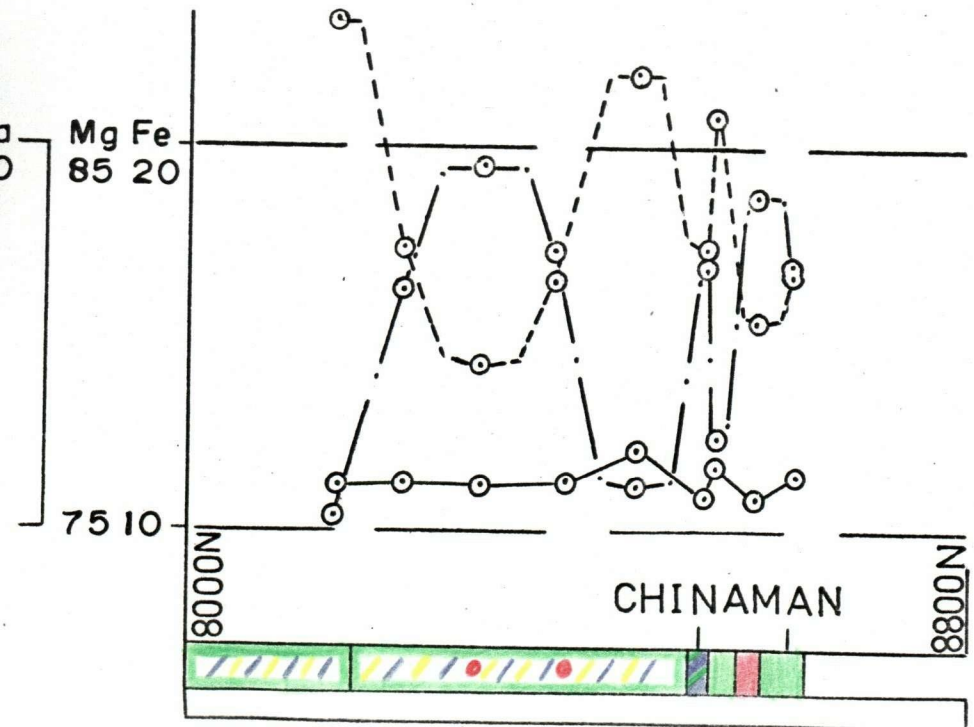

ELEMENTAL VARIATION IN
ORTHOPYROXENE
3050 CROSS-CUT

Mg —·—
Fe - - - - - - -
Ca ———

100'

PDT.
PXNITE.
HBLITE.
NORITE

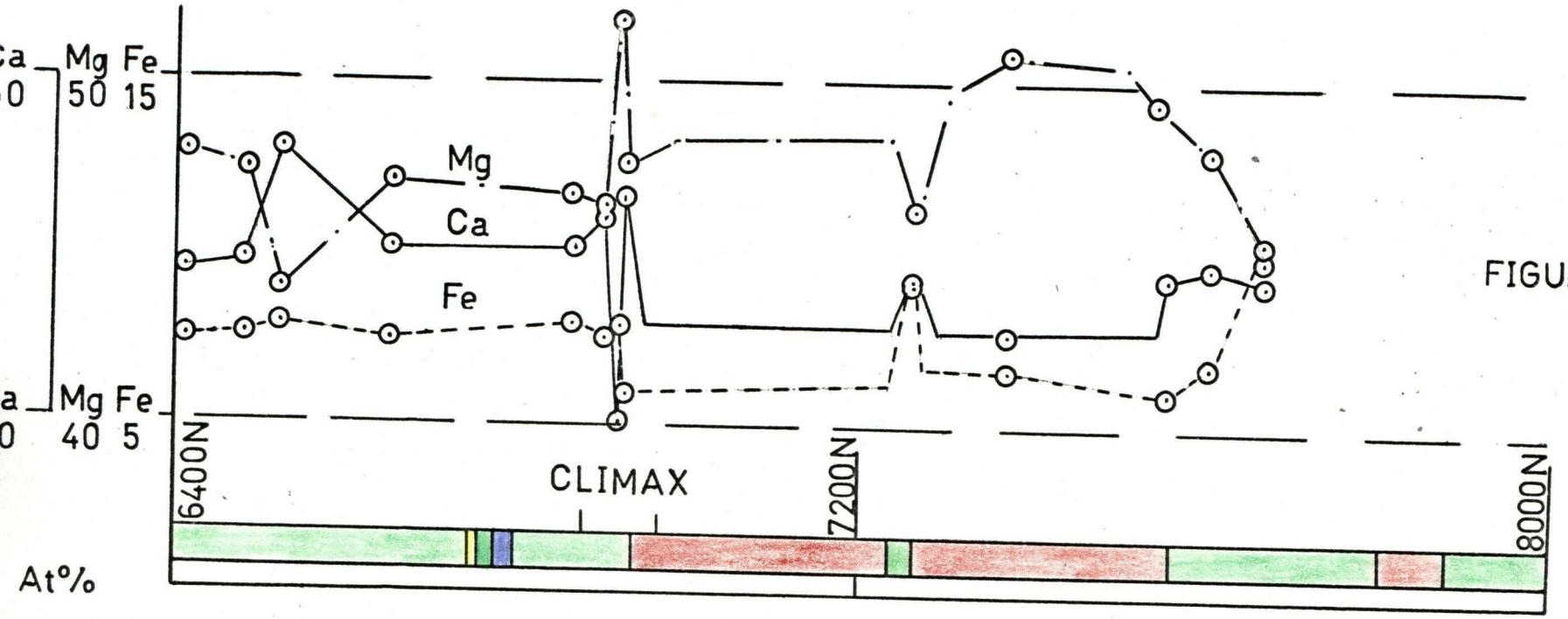

FIGURE 33

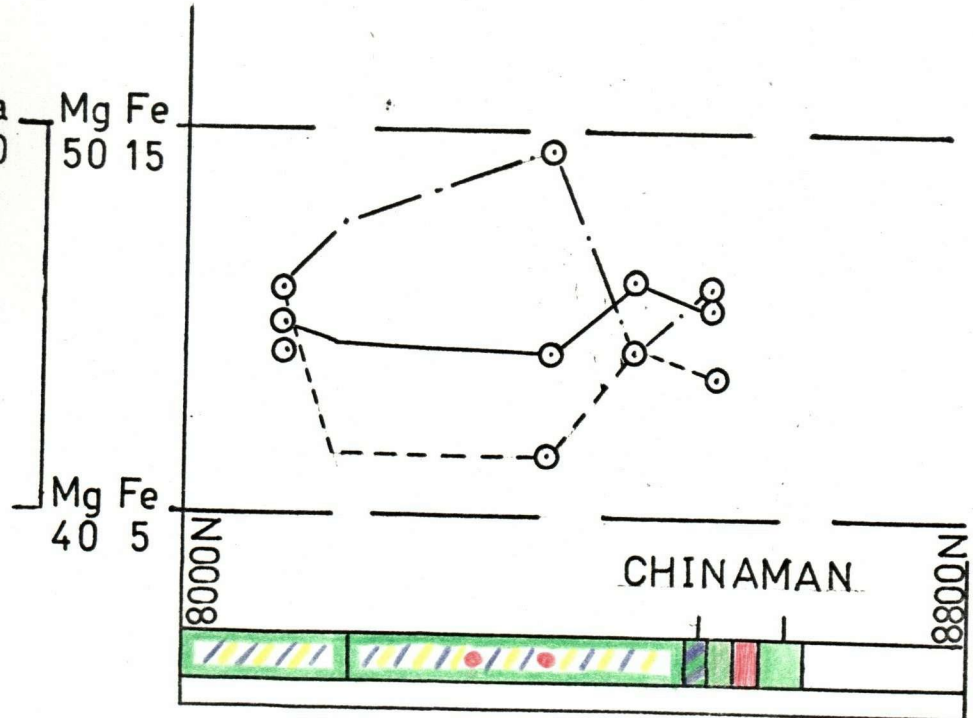

ELEMENTAL VARIATION IN
CLINOPYROXENE
3050 CROSS-CUT

Mg —·—

Fe - - - - - -

Ca ———

100'

PDT.

PX NITE.

HBLITE.

NORITE

vice-versa, and this relationship is dependant upon lithology. Ca generally shows clear inverse relationships with Mg and is sympathetic to Fe change except in the Climax ore zone.

Olivine, which is not plotted, may be compositionally related to a rock type. In the Climax orebody olivine in the footwall pyroxenite is lower in magnesium, Fo_{84}, than that in the hanging wall peridotite, Fo_{86}. This may be more apparent than real due to the uncertainty in analytical error.

Sulfide Analytical Techniques

Chemical analyses of sulfide minerals was made with a Joel electron microprobe at the Department of Metallurgy, U.B.C. This probe uses a 20^{o} take-off angle and was run at 25 Kev. and 0.8 milliamps. Standardization using pure metal standards is done manually and output is in digital form as relative intensities of sample to standard. The unrefined data is then prepared for computer corrections using the "MAJIC II" program and run on the U.B.C., IBM 370 computer. This program corrects for background, dead time loss, absorption effects, fluorescence effects and ionization penetration losses. It is believed that the results are quantitatively accurate to ±4% of the element present.

Twenty-nine samples were prepared and analyzed, yielding 29 pentlandite and 28 pyrrhotite compositions. These minerals were analyzed for Fe, Ni, Cu, Co, and S by difference. A complete tabulation of these analyses in weight percent and atomic percent is shown in Appendix 5.

Sulfide Analyses

Fig. 34, is a part of the Fe - Ni - S equilateral triangle which shows the chemical nature of the pentlandites and coexisting pyrrhotites.

FIGURE 34

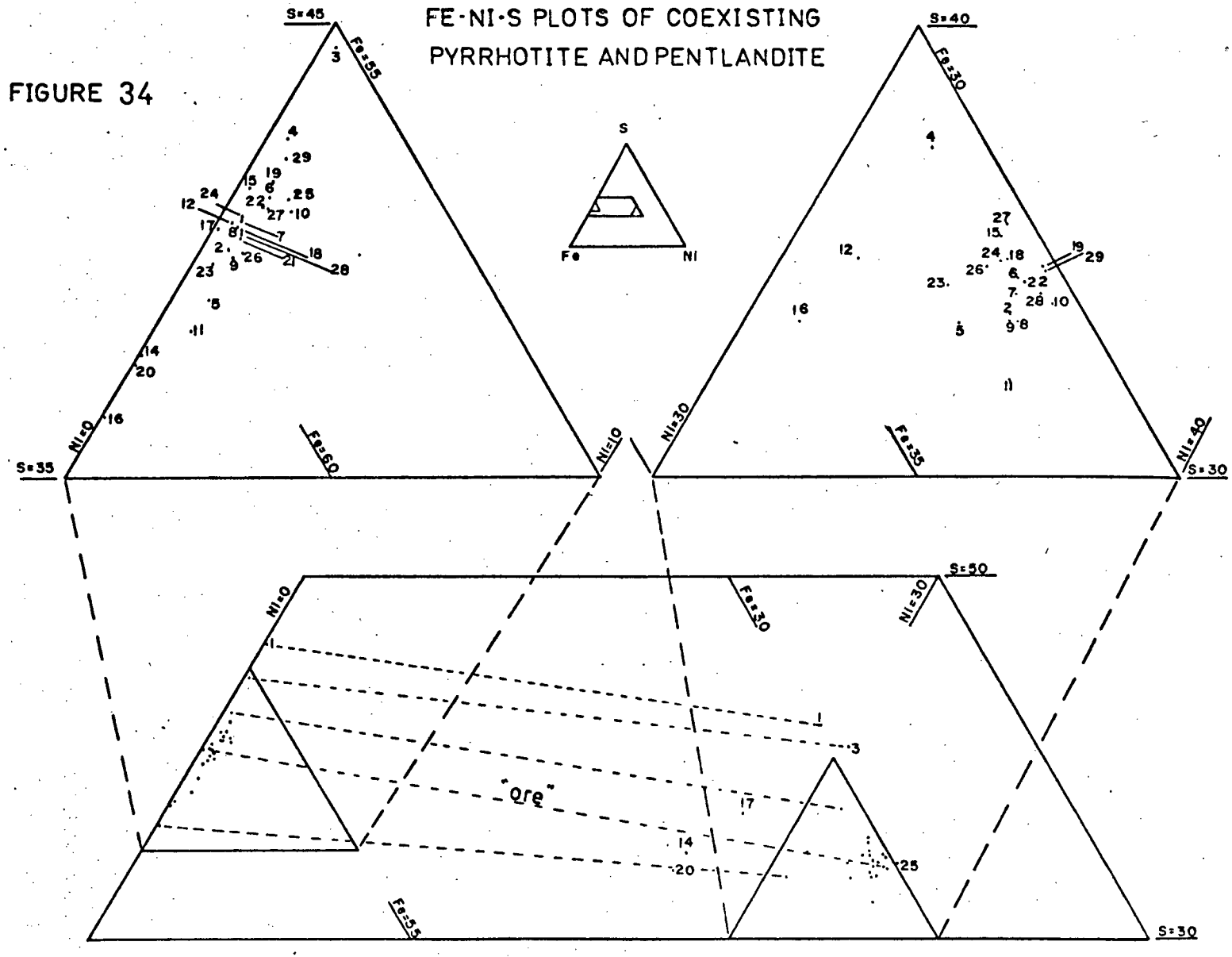
FE-NI-S PLOTS OF COEXISTING
PYRRHOTITE AND PENTLANDITE
S
Fe
Ni
S=45
Fe=55
Ni=0
S=35
Fe=60
Ni=10
S=40
Fe=30
Ni=30
Fe=35
Ni=40
S=30
S=50
Ni=0
Fe=30
Ni=30
"ore"
Fe=55
S=30

Pentlandite exhibits a wide variety of compositions with $Ni_{25.5}$ to $Ni_{35.8}$, $Fe_{29.0}$ to $Fe_{40.7}$ and $S_{32.1}$ to $S_{41.9}$ weight percent. A typical pentlandite, #7, yields a composition of $Fe_{30.17}$, $Ni_{33.91}$, $Co_{1.86}$, $S_{34.04}$. Pyrrhotite ranges from $Fe_{53.5}$, $S_{46.5}$ to $Fe_{63.7}$, $S_{36.3}$ and may contain Ni up to 1.26 weight percent. A typical pyrrhotite, #7, yields a composition of $Fe_{58.90}$ $Ni_{.37}$ $S_{40.73}$.

Tie-lines between the two minerals are generally parallel from the most sulfur-rich to sulfur-poor pair. This probably lends credence to the accuracy of analysis and equilibration between the mineral pair. The shifts in the tie-lines indicate a changing bulk composition of the sulfides and seem to be related to the petrology of the rock units from which the minerals are derived.

Illustrated in Fig. 35, is an elemental variation plot of pentlandite along the 3050 cross-cut. A pattern of parallel Fe - Ni variations is present in the pyroxenite south of the Climax orebody and a general increase in the Fe - Ni value is present as the ore zone is approached. Co content is high and irregular and then drops dramatically near and in the orebody. Within the Climax zone Ni values are extremely high and Co is consistently below 0.50 atomic percent. The hanging wall peridotite yields a pentlandite with Fe very high and Ni very low. The overall result appears to be one of Fe-rich, Ni-poor pentlandite in peridotite except in ore zones, and high Ni-Fe pentlandites in pyroxenites. Co values also appear higher in the pentlandites from pyroxenites than those from peridotites. The Chinaman zone pentlandites behave similarly to those in the Climax orebody. These pentlandites of high Ni content, sympathetic Fe values and low Co content seem to be distinctly characteristic of ore zones.

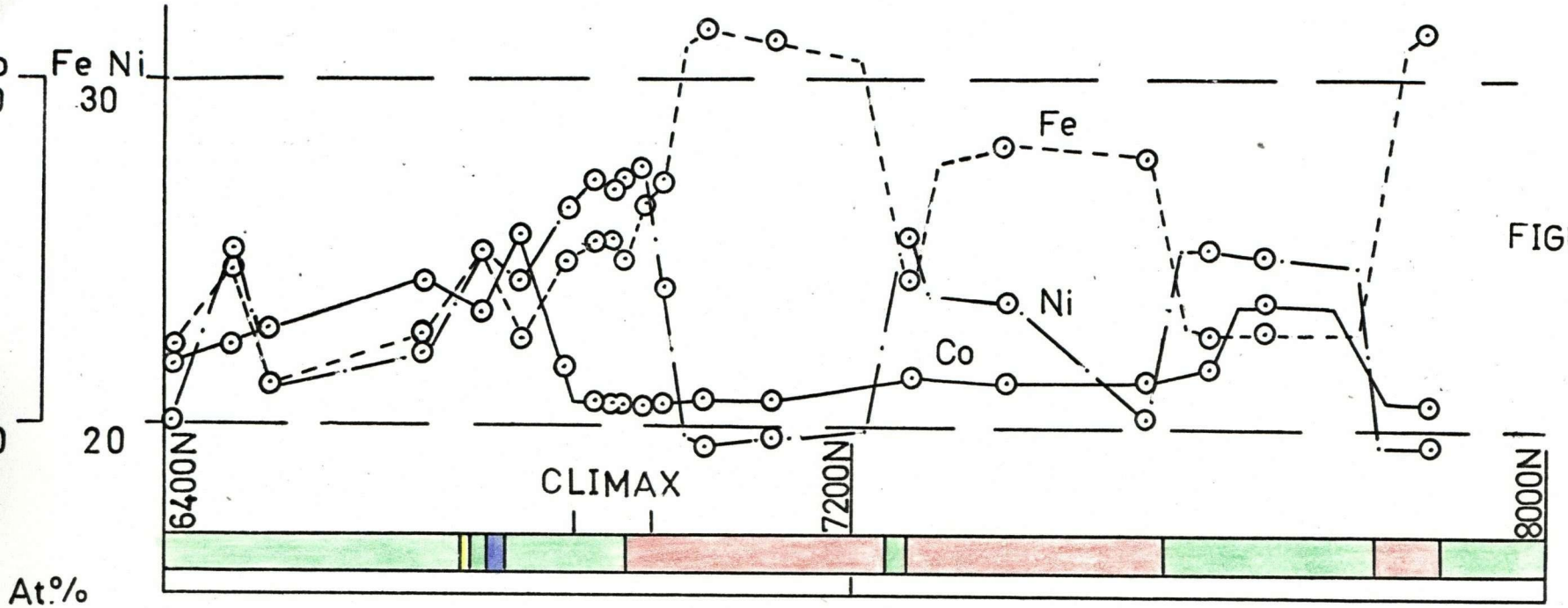

FIGURE 35

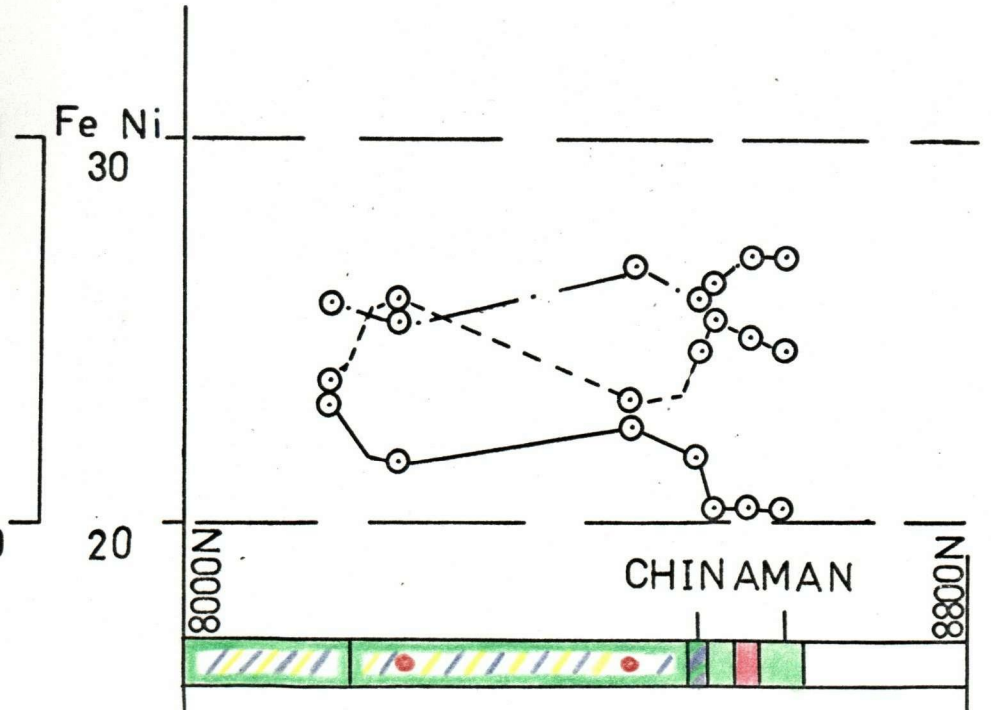

ELEMENTAL VARIATION IN
PENTLANDITE
3050 CROSS-CUT

Ni —·—
Fe - - - - - -
Co ———

100'

PDT.
PXNITE.
HBLITE.
NORITE

Pyrrhotite analyses have not been plotted as they appear to have a random and narrow Fe spread along the cross-cut. Further, their Ni content is generally low and large correction factors suggest questionable results. Three pyrrhotites with the greatest amount of Fe correspond to pentlandites that are Fe-rich. Within the two orebodies the pyrrhotite exhibits similar Fe contents with little fluctuation.

Elemental variations in two silicate minerals and one sulfide mineral along the 3050 cross-cut clearly vary with the different lithological units encountered and the orebodies. The marked variation in mineralogy between rock units limits the possible mechanisms of formation for the ultrabasic complex. These will be discussed in a later section.

THERMAL HISTORY OF THE ULTRABASIC COMPLEX

Introduction

Kretz, (1961), demonstrated that the distribution coefficient (K_D) relating Mg and Fe^{2+} distribution between coexisting Ca-rich and Ca-poor pyroxenes differs between magmatic (K_D = 0.73) and metamorphic (K_D = 0.57) assemblages. The distribution coefficient is dependant upon temperature, pressure and solid solution constituents other than Mg and Fe^{2+}. Atkins, (1969), however shows low K_D values from co-existing pyroxene pairs collected near the base of the Bushveld Complex (0.64 to 0.70). See Fig. 36. These low values are attributed mainly to the greater hydrostatic pressure under which these pyroxenes were formed. In this study the chemical nature of the pyroxenes resembles closely those from similar studies on the Skaergaard (Brown, 1957), the Stillwater (Hess, 1960), and the Bushveld (Atkins, 1969).

Wood and Banno, (1973), using an empirical approach, derived an expression for calculating equilibration temperatures of 2-pyroxene assemblages. Their method gives temperatures for almost all experimental data for multicomponent systems to within $\pm 60^{\circ}$ C of the observed temperatures. They stress that this empirical approach may lead to considerable error outside of the temperature-composition range covered by the experiments used in its derivations. As the temperature of formation and composition of the pyroxenes from Giant Mascot are believed compatible with those used in Wood and Banno's study, the use of their expression may be justified.

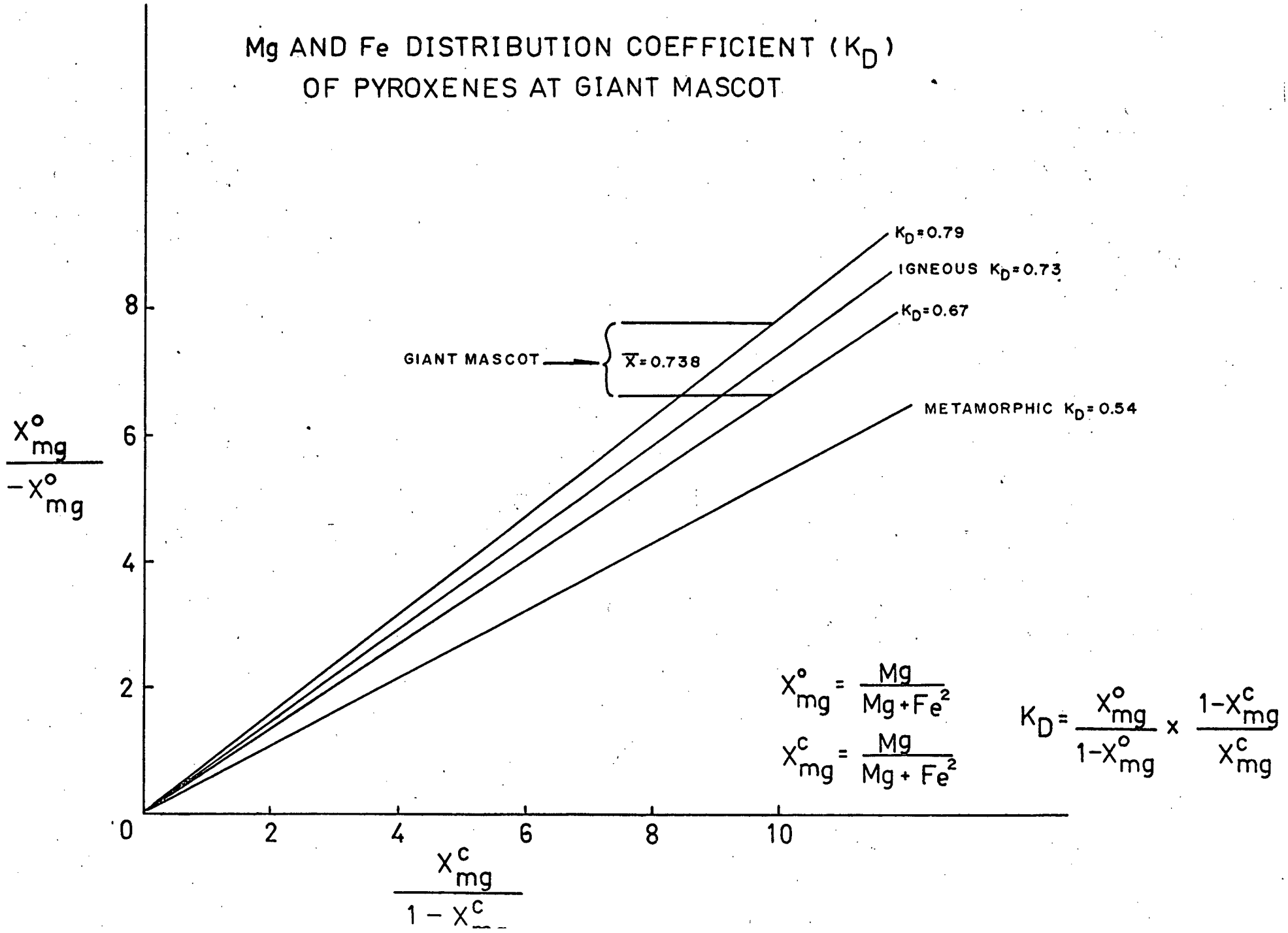
Mg AND Fe DISTRIBUTION COEFFICIENT (K_D)
OF PYROXENES AT GIANT MASCOT
K_D=0.79
IGNEOUS K_D=0.73
K_D=0.67
GIANT MASCOT
$\bar{X}$=0.738
METAMORPHIC K_D=0.54
$\frac{X^o_{mg}}{-X^o_{mg}}$
$\frac{X^c_{mg}}{1-X^c_{mg}}$
0
2
4
6
8
10
$X^o_{mg} = \frac{Mg}{Mg+Fe^2}$
$X^c_{mg} = \frac{Mg}{Mg+Fe^2}$
$K_D = \frac{X^o_{mg}}{1-X^o_{mg}} \times \frac{1-X^c_{mg}}{X^c_{mg}}$

Methods

The K_D values were determined using the following equation, (Kretz 1961, 1963):

$$K_D = \frac{X^o_{mg}}{1-X^o_{mg}} \cdot \frac{1-X^c_{mg}}{X^c_{mg}}$$

where $X^o_{mg} = \frac{Mg}{Mg + Fe^{2+}}$ in orthopyroxene.

and $X^c_{mg} = \frac{Mg}{Mg + Fe^{2+}}$ in clinopyroxene.

The expression for T(in ^oK), Wood and Banno 1973:

$$T = \frac{-10202}{\ln\left(\frac{a^{cpx}_{Mg_2Si_2O_6}}{a^{opx}_{Mg_2Si_2O_6}}\right) - 7.65X^{opx}_{mg} + 3.88(X^{opx}_{mg})^2 - 4.6}$$

where $a^{cpx}_{Mg_2Si_2O_6}$ is the activity of enstatite component in clinopyroxene.

and $a^{opx}_{Mg_2Si_2O_6}$ is the activity of enstatite component in orthopyroxene.

and $X^{opx}_{mg} = \frac{Fe^{2+}}{Fe^{2+} + Mg}$ in orthopyroxene.

The activity $a_{Mg_2Si_2O_6} = X_{Mg}^{M1} \times X_{Mg}^{M2}$, assumes the large ions present in the orthopyroxene and clinopyroxene structures occupy M2 sites while the smaller octahedrally coordinated ions occupy M1. The ions have been assigned to the two sites as follows;

M2	M1
Ca^{2+}	Al^{3+}
Na^{+}	Cr^{3+}
Mn^{2+}	Ti^{4+}
	Fe^{3+}

If the occupancies of the two sites by these ions are subtracted, the M2 and M1 sites that remain are filled by Mg^{2+} and Fe^{2+} ions in a random distribution. Thus $a_{Mg_2Si_2O_6}$ becomes;

$$\frac{Mg}{Mg+Fe^{2+}} \cdot (1-(Ca^{2+} + Na^{+} + Mn^{2+}))_{M2} \times \frac{Mg}{Mg+Fe^{2+}} \cdot (1-(Al^{3+} + Cr^{3+} + Ti^{4+} + Fe^{3+}))_{M1}$$

For the purposes of this study all Fe was considered Fe^{2+} following Wood and Banno, (1973). Also Mn^{2+} was not analyzed for in most pyroxenes but is considered to have an insignificant effect on the calculated temperature.

Giant Mascot Distribution Coefficients

Seventeen pairs of Ca-rich and Ca-poor coexisting pyroxenes were analyzed by electron microprobe. The resulting distribution coefficients (K_D) are listed in the right hand column of table 3. The

TEMPERATURE DATA OF COEXISTING PYROXENE PAIRS AND K_D VALUES.

TABLE 3.

Sample No.	X_{Fe}^{opx}	a_{En}^{cpx}	a_{En}^{opx}	$T^{\circ}c$	K_D
1 = 26A	.186	.091	.598	1035	.788
2 = 28A-2	.190	.064	.600	975	.695
3 = 32A-1	.202	.025	.608	835*	.714
4 = 34A-1	.205	.096	.561	1035	.620*
5 = 36A-3					
6 = 41A-1					
7 = 43A-1	.187	.063	.615	970	.743
8 = 44A-1	.190	.058	.600	960	.670
9 = 46A-1	.170	.156	.630	1140*	.749
11 = 47A-1	.144	.053	.676	970	.720
12 = 90A-1					
13 = 92A-1					
14 = 85A					
15 = 82A-1	.214	.062	.587	950	.739
16 = 78A-1	.130	.106	.711	1090	.870*
17 =104A	.133	.088	.624	1005	.769
18 =106A	.159	.074	.668	1010	.755
19 =108A	.230	.074	.544	975	.781
20 -114A					
21 =121A					
22 =130A	.236	.076	.560	970	.780
23 =132A					
24 =134A-2					
25 =136A	.166	.082	.656	1020	.685
26 =140A					
27 =152A-1	.224	.053	.559	925	.703
28 =156A-1	.211	.048	.587	915	.781
29 =160A-2					
30 =162A-1					

*anomolous

values range from 0.62 to 0.87 with a mean of 0.739. If the high and low values are discarded the range is more reasonable, (0.67 to 0.79), with a mean of 0.738. The high and low K_D values are from Fe-poor and Fe-rich pyroxene pairs respectively and they are anomalous with regard to the remaining 15 pairs.

The value of K_D obtained from this work suggests that the pyroxenes are magmatic. Although this value is greater than those of the Bushveld it is reasonable to assume that the high pressure of formation of Bushveld pyroxenes (~20km.) would result in a reduced K_D, (Atkins, 1969). The value obtained is more like that of the Skaergaard (~2km.) although that body appears to have formed at a higher temperature.

Pyroxene Geothermometry

Of the 17 pairs of pyroxenes analyzed, 15 yield remarkably similar temperatures. Disregarding the high and low values, representing pyroxenes extremely Ca-poor and Ca-rich respectively, the range of temperatures calculated for the Giant Mascot Ultramafite is 915° C to 1090° C. The mean of the 15 temperatures is 990° C. The error according to Wood and Banno should be no greater than ±60° C. All temperatures and pertinent data used in the calculations are listed in table 3. McTaggart, (pers. comm.), using the same methods calculated a temperature for a noritic rock at the mine and obtained a temperature of equilibration of 850° C.

The application of the Wood and Banno, (1973), expression for the temperatures of equilibration of clino- and orthopyroxenes yields

results that are remarkably consistent with other igneous assemblages (Bushveld, Skaergaard).

There seems to be no correlation between the temperatures of equilibration (formation) and K_D values. The bulk composition of the rock undoubtably has an effect on the K_D and T values but no correlation between a particular lithologic unit and a set of temperatures of K_D is readily seen. Those temperatures calculated from olivine-bearing rocks are slightly higher overall than those from pyroxenites but a high temperature from a pyroxenite provides the exception to the rule.

RADIOMETRIC AGES

Hornblende, and where possible a biotite concentrate was obtained from the rock to be analyzed. In one case the hornblende occurred as poikilitic grains enclosing orthopyroxenes and no attempt was made to separate them. The concentrates were subsequently sent to the Department of Geophysics at U.B.C. to be dated by the K-Ar method.

Ultrabasic Rocks

Four samples for radiometric dating were collected along the 3050 cross-cut (Fig. 37). They represent four different rock types, all rich in hornblende.

Sample 157A-1 was taken to represent the mineralized hornblendite of the Chinaman orebody. It consists of coarse 1 to 2 cm. prismatic hornblende with interstitial and massive mixtures of pyrrhotite, pentlandite and chalcopyrite. The hornblende is fresh megascopically but in thin-section some chlorite alteration is seen. The iron-nickel sulfides are penecontemporaneous with hornblende, but chalcopyrite appears to be locally later as it fills or reheals fractures in hornblende crystals.

The apparent age of crystallization of the hornblende yields an age of 108 ± 4 m.y. This age is also the minimum age of the main ore minerals although some chalcopyrite is younger than hornblende.

Sample 141A was collected approximately 100 feet east of the Chinaman orebody and is a coarse-grained feldspathic hornblendite. In hand-specimen it appears as a fresh, almost pegmatitic reaction rock

FIGURE 37

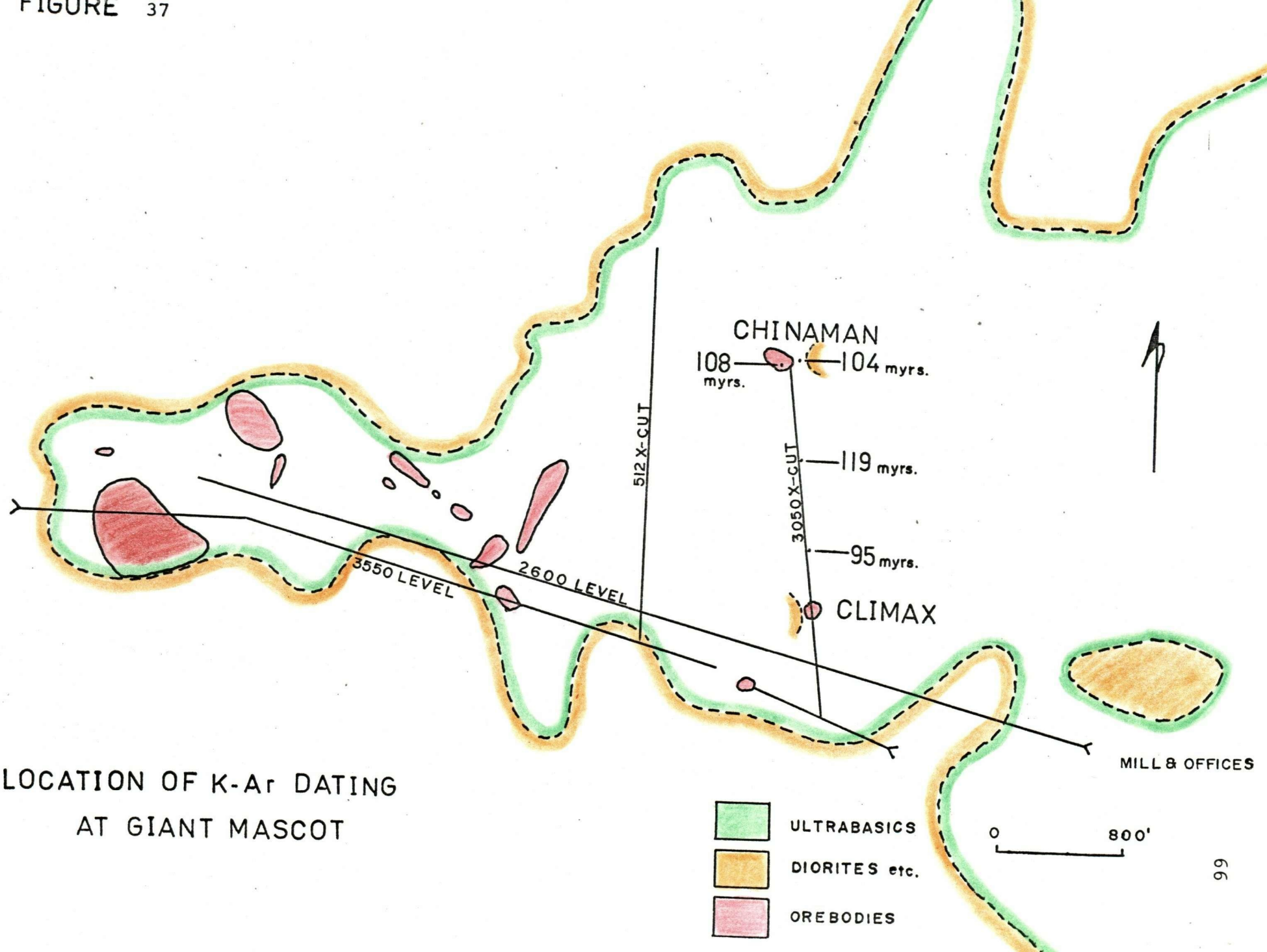

LOCATION OF K-Ar DATING
AT GIANT MASCOT

between the ultrabasics and a norite. Coarse 1 to 2 cm. hornblende crystals contain interstitial plagioclase. Minor chlorite and calcite are also seen in thin-section as alteration minerals and some quartz is present in the plagioclase-rich groundmass.

The apparent age of the hornblende crystallization is 104 ± 4 m.y. This date suggests a minimum age for the ultrabasic rocks and the enclosed norite body as the date obtained is that of the reaction margin of the two rock units.

Sample 120A is typical of a large volume of host rock within the complex. It is a hornblendic pyroxenite with large poikilitic hornblende crystals to 1 cm. containing orthopyroxenes from 0.2 to 2.0 mm. The groundmass is a mixture of tightly interlocking ortho- and clinopyroxenes. Radiometric dating was done on the whole rock.

The apparent age of the hornblendic pyroxenite was determined as 119 ± 4 m.y. This whole rock age may be somewhat high because of a dilution effect caused by the very low radiogenic nature of pyroxene. In any event, the available K-Ar dating places the minimum age of the ultrabasics between 104 ± 4 to 119 ± 4 m.y.

Sample 79A-2, was selected from a hornblendite dyke, as it represents the youngest rock unit seen in underground mapping. It is a fine-grained, 0.1 to 1.0 mm., monomineralic rock of oriented prisms of fresh hornblende. These fine-grained hornblende or feldspathic hornblende dykes cut all other rocks and contacts are knife-edge sharp. Most of these dykes or veins are 2 to 4 inches wide and follow a random, sinuous course. The apparent K-Ar age is 95 ± 4 m.y.

Granitoid Rocks

Several samples from the surrounding plutonic rocks were collected and three were selected for age dating. Their locations are shown in Fig. 38, along with some earlier age determinations.

Sample #7 was collected 0.1 miles west from the contact between high grade schists and plutonic rocks on the road to the mine. This sample (T. Richards, pers. comm.) probably represents the tonalite phase of the Spuzzum Pluton and is a foliated medium-grained fresh felsic rock. It consists of andesine, quartz, hornblende, biotite and minor chlorite. Both a biotite and hornblende K-Ar date was obtained at 79.4 ± 2.5 and 85.1 ± 2.8 m.y. respectively.

Sample #4 is a diorite that corresponds to Richards (1971) phase II diorite having hypersthene, clinopyroxene, hornblende and plagioclase as major constituents. This sample was collected within a few hundred feet of the ultrabasic complex. The location is about 400 feet along the lower haulage road, at the intersection of the road and a small tributary to Texas Creek. A hornblende-pyroxene concentrate of this sample gives a K-Ar date of 89.6 ± 3.1 m.y.

Sample #8 is a phase II diorite (Richards, 1971) collected several miles to the south of the mine. The sample location is 1.8 miles west of Haig junction on the north side of the Fraser River in a road cut on the main highway. This hornblende concentrate yielded a K-Ar date of 89.5 ± 2.8 m.y.

LOCATION OF K-Ar DATING OF SPUZZUM PLUTONIC ROCKS

FIGURE 38

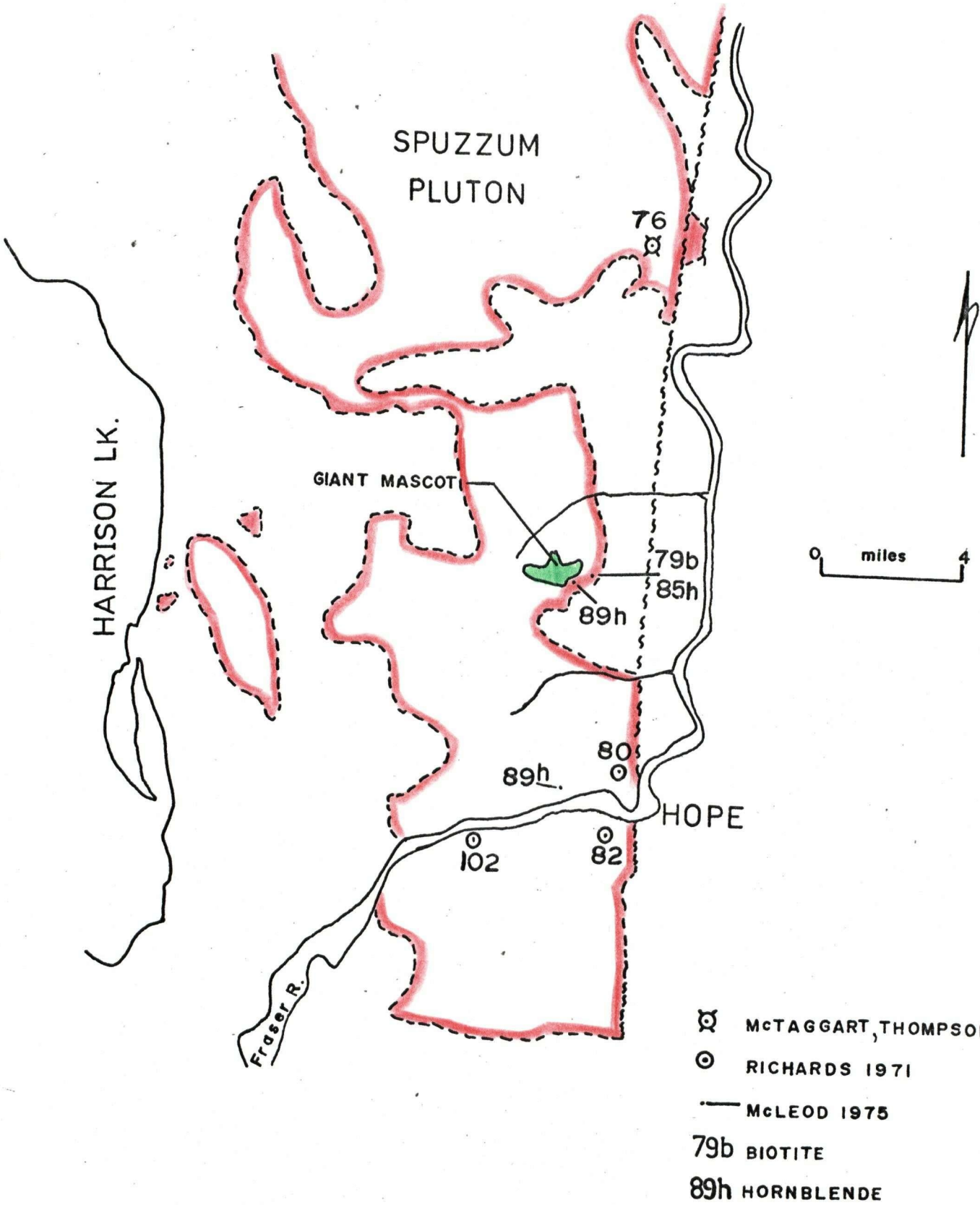

Discussion and Interpretation

Only one sample provided both a biotite and hornblende K-Ar date. In this case the hornblende gives an older date by nearly 6 m.y. It should be expected that hornblende would yield an older age as the mineral tends to "freeze in" radiogenic argon at a higher temperature than does biotite. This retention is due to a more compact crystal structure. However, the age spread appears too great for this to be the only reason and it is possible that unusually slow cooling of the initial magma would account for the difference.

Because of low potassium content in ultramafic samples, see table 4, they were reanalyzed and sample 157A-1 was dated twice. No significant differences were found.

Contamination of samples by the presence of pyroxene and chlorite though undesirable, is believed to have little or no effect on the resultant age, (R.L. Armstrong, pers. comm.).

The age of crystallization of the ultramafites, or at least the time when rocks ceased to lose radiogenic argon, ranges between 104 and 119 m.y. Late hornblendite dykes that cut the ultramafite are dated at 95 m.y. The enclosed norites or noritic phase must be at least 104 m.y. old. The Chinaman orebody in particular would seem to have a minimum age of 108 m.y., this would probably represent the age of all orebodies in the complex.

The surrounding plutonic rocks yield K-Ar ages that are concordant ages with Spuzzum intrusions (Richards, 1971). Tonalitic rocks, as suggested by Richards, are the younger at 79.4 to 85.1 m.y. Dioritic rocks near the ultramafite, similar petrologically to those several miles to the south and classified as phase II diorites by Richards (1971)

yield ages at both locations of 89.6 m.y. These dates agree fairly well with those of the type locality of Spuzzum plutonism (McTaggart and Thompson, 1967) northwest of Stout, British Columbia, a tonalitic rock dated at 76 m.y. The dating of the plutonic rocks alone suggest that the Giant Mascot Ultramafite is older than the Spuzzum Intrusions.

Comparison of K-Ar dates from ultramafites and surrounding Spuzzum diorites does not completely settle the problem of the relative ages of these two rock types because there are several varieties of diorite and not all of these have been sampled or dated. It is apparent, however that the ultramafite is at least as old and possibly older than certain diorites that do appear to belong to the Spuzzum Intrusions.

TABLE 4 . K/Ar samples and analytical results for ultrabasic and plutonic rocks at the Giant Mascot Property, near Hope, B.C.

Spec. No.	Min.	Rock	%K	Ar^{40*}/Ar^{40}	$Ar^{40*}_3:10^{-5}$ $Cm^3(stp)/g$	Age myr
79A-2	Hbl.	Hblite	0.183	0.64	0.07043	95±4
120A	Whole Rock	Hbl. pyrox.	0.130	0.43	0.06357	119±4
141A	Hbl.	Feld. Hblite	0.258	0.64	0.1093	104±4
157A-1	Hbl.	Min. Hblite	0.258	0.61	0.1154	108±4
4	Hbl. - pxn.	Dio.	0.334	0.43	0.1214	89.6±3.1
7a	Bio.	Q.D.	5.860	0.836	1.881	79.4±2.5
7b	Hbl.	Q.D.	0.464	0.580	0.160	85.1±2.8
8	Hbl.	Dio.	.536	0.580	0.1945	89.5±2.8

Constants used in age calculations:

$\lambda_e = 0.585 \times 10^{-10} yr^{-1}$

$\lambda_\beta = 4.72 \times 10^{-10} yr^{-1}$

$K^{40}/K = 1.19 \times 10^{-4}$

ORIGIN OF THE ULTRAMAFITE AND ITS ORES

Ruckmick and Noble (1959), Taylor (1967), and McTaggart (1971), classified the Giant Mascot Ultramafite as belonging to the Alaskan zoned type. Irvine, (1967) disqualified it on the grounds that it contains orthopyroxenes. Findlay (1969) disqualified it on this basis and suggested that it was "a variant of the 'normal' Cordilleran alpine-type intrusion". Naldrett (1973) is unable to classify it at all in his otherwise detailed classification system.

Early investigators of the Giant Mascot Ultramafite proposed diverse origins for the complex. Cairnes (1924) concluded that the ultrabasic rocks with their related ore minerals were magmatic in origin and cut the surrounding diorites. Cockfield and Walker (1933) believed that the ultrabasic rocks were intruded by surrounding diorite and that the ore was hydrothermal in origin. Horwood (1936, 1937) believed hornblendite to be the principal rock type, that the sulfide ore and pyroxenite had segregated from the hornblendite and that these were injected into their present position followed by related diorite intrusions.

McTaggart (1971) favors a metasomatic origin for zoned ultramafites and proposed that diorite and gabbros might be younger than the ultramafite. Muir, (1971) concluded that the Giant Mascot Ultramafite formed from a initial mass of hornblende pyroxenite which intruded along a diorite-metamorphic rock contact. Subsequently he suggested a number of plug-like olivine and sulfide bodies were intruded along the diorite-hornblende pyroxenite contact.

Aho (1956) whose work at Giant Mascot is the most detailed to date, offered two hypothesis of origin, magmatic and metasomatic. The magmatic

hypothesis invoked fractional crystallization of a basic parent magma followed by gravitative differentiation and final injection as a crystal mush into the surrounding diorites thus accounting for his massive orebodies. The metasomatic hypothesis was proposed to account for the origin of the zoned mineralized pipes by the addition or removal of SiO_2 and deposition of sulfides. He extended this hypothesis to the whole ultramafic mass and suggested that the large scale zoning from peridotite to pyroxenite and to hornblendite is caused by high temperature redistribution of silica, lime etc. in a pre-existing ultrabasic intrusion.

The origin of the ultramafic rocks and related sulfide mineralization is believed to be the result of a complex process. The orebodies and related rocks as described by Aho (1956), Muir (1971) and by the present author are similar in shape, mineral textures, mineral assemblages and relation of lithological units. On the other hand, the diverse origins and mechanisms of formation, as previously outlined, for the various orebodies and the related rocks seem incomplete or improbable to this author.

A geological map in Fig. 3, Aho (1956), shows the principal rock units in the area. The country rock is a diorite with inclusions of metamorphic rock. The ultramafite is a crudely zoned body with a hornblende reaction margin with hornblende pyroxenite grading inwards to pyroxenite and centers of peridotite. Inclusions within the ultramafite are high grade metamorphic schists and hornfelsed norite. Felsic inclusions and cross-cutting relationships at ultramafic-diorite contacts led Aho (1956) and Muir (1971) to postulate a younger age for the ultramafite. The possibility that these inclusions do not belong to the Spuzzum Intrusions is supported by the fact that they are usually norites as

opposed to Spuzzum diorites, they have a much better developed foliation and the plagioclase composition is usually much more clacic, basic bytownite as opposed to andesine-labradorite, characteristic of the Spuzzum. Also Aho (1956) states that ultramafic-diorite contacts show conflicting age relationships.

K-Ar age determinations support the idea that the ultramafite is older than the Spuzzum Diorite. This work and others yield ages of diorite crystallization from 80 to 89 m.y. with the oldest date obtained a few hundred feet from the south east corner of the ultramafite. The tonalite border phase of the Spuzzum appears younger and a hornblende-biotite pair dated at 85 and 79 m.y. respectively suggest a protracted cooling for the Spuzzum plutonism.

K-Ar dating of hornblendic rocks from within the ultramafite yield older ages of crystallization. From the center of the complex a hornblendic-pyroxenite yields a minimum age of crystallization of 119 m.y. and a coarse-grained hornblendite between an internal norite and ultramafic yields a date of 104 m.y. suggesting a minimum for both norite and ultramafite. Hornblende from the Chinaman orebody yields a minimum age of crystallization of 108 m.y. Young hornblendite dykes, observed to cut all ultramafic rock units, yield an age of 95 m.y., still older than Spuzzum rocks. It may be argued that the age difference is false and due to the capacity of ultramafic rocks for "freezing in" radiogenic components earlier than does diorite but this still places the ultramafite in a position of being at least as old as Spuzzum plutonism. More realistically, it can be argued that the ultramafic is the older rock mass and Spuzzum plutonism caused an uneven younging effect, resetting the radiogenic clock.

From the evidence obtained it is suggested that the ultramafite crystallization is a minimum of 15 m.y. older than the Spuzzum Intrusions and the actual age of the ultramafite may be considerably older. This sequence of events may well explain some of the secondary features seen by Aho in the study of the orebodies, the brecciation and protoclastic textures along the footwall of the 1900 and Chinaman ore zones and a crude metasomatic imprint (hornblendite margin) on the ultramafite itself.

Distribution coefficients for pyroxenes indicate origin by magmatic crystallization of Giant Mascot ultramafic rocks. Pyroxene geothermometry suggests equilibration with a minimum mean temperature of crystallization of 990°C. These considerations suggest that the Giant Mascot Ultramafite originated from a magmatic source and that Spuzzum Plutonism, intermediate in composition, did not effect K_D's or temperatures of pyroxene equilibration. Further, at temperatures of formation in the range of 1000°C a sulfide liquid could coexist with the ultramafic magma.

Chemical analyses of silicates and a sulfide mineral within the ultramafite show marked compositional variations from peridotites to pyroxenites. Pentlandites are different compositionally in each of the two rock units and are different again in ore zones. It seems certain that no theory of single magmatic injection or accumulation can explain these observations but that multiple injections of different compositions, possibly followed by separate ore injections, may.

Textures must be taken into account in working out a hypothesis of origin. Texturally the peridotites show olivine-pyroxene or olivine-hornblende textural types indistinguishable from heteradcumulates found in layered rocks from Rhum, Skaergaard etc. Pyroxenites appear adcumulate-like in texture although heteradcumulate-like textures are seen.

In particular, hornblende in pyroxenites forms clear heteradcumulate textures.

Microscopically olivines and pyroxenes appear somewhat deformed near contacts suggesting movement after some crystallization. This is also true of some sulfides, particularly chalcopyrite in the Chinaman orebody. Between the contact of peridotite and websterite at the Climax ore zone this deformation is noted along with variable amounts of olivine which appear to make a hybrid-type rock between the two end member rock units. It has been suggested by Muir (1971) that a similar occurrence in the 4600 orebody is the result of mixing of two crystal mushes to produce what he called a "hybrid zone".

Structurally, the ore zones appear related to lithological contacts mainly between peridotite and pyroxenite, forming steeply plunging pipe-like orebodies with the sulfides concentrated mainly on the footwall of the pipe. The ore zones are either massive sulfide concentrations between the two principal ultramafic phases or in a pipe-like body, zoned from hornblende rich rocks to peridotite in the cores with ore minerals concentrated along the footwall. The proximity of noritic phases within the ultramafite appear to have some influence, possibly structural, on the localization of ore.

The majority of the orebodies lie along a line near the south-west part of the complex with some exceptions, the Chinaman being more central to the ultramafite. The ore zones appear to terminate downwards at approximately the 2600 foot elevation. This termination may be influenced by the bottoming of the ultramafic rocks at 250 to 400 feet below this level as indicated by downhole drilling which encounters metamorphic and dioritic rocks. Some orebodies reach the surface; others weaken or

diminish, or are faulted off.

The author considers the following hypotheses for the origin of the Giant Mascot Ultramafite and its ores:

(1) Multiple injections of ultrabasic magmas, of differing compositions, to form a zoned complex of the Alaskan type (Ruckmick and Noble, 1959).

(2) The emplacement of an ultramafic body in a solid or magmatic state with subsequent metasomatic modification by Spuzzum Plutonism.

(3) Multiple injection of crystal mush and sulfide melts derived from a differentiating intrusion located at some greater depth.

(4) Diapiric re-emplacement of rudely stratiform sequences of cumulates and sulfides still in a "mushy" form and derived from a differenting subvolcanic intrusion (Irvine, 1974).

The first hypothesis would account for the origin of the ultramafite provided that more than one center of injection was operative at one time within the stock and that subsequently the Spuzzum intrusions disrupted and rearranged the zoning, and metasomatized the ultramafite. Also the size and age relationships of the ultramafite to the surrounding granitic terrane is remarkably similar to those of the Alaskan type.

It must be pointed out however, that the Giant Mascot Ultramafite differs in several important respects from the Alaskan type. These differences are: (1) the lack of graded layering in rhythmical beds as noted in some Alaskan Complexes; (2) the presence of several crudely zoned peridotite centers; (3) late hornblendite dykes cutting all rock

units at Giant Mascot; (4) the abundance of orthopyroxene; (5) the presence of plagioclase; (6) the restricted compositional range of olivine (Fo_{84}-Fo_{86}); (7) the restricted compositional range of clinopyroxene ($Di_{89}Hed_{11}$-Di_{79} Hed_{21}) compared to Alaskan clinopyroxene ($Di_{99}Hed_{1}$-$Di_{70}Hed_{30}$); and (8) the presence of abundant Ni and Cu sulfides at Giant Mascot. Some of these chemical differences may be the result of differing compositions of initial magmas or the much smaller size (and therefore less differentiated?) of the Giant Mascot body. Naldrett (1973) suggests the chemical differences may not be attributed to different mechanisms of formation but to the depths at which ultramafic magmas have originated. Furthermore, there are serious objections to the Ruckmick-Noble hypothesis. The younger, more ultrabasic magmas in Alaska are not seen to cut the older less ultrabasic rocks. Further, there remains the more general problem of producing a dunite or peridotite magma.

The second mechanism, involving metasomatism of a pre-existing ultramafite has some support in that alpine ultramafites to the northwest of Giant Mascot in the vicinity of The Old Settler mountain show increasing metamorphic grade where in contact with Spuzzum diorite. Pyroxenites are there developed with minor Ni-Cu showings and these resemble those at Giant Mascot. Trommsdorff and Evans, (1972), have described, in the Swiss Alps, serpentinites metamorphosed to pyroxene, amphibole and olivine. Thus, if an alpine ultramafite were engulfed by the Spuzzum magmas, conversion and metasomatism might occur and give rise to a zoned body with this mineral assemblage. Nickel mineralization could possibly result by redistribution and concentration during metamorphism of nickel originally held in silicates such as olivine and per-

haps released during serpentinization.

This mechanism is not acceptable for Giant Mascot because sulfide textures suggest a magmatic origin with precipitation from a liquid which would be at least at 1000°C. Temperatures of formation or equilibration of the ultramafite (2-pyroxene geothermometer) was apparently near 1000°C., much higher than would be reasonably expected in a sizeable inclusion heated by Spuzzum diorite magma. Furthermore, textures of the principal ultrabasic minerals are more magmatic-looking than metamorphic.

Although the general hypothesis seems untenable, it seems certain that the coarse-grained hornblendite margin is metasomatic, but the metamorphic effect extends not much further than 100 yards. In addition, during the emplacement of the Spuzzum, there were developed late hornblendite dykes which cut all rock units within the complex, and there was also some redistribution of ore minerals (which, incidentally, led Aho to postulate a hydrothermal origin for some orebodies).

The third hypothesis, injection of crystal mushes from a differentiating body (Bowen and Tuttle, 1949), appears to offer a plausible explanation for the genesis of the Giant Mascot Complex. Several injections of mushes ranging in composition from hornblendic pyroxenite, to pyroxenite, to peridotite in that order with the later, more magnesian, magmas emplaced along several centers would account for the crude zonation of the ultramafite on the whole and the zonation around some ore zones. The ore-forming sulfide melts would be, apparently, injected last or along with the peridotite mush which, on cooling, formed the host rock for the net-textured and massive sulfides.

This hypothesis although plausible is complex and incomplete. A simpler and more complete one, that of Irvine (1974), retains the idea

of crystal mushes derived from a differentiating body but offers an alternative method of emplacement.

A fourth hypothesis, making use of Irvine's mechanism (1974), involves diapiric re-emplacement of rudely stratiform sequences of "mushy" cumulates and sulfides, that have precipitated in a differentiating subvolcanic magma chamber in the order: sulfidic peridotite, pyroxenite to hornblende pyroxenite. These magmas may represent the earliest Spuzzum magmatism.

Diapirism could result from additions of magmas (Spuzzum?) from depth through feeders into the magma chamber, from upward force applied by the rising Spuzzum magmas or from tectonic compression. Although erosion has removed the postulated overlying volcanoes, to the east, the Spences Bridge (Lower Cretaceous) and the Kingsvale (late Lower Cretaceous) Groups ranging in composition from andesites to basalts (Rice, 1947) show that volcanism was widespread at this time.

This process of re-emplacement by diapirism might readily explain the crude zonation within the ultramafite (excluding the marginal hornblendite) and accounts very well for several features seen on the 3050 cross-cut such as:

(1) The sharp change in mineral composition both silicates and sulfide from one rock type to another.

(2) The hybrid pyroxenite on the footwall of the Climax orebody, possibly the consequence of mixing of two crystal mushes.

(3) The strained silicates in the Climax zone between pyroxenite and peridotite.

(4) The protoclastic zone on the footwall of the Chinaman orebody.

(5) The close spatial relationship of sulfides to peridotite and particularly net-textured peridotites in the ore zones.

(6) The heteradcumulate-like nature of the silicates.

With the metasomatic effects of subsequent Spuzzum magmas on the ultramafite, this mechanism appears to account reasonably well for the complex geological features observed at Giant Mascot.

Richards (1971) noted several small ultrabasic bodies in the Spuzzum, from hornblendite up to 5 feet long, to peridotite and pyroxenite lenses, about 6 inches in length. These are aligned with the foliation in the diorite or cut across foliation but are, nevertheless, irregularly elongated along foliation directions. Pyroxenite contains augite about 10% more Fe-rich and hypersthene 10-20% more Fe-rich than those at Giant Mascot. In addition these small bodies all contain quartz and andesine, and thus differ from ultramafites at Giant Mascot. Richards (1971) suggests that these bodies are formed by metasomatic replacement of the diorites along pre-existing fractures. An alternative is that these are strongly metamorphosed ultramafic xenoliths. Chemical comparisons between these small pyroxenite lenses and Spuzzum diorites strongly support the first hypothesis.

CONCLUSIONS

A brief summary of some of the more important findings made during the course of this study are given below:

(1) K-Ar dating indicates that the ultramafite (119 m.y.) is as old as or probably older than Spuzzum Plutonism (89 m.y.).

(2) Formation or equilibration of pyroxene pairs occurred at a mean minimum temperature of 990°C.

(3) Pyroxene pairs have a mean distribution coefficient of 0.738, indicative of magmatic formation.

(4) Pyroxene, and particularly orthopyroxene, is markedly different in adjacent pyroxenites and peridotites, with Mg-rich pyroxenes in peridotite.

(5) The composition of olivine appears to vary little but the most Mg-rich is found in the Climax hanging wall.

(6) Pentlandite is Fe- and Ni-rich with little Co in ore-bodies, is Co-rich and slightly Fe- and Ni-poor in pyroxenites and is Fe-rich and Ni-poor in peridotite.

(7) Mineral textures in the more magnesian rock units are similar to cumulate textures observed in layered complexes.

(8) Contacts between ultramafic rock units are usually sharp on a megascopic scale and gradational microscopically.

(9) The Climax and Chinaman orebodies are steeply plunging pipe-like bodies with the higher grade sections concentrated in the trough or footwall zone.

(10) The Climax orebody lies at a contact between pyroxenite and peridotite whereas the Chinaman appears to be crudely zoned around a peridotite core. Both are spatially related to a norite body.

In conclusion, the writer maintains that the genesis of the Giant Mascot Ultramafite involves a diapiric re-emplacement of rudely stratiform crystal mushes and sulfides from a differentiating sub-volcanic body, possibly an early phase of Spuzzum magma activity. Subsequently this material was engulfed by the rising Spuzzum dioritic magmas and a metasomatic hornblendite marginal zone was imposed on the ultramafite.

REFERENCES CITED

Aho, A.E. (1956) Geology and genesis of ultrabasic nickel - copper - pyrrhotite deposits at the Pacific Nickel Property, southwestern British Columbia. Econ. Geol. vol. 51, pp. 444-481.

Armstrong, R.L. (pers. comm.) Associate Professor, Dept. of Geological Sciences, Univ. of B.C.

Atkins, F.B. (1969) Pyroxenes of the Bushveld Intrusion, South Africa. Journ. of Pet., vol. 10, pp. 222-249.

Bowen, N.L., and Tuttle, O.F. (1949) The System $MgO-SiO_2-H_2O$. Geol. Soc. Amer., Bull. 60, pp. 439-460.

Brown, G.M. (1957) Pyroxenes from the early and middle stages of fractionation of the Skaergaard intrusion, East Greenland. Miner. Mag. 31, pp. 511-543.

Cairnes, C.E. (1924) Nickeliferous mineral deposit, Emory Creek, Yale Mining Division, British Columbia. Geol. Surv. Can., Summ. Rept., pp. 100-106.

_____ (1930) The serpentine belt of Coquihalla Region, Yale District, British Columbia. Geol. Surv. Can., Summ. Rept. for 1929, pp. 144-197.

Cockfield, W.E., and Walker, J.F. (1933) The nickel bearing rocks near Choate, British Columbia. Geol. Surv., Can. Summ. Rept., pp. 62-68.

Craig, J.R., and Kullerud, G. (1969) Phase relations in the Cu-Fe - Ni-S system and their application to magmatic ore deposits, in Magmatic Ore Deposits, Monograph 4, Econ. Geol., pp. 344-358.

Findlay, D.C. (1969) Origin of the Tulameen ultramafic gabbro complex, southern British Columbia. Can. J. Earth. Sci., vol. 6, pp. 399-426.

Hess, H.H. (1960) Stillwater igneous complex, Montana: a quantitative mineralogical study. Mem. geol. Soc. Am. 80.

Horwood, H.C. (1936) Geology and mineral deposits at the mine of B.C. Nickel Mines, Ltd., Yale District, British Columbia. Geol. Surv. Can., Memoir 190.

_____ (1937) Magmatic segregation and mineralization of the B.C. Nickel Mine, Choate, B.C. Trans. Royal Soc. Canada, sec 4, pp. 5-14.

Hutchison, W.W. (1970) Geological Survey paper Series, Age Determinations and Geological Studies. Geol. Surv. Can., Paper 71-2.

Irvine, T.N. (1967) The Duke Island Ultramatic Complex, southeastern Alaska. Ultramafic and related rocks (ed. P.J. Wyllie), pp. 84-96, New York John Wiley and Sons.

_____ (1974) Petrology of the Duke Island Ultramafic Complex Southeastern Alaska. Geol. Soc. Amer., Mem. 138.

Kretz, R. (1961) Some applications of thermodynamics to coexisting minerals of variable composition. J. Geol. 69, pp. 361-387.

_____ (1963) Distribution of magnesium and iron between orthopyroxene and calcic pyroxene in natural mineral assemblages. Ibid. 71, pp. 772-785.

Kullerud, G., Yund, R.A., and Moh, G.H. (1969) Phase relations in the Cu-Fe-S, Cu-Ni-S, and Fe-Ni-S systems, in Magmatic Ore Deposits, Monograph 4, Econ. Geol., pp. 323-343.

Mattinson, J.M. (1970) Uranium-Lead Geochronology of the Northern Cascades, Washington (abs.) Geol. Soc. Amer., Cordilleran Section, 66th Annual Meeting, pp. 116.

McTaggart, K.C., and Thompson, R.M. (1967) Geology of part of the northern Cascades in southern British Columbia. Can. J. Earth Sci., vol. 4, pp. 1191-1228.

McTaggart, K.C. (1970) Tectonic History of the Northern Cascade Mountains. Geol. Assoc. of Canada, special paper No. 6, pp. 137-148.

_____ (1971) On the origin of ultramafic rocks. Bull. Geol. Soc. Amer., vol. 82, pp. 23-42.

Monger, J.W.H. (1970) Hope map-area, west half, British Columbia. Geol. Surv. Can., Paper 69-47.

Muir , J.E. (1971) A study of the petrology and ore genesis of the Giant Nickel 4600 Orebody, Hope, B.C. Unpublished M.Sc. thesis, University of Toronto, Toronto, Canada.

Naldrett, A.J. (1973) Nickel sulfide deposits - Their classification and genesis, with special emphasis on deposits of volcanic association. Can. Inst. Mining Met., vol. 76, pp. 183-201.

Read, P.B. (1960) Geology of the Fraser Valley between Hope and Emory Creek, British Columbia. Unpublished M.A.Sc. thesis, University of British Columbia.

Rice, H.M.A. (1947) Geology and Mineral Deposits of the Princeton Map-Area, British Columbia. Geol. Surv. Can., Mem. 243.

Richards, T.A. (1971) Plutonic rocks between Hope, B.C. and the 49th parallel. Unpublished Ph.D. thesis, University of British Columbia.

Roddick, J.A. and Hutchison, W.W. (1969) Northwestern part of Hope Map-area, British Columbia. Geol. Surv. Can., Paper 69-1A, pp. 29-38.

Ruckmick, J.C., and Noble, J.A. (1959) Origin of the ultramafic complex at Union Bay, southeastern Alaska. Bull. Geol. Soc. Amer., 70, pp. 981-1018.

Streckeisen, A. (1967) Classification and Nomenclature of Igneous Rocks, (Final Report of an Inquiry). Neues Jahrbuch für Mineralogie, Abhandlungen 107, pp. 144-240., in Geotimes, October 1973.

Sutherland-Brown, A., et.al. (1971) Metallogeny the Canadian Cordillera. Can. Inst. Mining Met., vol. 74, pp. 121-145.

Taylor, H.P., Jr. (1967) The zoned ultramafic complexes of southeastern Alaska, in Ultramafic and related rocks (ed. P.J. Wyllie), New York, John Wiley and Sons.

Trommsdorff, V., and Evans, B.W. (1972) Progressive metamorphism of Antigorite schist in the Bergell Tonalite aureole (Italy). Am. Jour. Sci., vol. 272, pp. 423-437.

Wood, B.J., and Banno, S. (1973) Garnet-Orthopyroxene and Orthopyroxene - Clinopyroxene relationships in simple and complex systems. Contr. Mineral. Petrol., vol. 42, pp. 109-124.

Appendix 1

Sample Location Map

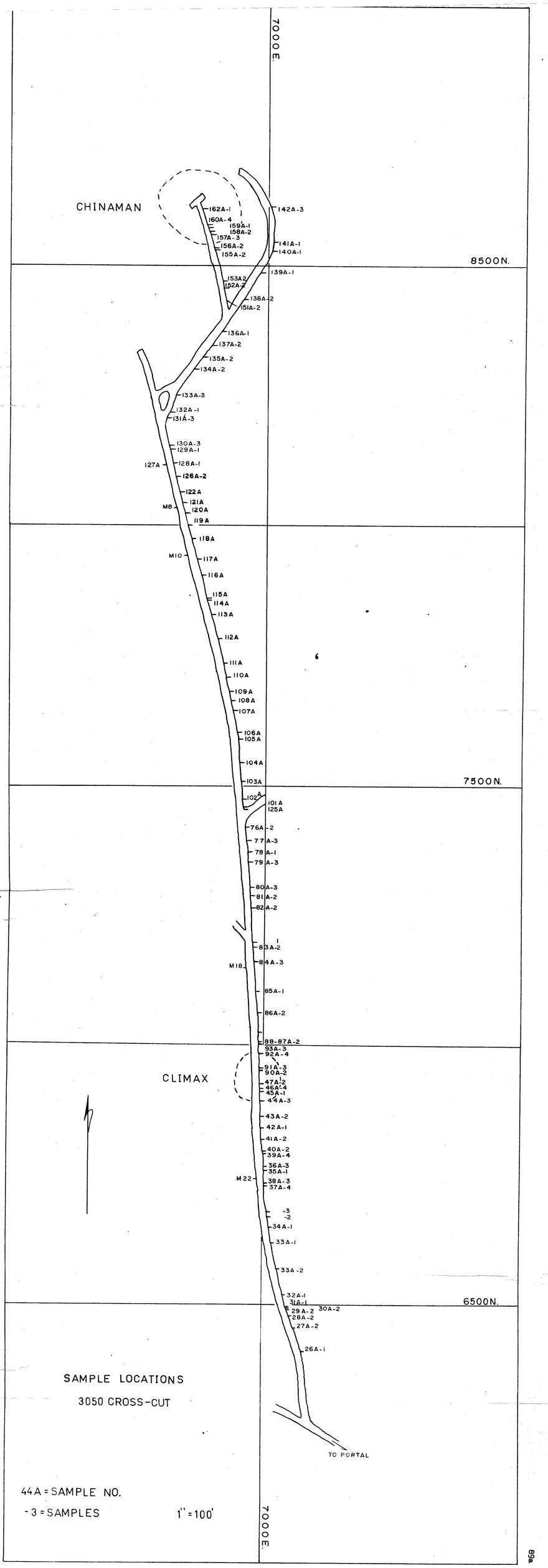
7000E.
CHINAMAN
162A-1
160A-4
159A-1
158A-2
157A-3
156A-2
155A-2
142A-3
141A-1
140A-1
8500N.
139A-1
153A2
152A-2
138A-2
151A-2
136A-1
137A-2
135A-2
134A-2
133A-3
132A-1
131A-3
130A-3
129A-1
127A
128A-1
126A-2
122A
M8
121A
120A
119A
118A
M10
117A
116A
115A
114A
113A
112A
111A
110A
109A
108A
107A
106A
105A
104A
103A
102A
101A
125A
7500N.
76A-2
77A-3
78A-1
79A-3
80A-3
81A-2
82A-2
83A-2
M18
84A-3
85A-1
86A-2
88-87A-2
93A-3
92A-4
91A-3
90A-2
CLIMAX
47A-2
46A-4
45A-1
44A-3
43A-2
42A-1
41A-2
40A-2
39A-4
36A-3
35A-1
M22
38A-3
37A-4
-3
-2
34A-1
33A-1
33A-2
32A-1
31A-1
30A-2
29A-2
28A-2
27A-2
26A-1
6500N.
SAMPLE LOCATIONS
3050 CROSS-CUT
TO PORTAL
44A = SAMPLE NO.
-3 = SAMPLES
1" = 100'
7000E.

Appendix 2

Geology of Climax

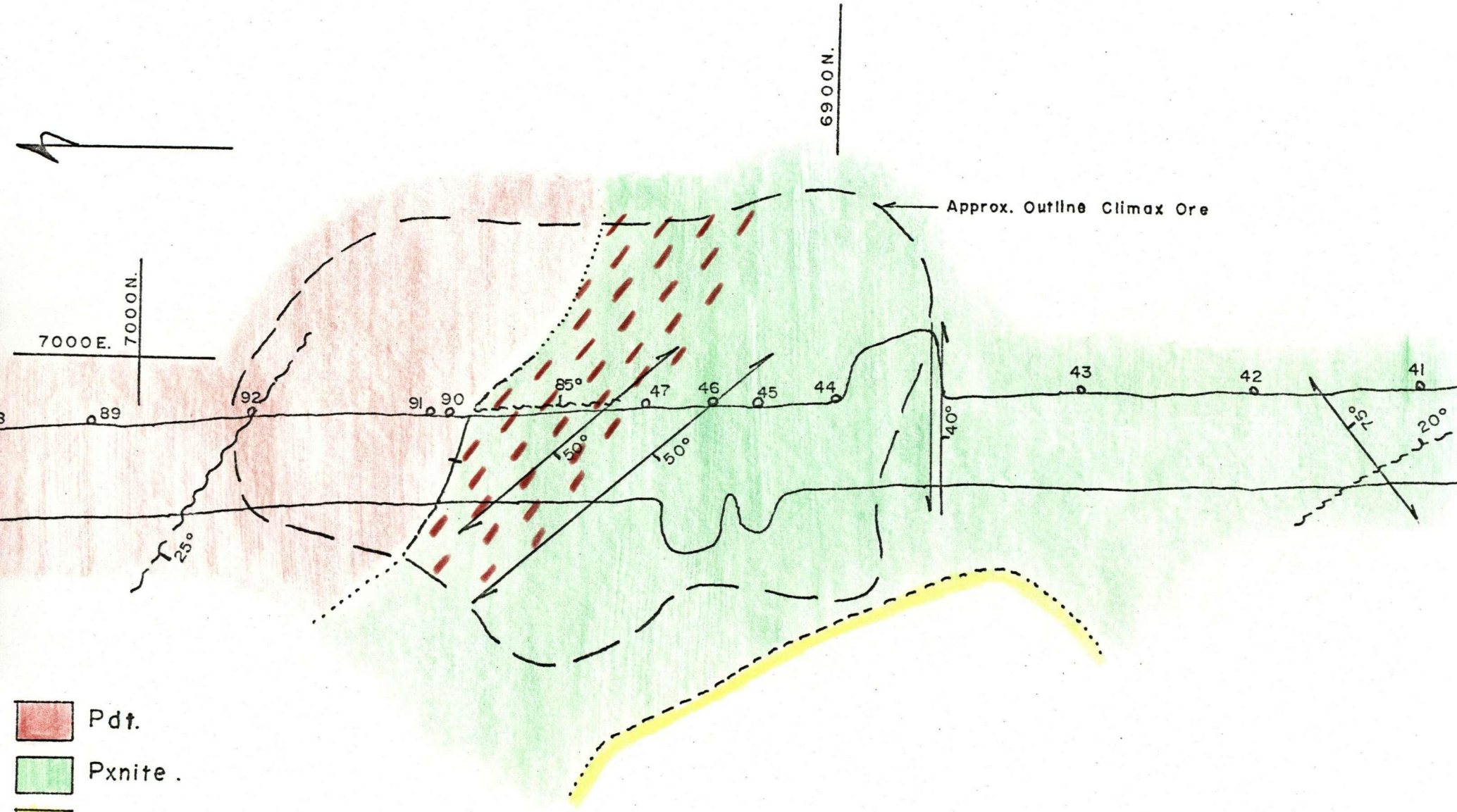

GEOLOGY OF CLIMAX

3050 X-CUT

91

Appendix 3

Cu, Ni, and Cu/(Cu+Ni) Assay Contour Plots, Chinaman and Climax Orebodies

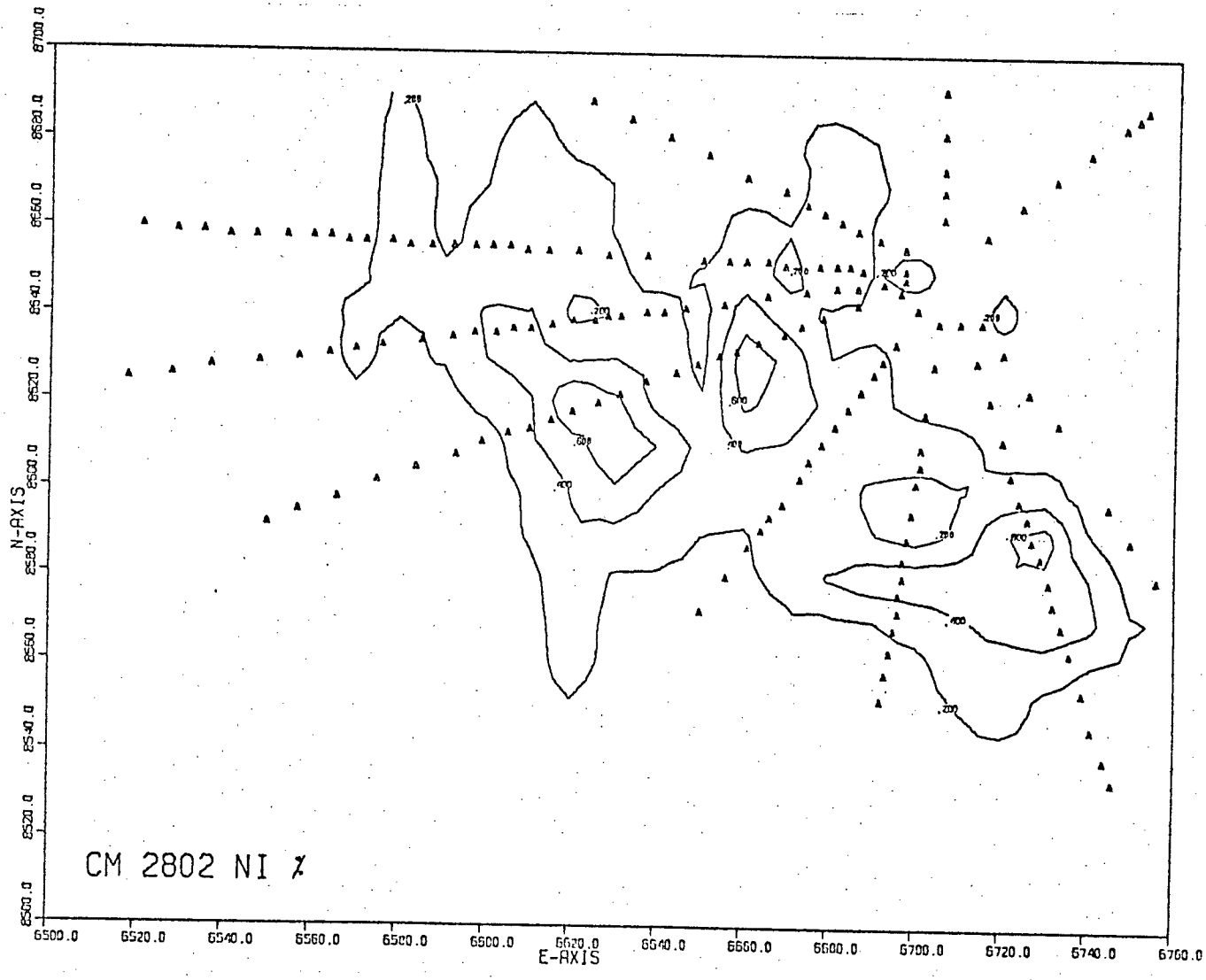
CM 2802 NI χ
N-AXIS
E-AXIS
8700.0
8620.0
8600.0
8580.0
8560.0
8540.0
8520.0
8500.0
6500.0
6520.0
6540.0
6560.0
6580.0
6600.0
6620.0
6640.0
6660.0
6680.0
6700.0
6720.0
6740.0
6760.0

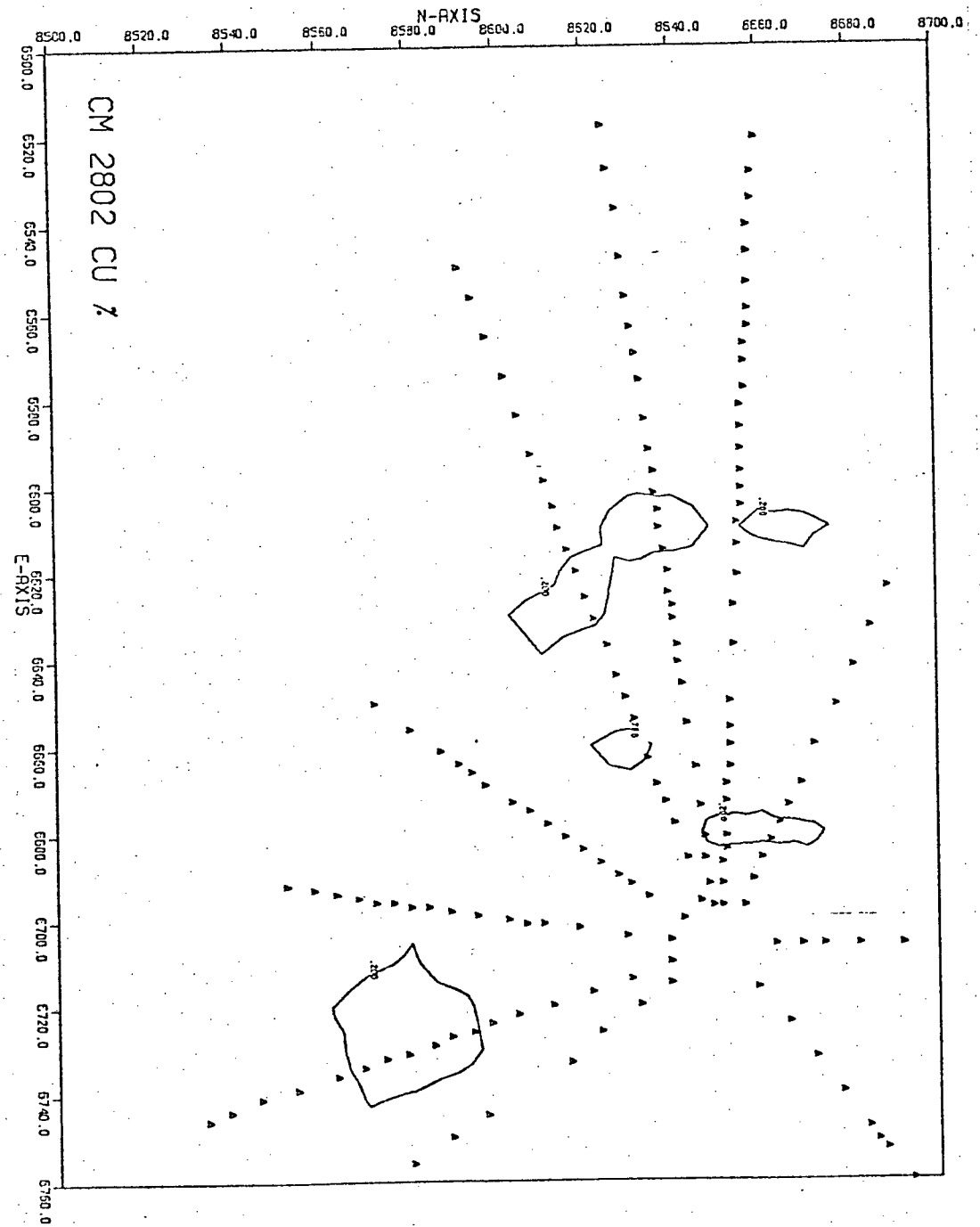
CM 2802 CU %
N-AXIS
8500.0
8520.0
8540.0
8560.0
8580.0
8600.0
8620.0
8640.0
8660.0
8680.0
8700.0
E-AXIS
6500.0
6520.0
6540.0
6560.0
6580.0
6600.0
6620.0
6640.0
6660.0
6680.0
6700.0
6720.0
6740.0
6760.0

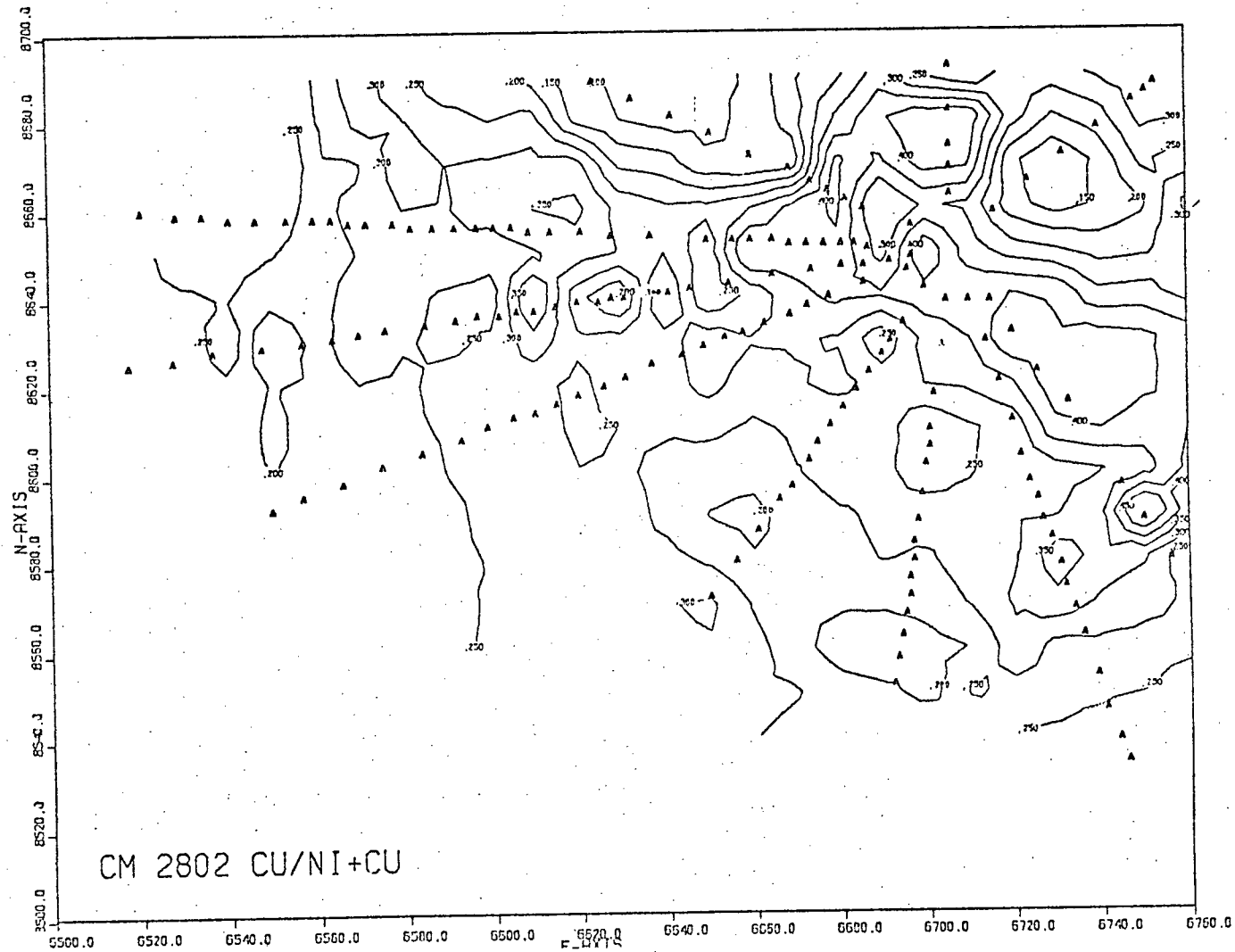
CM 2802 CU/NI+CU
N-AXIS
E-AXIS
8700.0
8580.0
8660.0
8640.0
8620.0
8600.0
8580.0
8560.0
8540.0
8520.0
8500.0
6500.0
6520.0
6540.0
6560.0
6580.0
6600.0
6620.0
6640.0
6660.0
6680.0
6700.0
6720.0
6740.0
6760.0

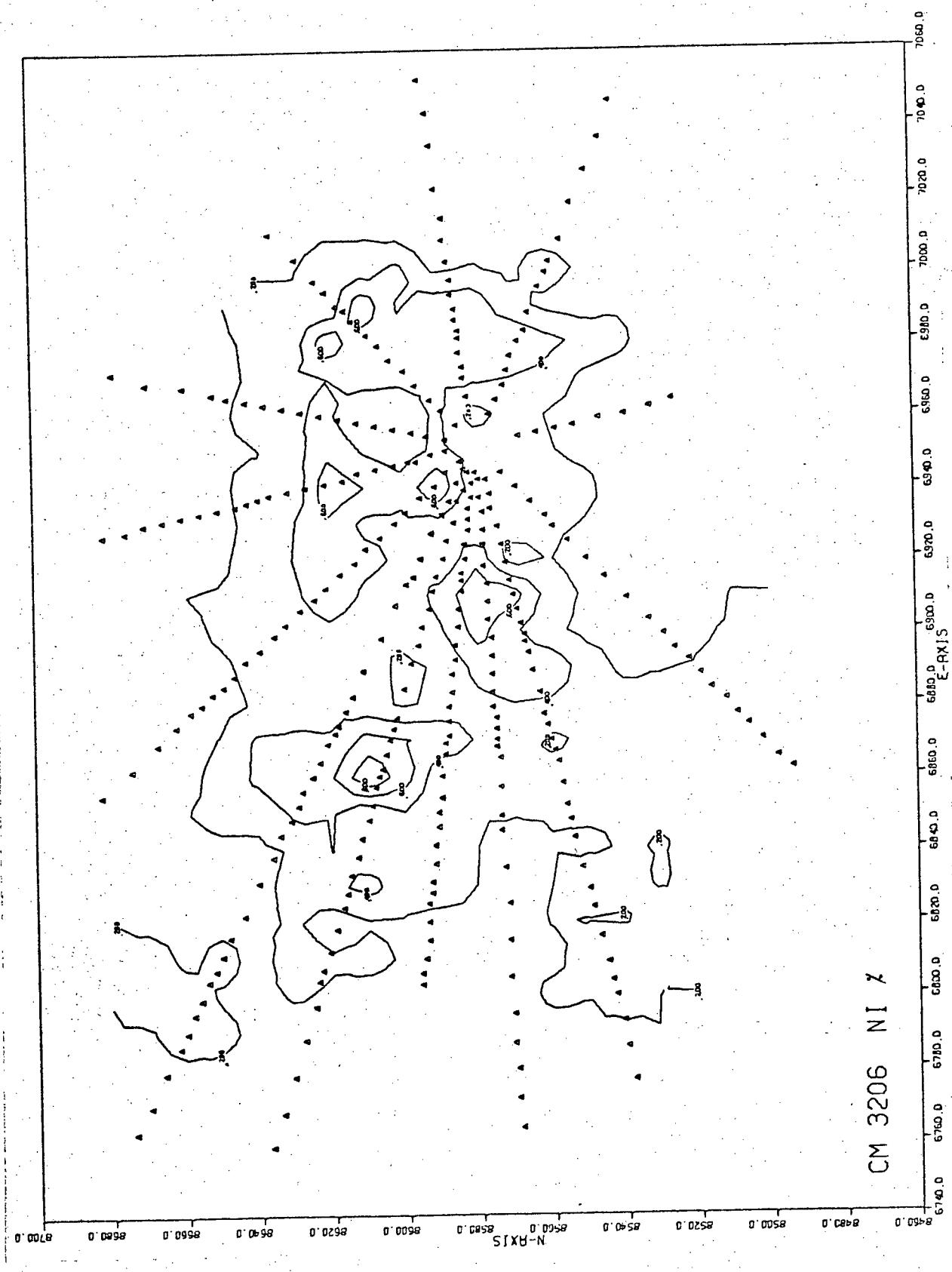
CM 3206 NI %
N-AXIS
E-AXIS
8460.0
8480.0
8500.0
8520.0
8540.0
8560.0
8580.0
8600.0
8620.0
8640.0
8660.0
8680.0
8700.0
6740.0
6760.0
6780.0
6800.0
6820.0
6840.0
6860.0
6880.0
6900.0
6920.0
6940.0
6960.0
6980.0
7000.0
7020.0
7040.0
7060.0

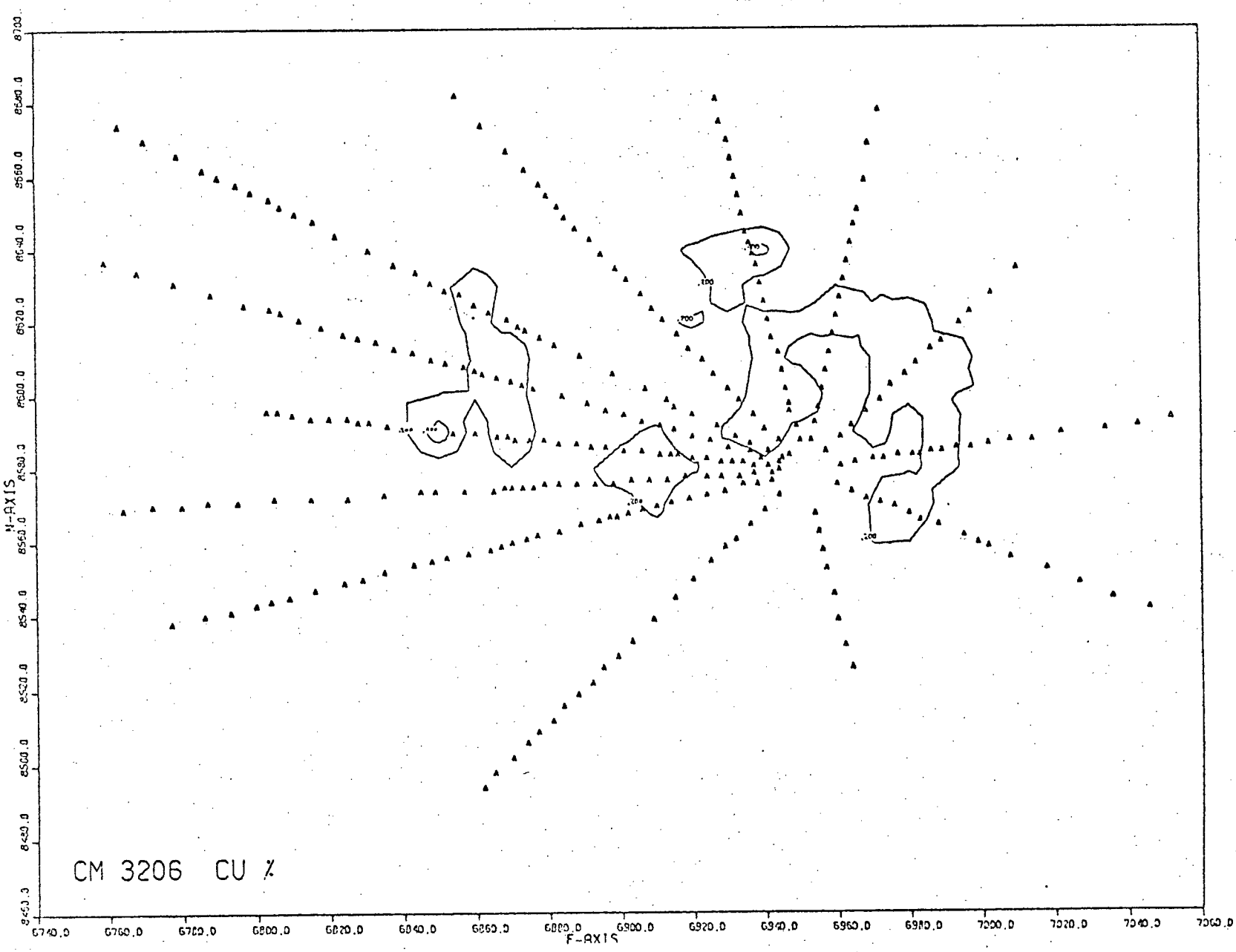
CM 3206 CU %
H-AXIS
F-AXIS
6740.0
6760.0
6780.0
6800.0
6820.0
6840.0
6860.0
6880.0
6900.0
6920.0
6940.0
6960.0
6980.0
7000.0
7020.0
7040.0
7060.0
8700
8580.0
8560.0
8540.0
8520.0
8500.0
8480.0
8460.0

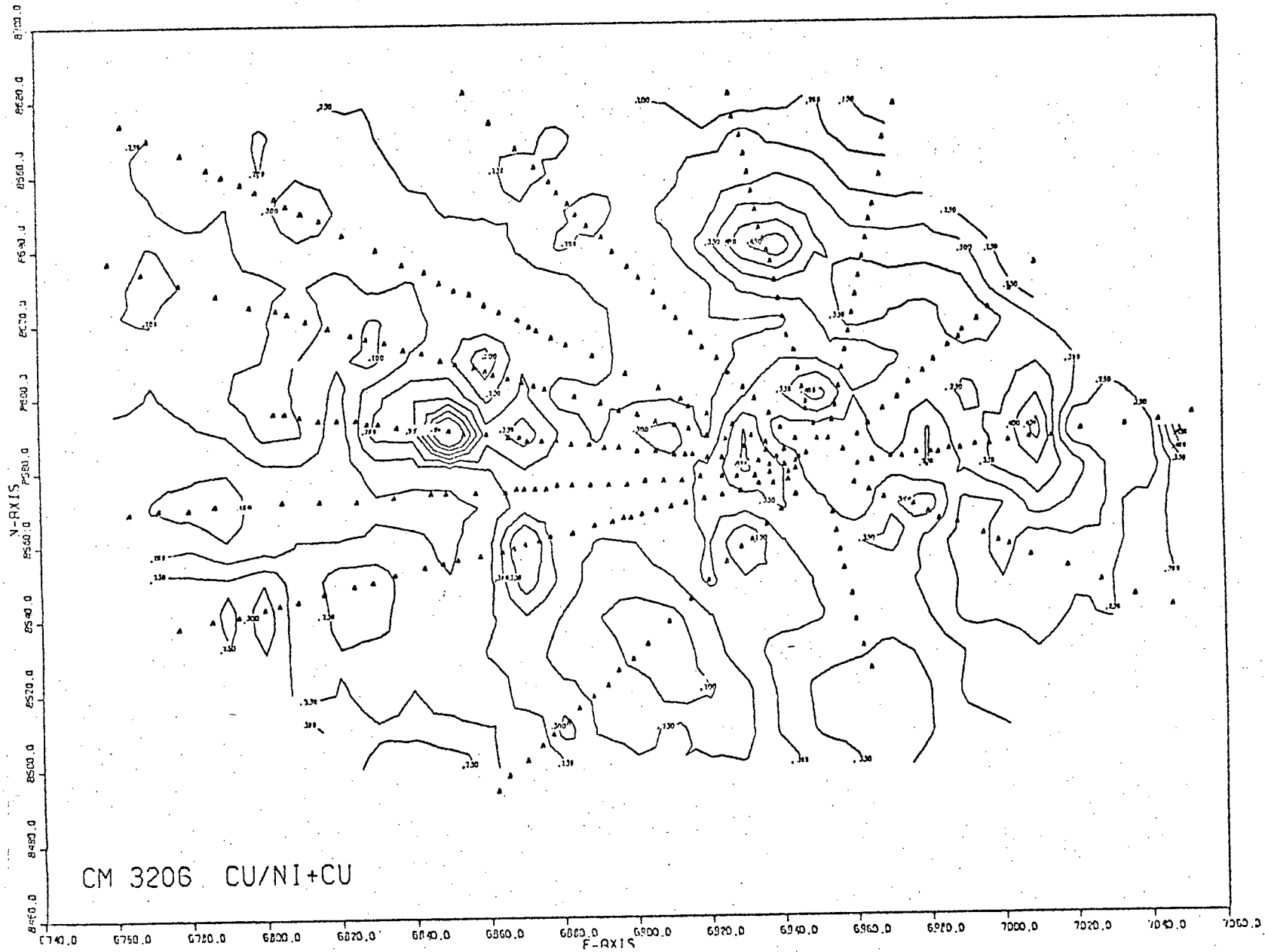
CM 3206 CU/NI+CU
N-AXIS
E-AXIS
6740.0
6760.0
6780.0
6800.0
6820.0
6840.0
6860.0
6880.0
6900.0
6920.0
6940.0
6960.0
6980.0
7000.0
7020.0
7040.0
7060.0
8460.0
8480.0
8500.0
8520.0
8540.0
8560.0
8580.0
8600.0

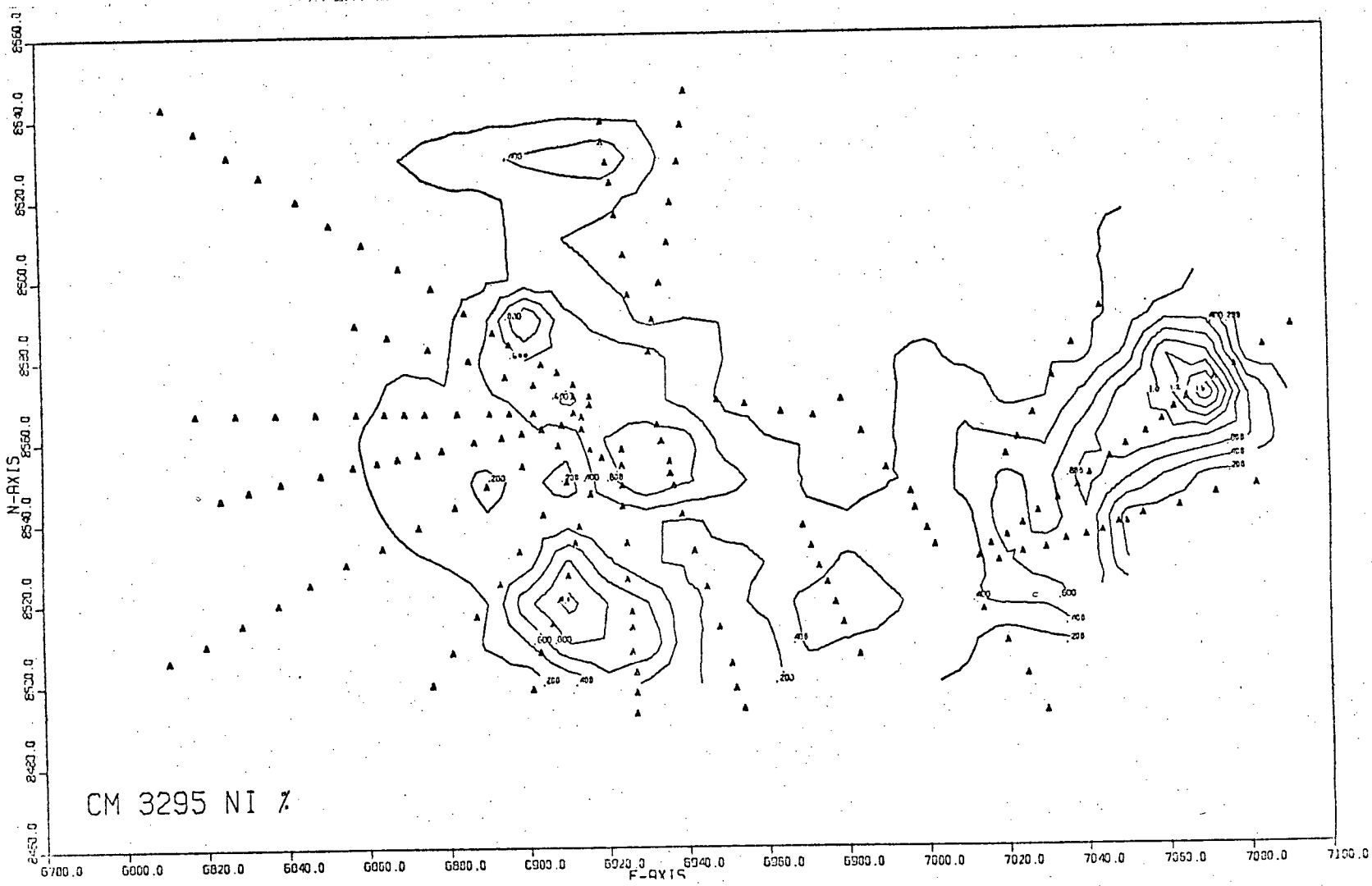
CM 3295 NI %
N-AXIS
E-AXIS
8560.0
8540.0
8520.0
8500.0
8480.0
8460.0
6780.0
6800.0
6820.0
6840.0
6860.0
6880.0
6900.0
6920.0
6940.0
6960.0
6980.0
7000.0
7020.0
7040.0
7060.0
7080.0
7100.0

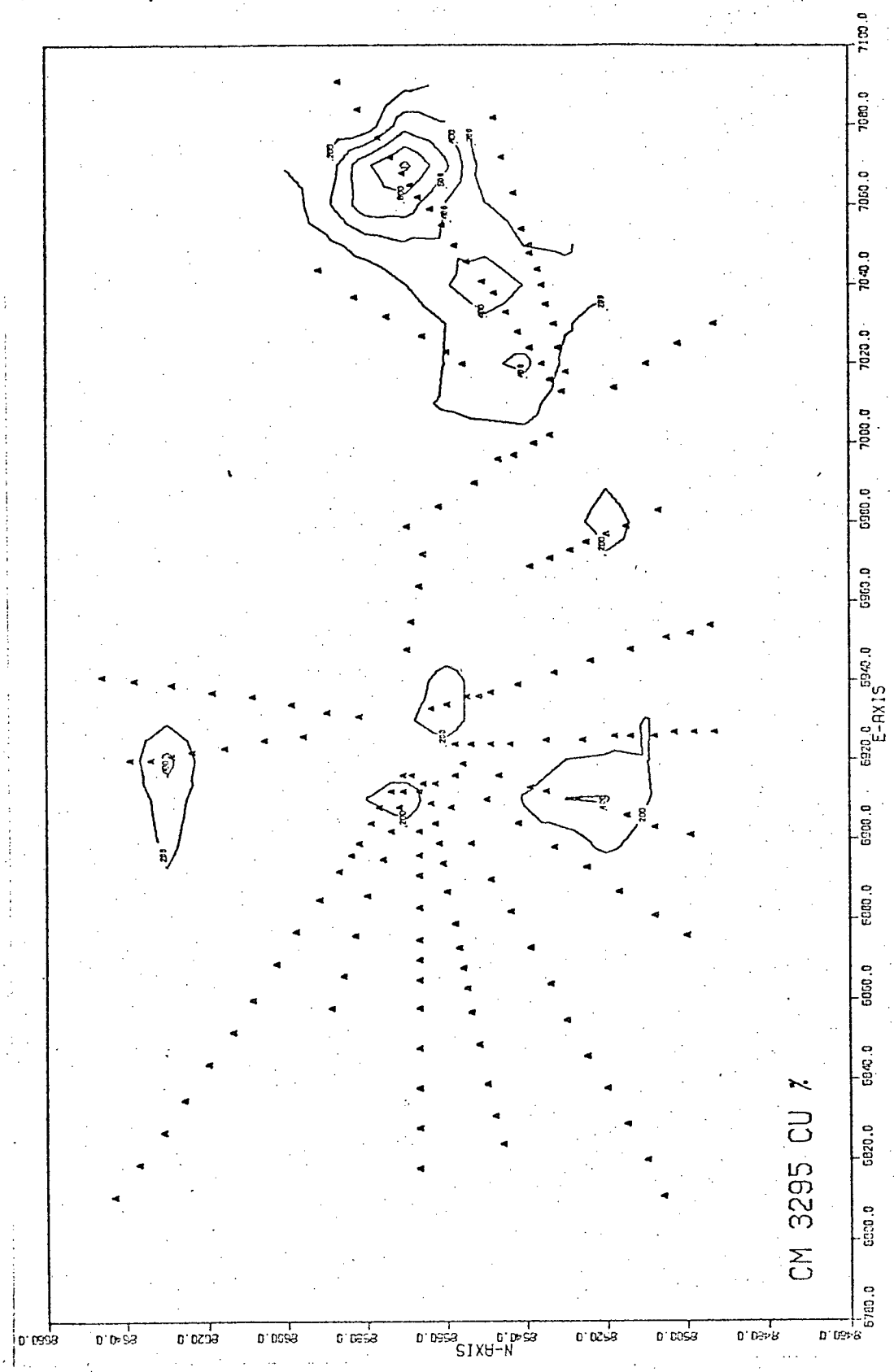
CM 3295 CU %
N-AXIS
E-AXIS
8460.0
8500.0
8520.0
8540.0
8560.0
8580.0
8600.0
8620.0
8640.0
8660.0
6780.0
6800.0
6820.0
6840.0
6860.0
6880.0
6900.0
6920.0
6940.0
6960.0
6980.0
7000.0
7020.0
7040.0
7060.0
7080.0
7100.0

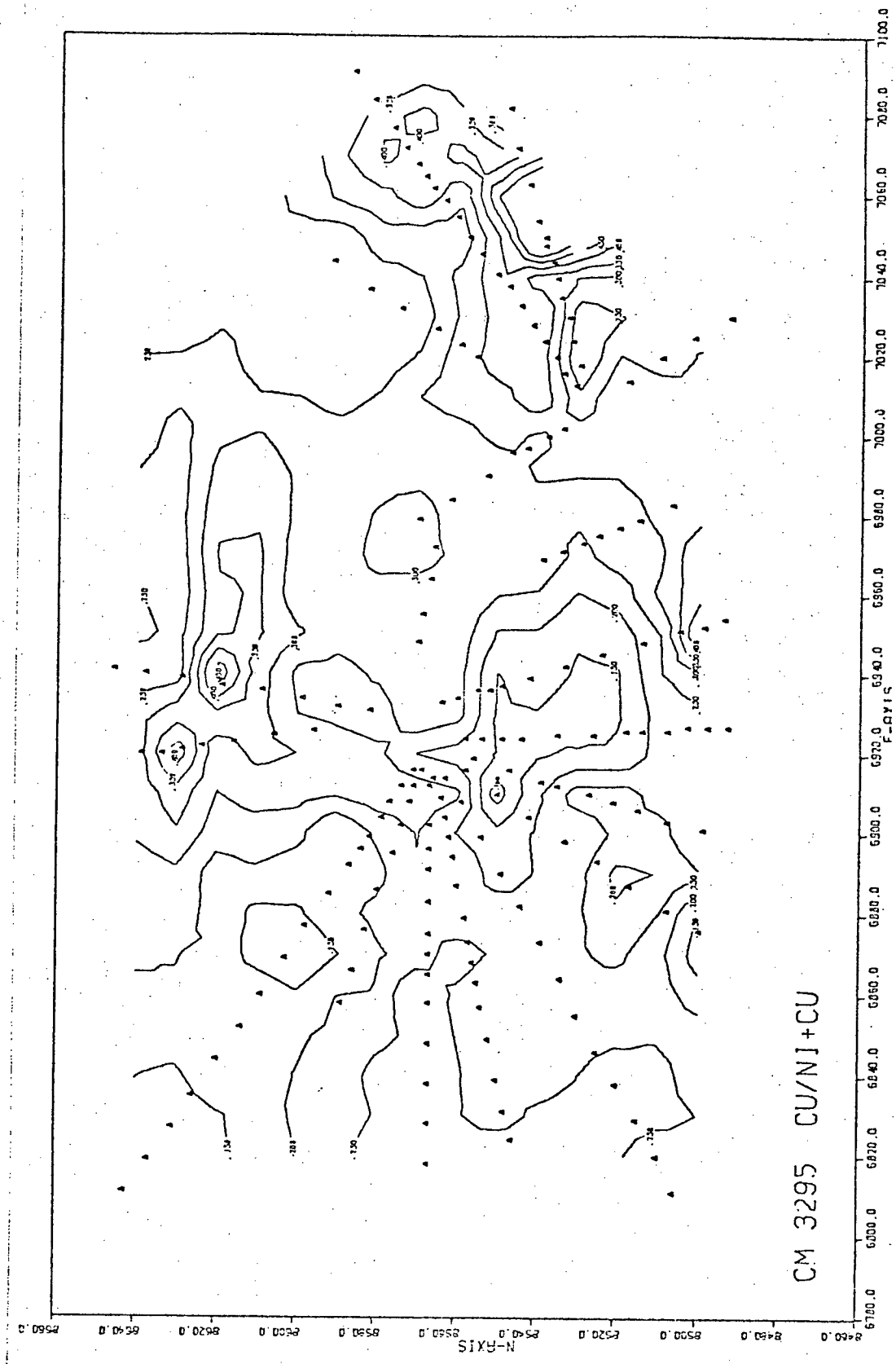
CM 3295 CU/NI+CU
N-AXIS
E-AXIS

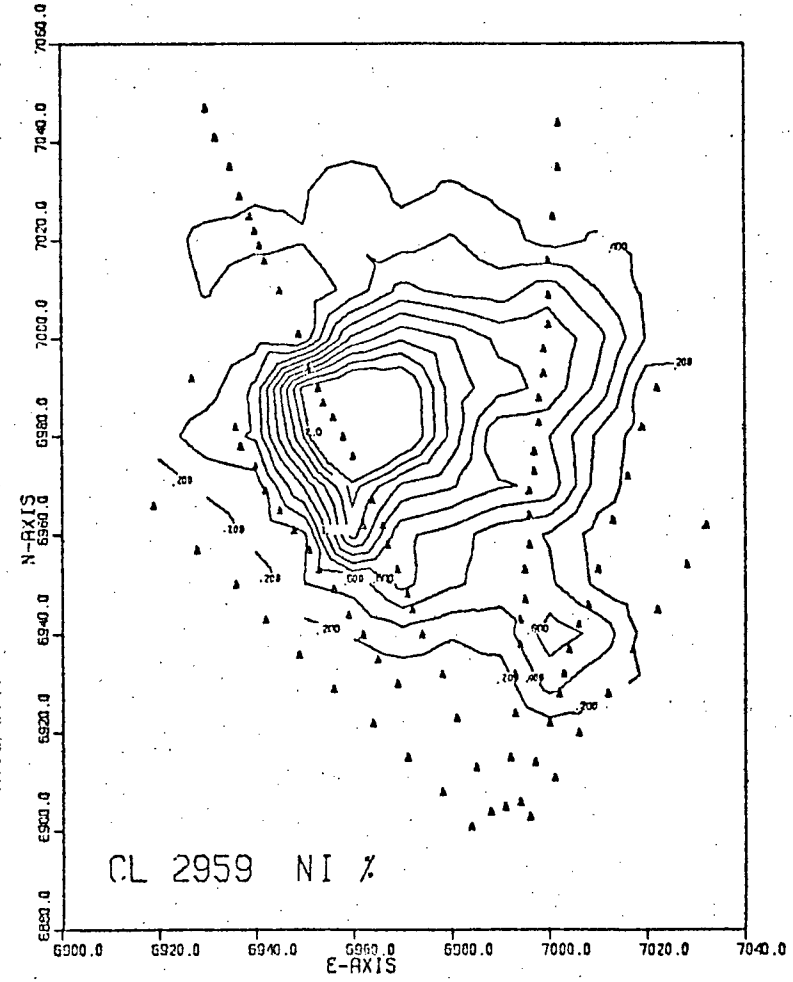
CL 2959 NI %
N-AXIS
E-AXIS
6900.0
6920.0
6940.0
6960.0
6980.0
7000.0
7020.0
7040.0
7060.0

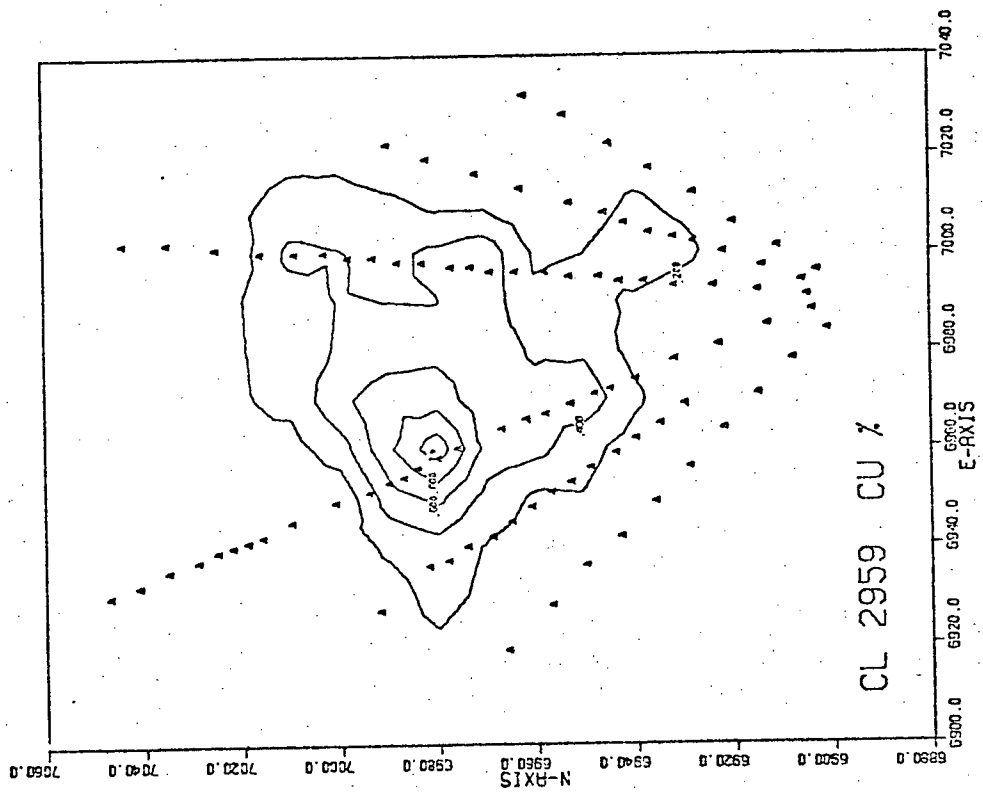
CL 2959 CU %
E-AXIS
N-AXIS
6900.0
6920.0
6940.0
6960.0
6980.0
7000.0
7020.0
7040.0
7060.0

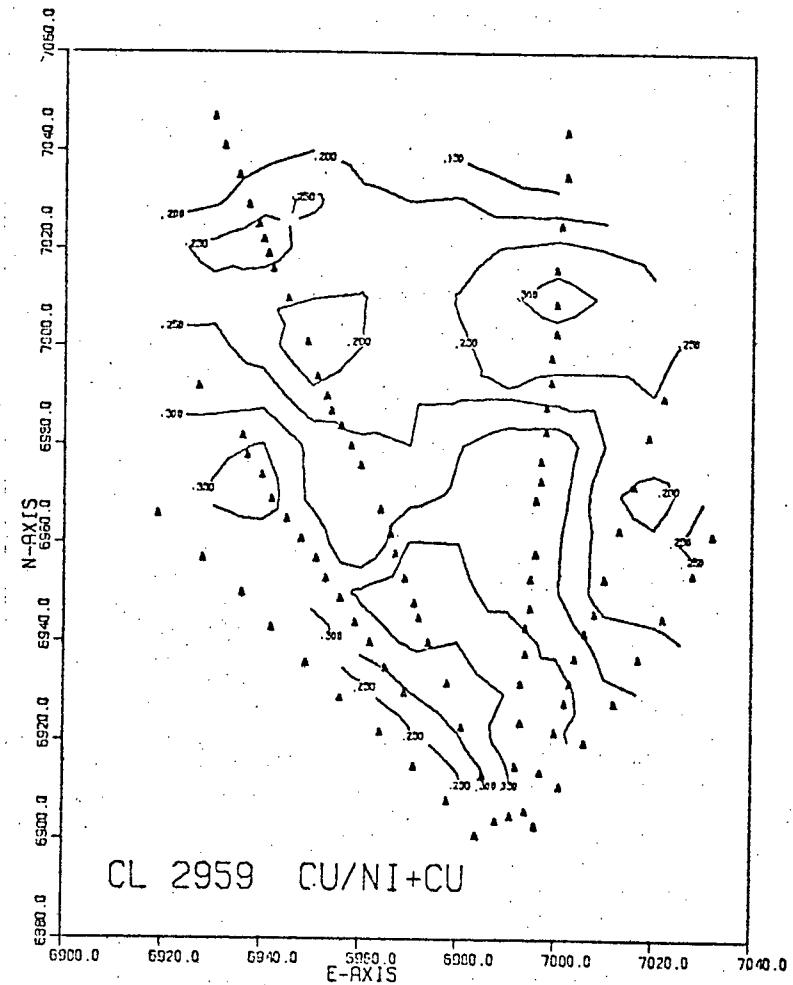
CL 2959 CU/NI+CU
N-AXIS
E-AXIS
6900.0
6920.0
6940.0
6960.0
6980.0
7000.0
7020.0
7040.0

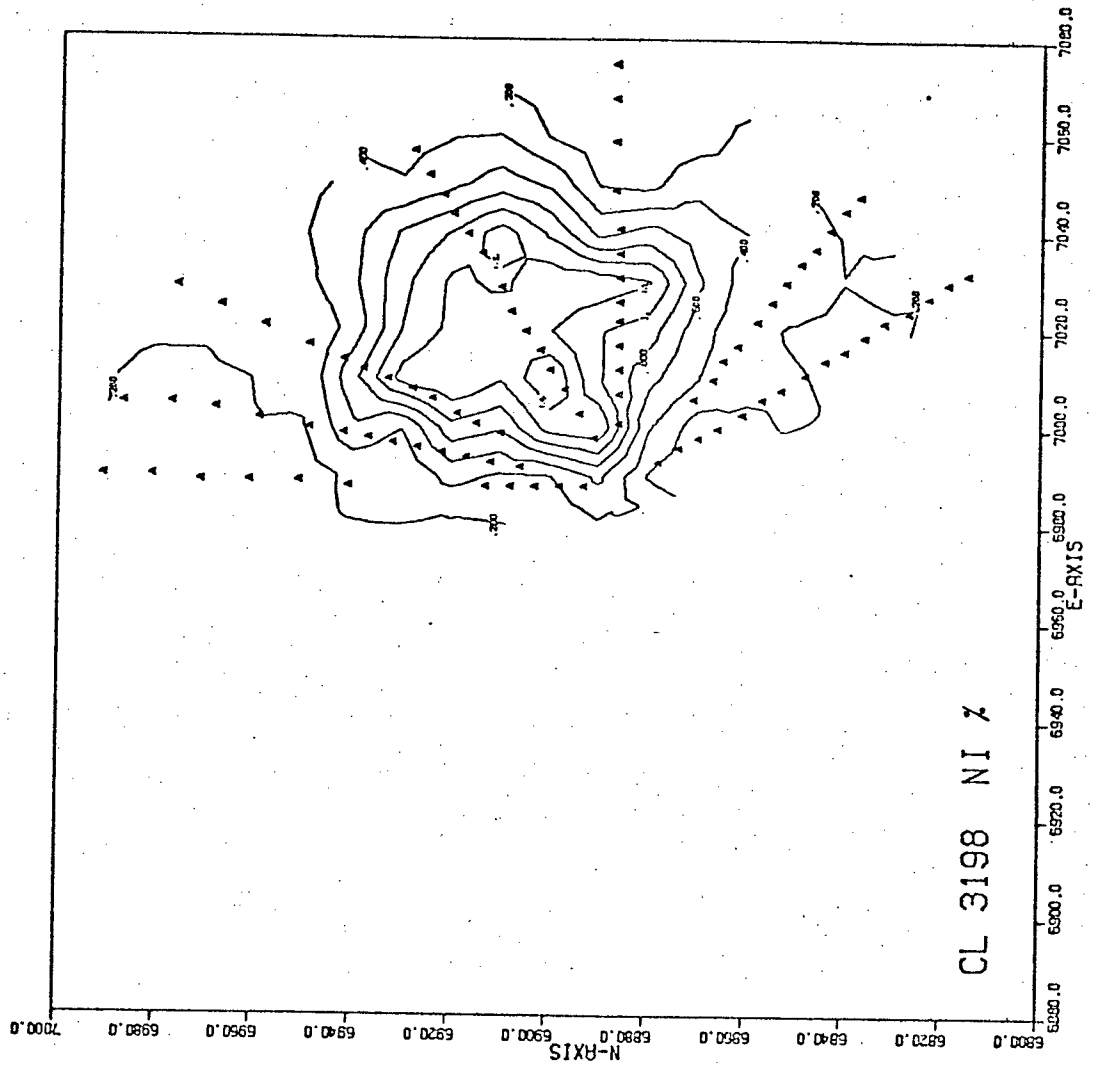
CL 3198 NI %
N-AXIS
E-AXIS
6800.0
6820.0
6840.0
6860.0
6880.0
6900.0
6920.0
6940.0
6960.0
6980.0
7000.0
7000.0
7020.0
7040.0
7050.0
7060.0

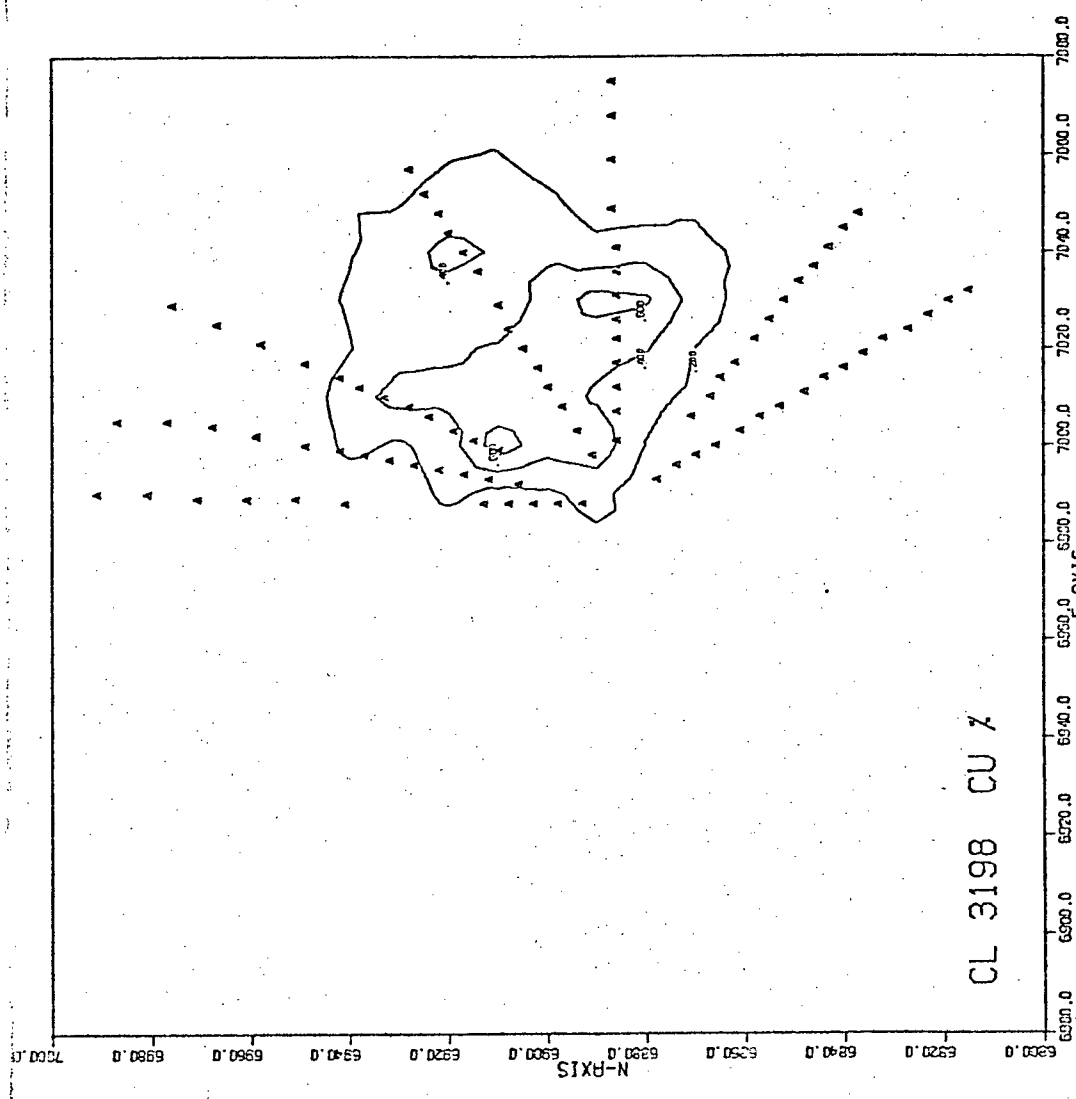
CL 3198 CU %
N-AXIS
E-AXIS
6880.0
6920.0
6960.0
7000.0
7040.0
7080.0
7120.0
7160.0
7200.0
7240.0
7280.0
7320.0
7360.0
7400.0
7440.0
7480.0
7520.0
7560.0
7600.0
6900.0
6920.0
6940.0
6960.0
6980.0
7000.0
7020.0
7040.0
7060.0
7080.0
7100.0
7120.0
7140.0
7160.0
7180.0
7200.0

CL 3198 CU/NI+CU
N-AXIS
E-AXIS
7000.0
6980.0
6960.0
6940.0
6920.0
6900.0
6880.0
6860.0
6840.0
6820.0
6800.0
6900.0
6920.0
6940.0
6960.0
6980.0
7000.0
7020.0
7040.0
7060.0
7080.0

Appendix 4

Microprobe Analyses of Silicates

N.B. For sample number correlation see p. 62.

MICROPROBE ANALYSIS OF ORTHOPYROXENES

	1	2	3	4	5	6	7	8
Si	55.37	54.84	54.18	54.90	53.40	54.695	54.567	54.96
Al	3.13	2.62	2.38	2.28	2.64	2.128	2.110	1.52
Ti	.23	.18	.07	.24	.32	.239	.420	.20
Cr	.42	.12	.23	.19	.26	.190	.252	.12
Fe	12.09	12.74	13.41	12.68	13.94	14.062	12.236	11.93
Mn	n.d.	n.d.	n.d.	n.d.	n.d.	n.d.	n.d.	n.d.
Mg	29.72	30.03	29.78	27.60	26.47	28.631	29.896	28.49
Ca	.68	.69	.35	1.09	1.24	1.154	.796	1.20
Na	.03	-	-	-	.07	.012	.052	.02
K	n.d.	n.d.	n.d.	n.d.	n.d.	n.d.	n.d.	n.d.
	101.67	101.22	100.40	98.95	98.34	101.111	100.329	98.44

Oxides

Formulae based on 6 oxygens

	1		2		3		4		5		6		7		8	
Si	1.928	2.00	1.925	2.00	1.924	2.00	1.968	2.00	1.944	2.00	1.937	2.00	1.932	2.00	1.977	2.00
Al	.072		.075		.076		.032		.056		.063		.068		.023	
Al	.056	1.99	.033	2.01	.024	2.020	.064	1.972	.057	1.99	.026	2.01	.020	2.01	.041	1.98
Ti	.006		.005		.002		.006		.009		.006		.011		.005	
Cr	.012		.003		.006		.005		.007		.005		.007		.003	
Fe	.352		.374		.398		.380		.424		.416		.362		.359	
Mn	-		-		-		-		-		-		-		-	
Mg	1.543		1.572		1.577		1.475		1.437		1.511		1.577		1.527	
Ca	.025		.026		.013		.042		.048		.044		.030		.046	
Na	.002		-		-		-		.005		.001		.003		.001	
K	-		-		-		-		-		-		-		-	

Mg =	80.45%	79.65%	79.30%	77.75%	75.25%	76.65%	80.05%	78.85%
Fe =	18.25%	18.95%	20.05%	20.00%	22.20%	21.10%	18.40%	18.65%
Ca =	1.30%	1.40%	0.65%	2.25%	2.55%	2.25%	1.55%	2.50%

cont'.d..../2

	9	10	11	12	13	14	15	16
Si	56.075	56.325	56.869	57.247	53.824	55.544	53.232	55.62
Al	2.074	1.673	1.595	2.316	2.557	2.279	2.166	1.78
Ti	.165	.134	.205	.384	.197	.248	.320	.04
Cr	.344	.370	.214	.370	.323	.482	.173	.12
Fe	11.305	12.028	9.612	8.809	8.500	8.190	13.920	8.67
Mn	.160	.140	n.d.	n.d.	n.d.	n.d.	n.d.	n.d.
Mg	30.863	31.131	32.088	32.526	31.164	32.482	28.772	32.44
Ca	1.110	1.043	1.079	.648	.759	1.212	.526	.92
Na	.011	-	.042	.081	-	-	.057	-
K	-	-	n.d.	n.d.	n.d.	n.d.	n.d.	n.d.
	102.107	101.844	101.704	102.381	97.325	100.437	99.166	99.59

Oxides

Formulae based on 6 oxygens

	9		10		11		12		13		14		15		16	
Si	1.942	2.00	1.960	2.00	1.959	2.00	1.949	2.00	1.931	2.00	1.930	2.00	1.922	2.00	1.950	2.00
Al	.058		.040		.041		.051		.069		.070		.078		.050	
Al	.027	2.007	.028	1.996	.024	2.002	.042	1.99	.039	2.003	.020	2.00	.014	2.02	.023	2.06
Ti	.004		.003		.005		.010		.005		.006		.009		.001	
Cr	.009		.010		.006		.010		.009		.013		.005		.003	
Fe	.327		.350		.277		.251		.255		.238		.420		.254	
Mn	.005		.004		n.d.		n.d.		n.d.		-		-		-	
Mg	1.593		1.562		1.647		1.650		1.666		1.683		1.549		1.695	
Ca	.041		.039		.040		.024		.029		.045		.020		.034	
Na	.001		-		.003		.005		-		-		.004		-	
K	-		-		-		n.d.		n.d.		-		-		-	
	Mg = 81.20%		Mg = 80.00%		Mg = 83.75%		Mg = 85.65%		Mg = 85.45%		Mg = 85.60%		Mg = 77.85%		Mg = 85.40%	
	Fe = 16.70%		Fe = 18.00%		Fe = 14.15%		Fe = 13.10%		Fe = 13.05%		Fe = 12.10%		Fe = 21.15%		Fe = 12.70%	
	Ca = 2.10%		Ca = 2.00%		Ca = 2.10%		Ca = 1.25%		Ca = 1.50%		Ca = 2.30%		Ca = 1.00%		Ca = 1.70%	

Cont'd...

	17	18	19	20	21	22	23	24
Si	57.507	55.094	53.074	55.016%	52.171	51.954	52.303	56.229
Al	1.985	1.638	2.953	2.962	2.079	2.935	4.912	2.425
Ti	.093	.144	.170	.154	.198	.155	.053	.060
Cr	.185	.062	.065	.808	-	.038	-	.217
Fe	8.895	10.538	15.021	9.557	24.146	15.634	11.495	9.710
Mn	n.d.	n.d.	n.d.	n.d.	n.d.	n.d.	n.d.	n.d.
Mg	32.504	31.253	28.176	31.122	22.211	28.441	30.161	32.246
Ca	1.122	.937	1.286	2.275	.816	.636	.661	.619
Na	-	.005	-	.267	-	.033	.037	.058
K	n.d.	n.d.	n.d.	n.d.	n.d.	n.d.	n.d.	n.d.
	102.291	99.671	100.749	102.161	101.621	99.826	99.622	101.564

Oxides

Formulae based on 6 oxygens

	17		18		19		20		21		22		23		24	
Si	1.961	2.00	1.947	2.00	1.900	2.00	1.902	2.00	1.926	2.00	1.883	2.00	1.860	2.00	1.939	2.0
Al	.039		.053		.100		.098		.074		.117		.140		.061	
Al	.041	2.04	.015	2.01	.025	2.03	.023	2.03	.016	2.02	.008	2.05	.066	2.03	.037	2.0
Ti	.024		.004		.005		.004		.005		.004		.001		.001	
Cr	.005		.002		.002		.022		-		.001		-		.006	
Fe	.254		.311		.450		.276		.746		.474		.342		.280	
Mn	-		-		-		-		-		-		-		-	
Mg	1.652		1.646		1.503		1.604		1.222		1.536		1.599		1.657	
Ca	.041		.035		.049		.084		.032		.025		.025		.023	
Na	-		-		-		.018		-		.002		.002		.004	
K	-		-		-		-		-		-		-		-	

Mg = 84.80%	Mg = 82.60%	Mg = 75.10%	Mg = 81.65%	Mg = 61.10%	Mg = 75.45%	Mg = 81.30%	Mg = 84.50
Fe = 13.10%	Fe = 15.65%	Fe = 22.45%	Fe = 14.05%	Fe = 37.30%	Fe = 23.35%	Fe = 17.40%	Fe = 14.30
Ca = 2.10%	Ca = 1.75%	Ca = 2.45%	Ca = 4.30%	Ca = 1.60%	Ca = 1.20%	Ca = 1.30%	Ca = 1.20

	25	26	27	28	29	30
Si	54.253	54.121	54.209	55.614	55.035	54.919
Al	2.593	2.452	1.819	2.175	3.027	2.344
Ti	.101	.156	.057	.054	.035	.184
Cr	.315	.232	.385	.032	.309	.545
Fe	11.130	11.778	14.489	14.267	10.236	11.225
Mn	n.d.	n.d.	n.d.	n.d.	n.d.	n.d.
Mg	31.270	32.071	28.179	29.889	31.484	30.576
Ca	.675	.529	1.066	.919	.498	.792
Na	-	.002	-	-	.022	.059
K	n.d.	n.d.	n.d.	n.d.	n.d.	n.d.
	100.337	101.341	100.204	102.95	100.646	100.644

Oxides

Formulae based on 6 oxygens

	25	26	27	28	29	30
Si	1.912 } 2.00	1.896 } 2.00	1.942 } 2.00	1.933 } 2.00	1.921 } 2.00	1.929 } 2.00
Al	.088	.101	.058	.067	.079	.071
Al	.020	.003	.019	.022	.045	.026
Ti	.003	.001	.001	.001	.001	.005
Cr	.009	.006	.011	.001	.008	.015
Fe	.328 } 2.03	.345 } 2.046	.434 } 2.01	.415 } 2.02	.299 } 2.01	.330 } 2.01
Mn	-	-	-	-	-	-
Mg	1.642	1.674	1.505	1.548	1.638	1.601
Ca	.025	.020	.041	.034	.019	.030
Na	-	-	-	-	.001	.004
K	-	-	-	-	-	-
	Mg = 82.30%	Mg = 82.20%	Mg = 76.05%	Mg = 77.50%	Mg = 83.75%	Mg = 81.65%
	Fe = 16.45%	Fe = 16.85%	Fe = 21.90%	Fe = 20.80%	Fe = 15.30%	Fe = 16.85%
	Ca = 1.25 %	Ca = 0.95%	Ca = 2.05%	Ca = 1.70%	Ca = 0.95%	Ca = 1.50%

MICROPROBE ANALYSIS OF CLINOPYROXENES

	1	2	3	4	7	8	9	10	11
Si	54.00	52.11	52.47	52.87	51.918	53.19	53.803	54.175	53.937
Al	3.52	2.97	3.66	2.60	2.472	1.37	3.109	2.890	1.902
Ti	.45	.50	.58	.40	.402	.28	.344	.453	.288
Cr	.58	.39	.36	.31	.503	.32	.528	.580	.609
Fe	4.64	4.92	5.04	4.53	5.052	4.63	4.961	4.678	3.761
Mn	n.d.	n.d.	n.d.	n.d.	n.d.	n.d.	.093	.060	n.d.
Mg	16.80	17.06	15.72	16.01	16.625	16.46	18.106	17.778	17.242
Ca	21.69	22.47	23.87	21.29	22.381	22.74	19.456	18.483	23.537
Na	.39	.46	.57	.20	.364	.31	.394	.447	.315
K	n.d.	n.d.	n.d.	n.d.	n.d.	n.d.	-	-	-
	101.07	100.88	102.27	98.21	100.717	99.30	100.794	99.544	102.491

Oxides

Formulae based on 6 Oxygens

	1		2		3		4		7		8		9		10		11	
Si	1.914	2.000	1.898	2.00	1.891	2.00	1.959	2.00	1.914	2.00	1.961	2.00	1.937	2.00	1.964	2.00	1.941	2.00
Al	.086		.102		.109		.041		.086		.039		.063		.036		.059	
Al	.064	2.003	.025	2.03	.046	2.03	.072	1.98	.021	2.02	.020	2.005	.069	1.99	.087	1.97	.022	2.01
Ti	.012		.014		.016		.011		.011		.008		.009		.012		.008	
Cr	.017		.011		.010		.009		.014		.009		.015		.017		.017	
Fe	.140		.150		.152		.140		.156		.143		.149		.142		.113	
Mn	-		-		-		-		-		-		.003		.002		-	
Mg	.904		.926		.844		.884		.914		.905		.971		.961		.925	
Ca	.839		.877		.922		.845		.884		.898		.750		.718		.907	
Na	.027		.032		.040		.014		.026		.022		.027		.031		.022	
K	-		-		-		-		-		-		-		-		-	

Mg = 48.00	Mg = 47.50	Mg = 43.95	Mg = 47.25%	Mg = 46.80%	Mg = 46.40	Mg = 5195%	Mg = 52.75%	Mg = 47.60%
Fe = 4.45	Fe = 7.65	Fe = 7.90	Fe = 7.50%	Fe = 8.00%	Fe = 7.55	Fe = 7.95%	Fe = 7.80%	Fe = 5.80%
Ca = 44.55	Ca = 44.85	Ca = 48.15	Ca = 45.25%	Ca = 45.20%	Ca = 46.05	Ca = 40.10%	Ca = 39.45%	Ca = 46.60%

cont'd... ./2

	15	16	17	18	19	22	25	27	28
Si	51.768	52.24	54.027	53.663	50.783	53.007	52.207	52.253	52.361
Al	2.109	2.06	1.803	2.167	3.913	3.503	3.786	2.792	3.039
Ti	.466	.16	.054	.100	.359	.483	.308	.348	.381
Cr	.504	.95	.697	.738	.201	.086	.660	.382	.289
Fe	6.019	4.23	3.857	4.503	6.479	6.882	4.285	5.926	5.631
Mn	n.d.	n.d.	n.d.	n.d.	n.d.	n.d.	n.d.	n.d.	n.d.
Mg	16.859	18.22	18.260	17.645	15.547	16.020	17.541	15.474	16.543
Ca	22.447	20.88	22.690	22.800	21.270	21.681	22.009	22.422	23.291
Na	.344	.49	.194	.294	.393	.504	.486	.435	.337
K	n.d.	n.d.	n.d.	n.d.	n.d.	n.d.	n.d.	n.d.	n.d.
	100.517	99.23	101.582	101.910	98.945	102.166	101.282	100.032	101.872

Oxides

Formulae based on 6 Oxygens

Si	1.904 } 2.00	1.923 } 2.00	1.940 } 2.00	1.928 } 2.00	1.892 } 2.00	1.911 } 2.000	1.885 } 2.00	1.924 } 2.00	1.897 } 2.00
Al	.091	.077	.060	.072	.108	.089	.115	.076	.103
Ti	.005								
Al	-	.012	.016	.020	.064	.060	.046	.045	.027
Ti	.006	.004	.001	.003	.010	.013	.008	.009	.010
Cr	.015	.028	.019	.021	.006	.002	.019	.011	.008
Fe	.185	.130	.116	.135	.202	.207	.129	.182	.171
Mn	n.d. } 2.04	n.d. } 2.03	n.d. } 2.01	n.d. } 2.022	n.d. } 2.02	n.d. } 2.01	n.d. } 2.03	- } 2.01	- } 2.04
Mg	.924	.999	.977	.945	.863	.861	.944	.849	.893
Ca	.885	.823	.873	.878	.849	.838	.852	.885	.904
Na	.024	.035	.013	.020	.028	.035	.034	.031	.024
K	n.d.	n.d.	n.d.	n.d.	n.d.	n.d.	n.d.	-	-

Mg = 46.35%	Mg = 51.15	Mg = 49.70%	Mg = 48.25%	Mg = 45.10%	Mg = 45.00%	Mg = 49.05%	Mg = 44.35%	Mg = 45.40%
Fe = 9.30%	Fe = 6.70	Fe = 5.90%	Fe = 6.90%	Fe = 10.55%	Fe = 10.80%	Fe = 6.70%	Fe = 9.45%	Fe = 8.70%
Ca = 44.35%	Ca = 42.15	Ca = 44.40%	Ca = 44.85%	Ca = 44.35%	Ca = 44.20%	Ca = 44.25%	Ca = 46.20%	Ca = 45.90%

MICROPROBE ANALYSIS OF OLIVINES

	1	11	12	12A	13	13A	14
Si	39.90	39.88	40.892	40.490	40.892	40.185	40.226
Al	-		-	-	-	-	-
Ti	-		-	-	.033	.010	-
Cr	-		-	-	-	-	-
Fe	18.04	15.94	14.774	14.838	12.942	14.002	13.251
Mn	-		.147	.134	n.d.	n.d.	n.d.
Mg	44.13	45.81	45.650	45.984	47.235	47.404	47.043
Ca	-		-	-	-	.004	.004
Na	-		.004	.004	-	-	-
K	-		-	-	n.d.	n.d.	n.d.
	102.07	101.63	101.467	101.450	101.102	101.605	100.524

Oxides

Formulae based on 4 oxygens

Si	.993	.989	1.007	.999	1.003	.988	.995
Al			-	-	-	-	-
Ti			-	-	-	-	-
Cr			-	-	-	-	-
Fe	.376	.330	.304	.306	.265	.288	.274
Mn			.003	.003	-	-	n.d.
Mg	1.637	1.692	1.677	1.692	1.727	1.737	1.735
Ca			-	-	-	-	-
Na			.0002	.0002	-	-	-
K			-	-	-	-	n.d.
	Fo = 81.20% Fa = 18.80%	Fo = 83.80% Fa = 16.20%	Fo = 84.60% Fa = 15.40%	Fo = 84.70% Fa = 15.30%	Fo = 86.65% Fa = 13.35%	Fo = 85.80% Fa = 14.20%	Fo = 86.35% Fa = 13.65%

cont'd... ./2

	16	17	20	23	24	26	29
Si	39.460	40.143	38.045	39.794	40.363	38.886	39.347
Al	-	.549	.036	-	-	.020	-
Ti	.020	-	.002	.040	-	-	.035
Cr	-	.370	.089	-	-	-	-
Fe	14.150	15.139	19.791	15.456	14.381	16.986	14.724
Mn	n.d.	n.d.	n.d.	n.d.	-	n.d.	n.d.
Mg	47.130	45.662	44.363	45.654	46.826	45.512	45.886
Ca	-	.016	-	.047	-	-	-
Na	-	-	-	-	-	.002	-
K	n.d.	n.d.	n.d.	n.d.	-	n.d.	n.d.
	100.760	101.879	102.326	100.991	101.570	101.406	99.992

Oxides — Formulae based on 4 oxygens

Si	.980	.988	.957	.991	.993	.973	.987
Al	-	.016	.001	-		-	-
Ti	-	-	-	.001		-	-
Cr	-	.007	.002	-		-	-
Fe	.294	.312	.416	.322	.296	.355	.309
Mn	n.d.	n.d.	-n.d.	n.d.		-	-
Mg	1.745	1.676	1.664	1.694	1.717	1.698	1.716
Ca	-	-	-	.001		-	-
Na	-	-	-	-		-	-
K	n.d.	n.d.	-n.d.	n.d.	-	-	-
	Fo = 85.55% Fa = 14.45%	Fo = 84.30% Fa = 15.70%	Mg = 80.0% Fe = 20.0%	Fo = 84.0% Fa = 16.0%	Fo = 85.40% Fa = 14.60%	Fo = 82.70% Fa = 17.30%	Fo = 84.80% Fa = 15.20%

Appendix 5

Microprobe Analyses of Sulfides

SULFIDE SAMPLE No. CORRELATION

1	=	26A
2	=	28A-2
3	=	32A-1
4	=	34A-1
5	=	36A-3
6	=	41A-1
7	=	43A-1
8	=	44A-1
9	=	46A-1
10	=	47A-1
11	=	90A-1
12	=	92A-1
13	=	87A
14	=	85A
15	=	82A-1
16	=	78A-1
17	=	104A
18	=	106A
19	=	108A
20	=	114A
21	=	121A
22	=	130A-1
23	=	132A-1
24	=	140A-1
25	=	152A-1
26	=	156A-1
27	=	157A-1
28	=	160A-2
29	=	162A-1

ELECTRON MICROPROBE ANALYSES OF PENTLANDITE AND PYRRHOTITE

		1	2	3	4	5	6	7
Pentlandite	Wt%							
	Fe	28.77	29.99	27.30	28.41	30.55	27.29	30.17
	Ni	27.31	33.53	28.70	28.90	32.16	31.09	33.91
	Cu	-	.02	.02	.03	.03	.01	.02
	Co	2.01	2.85	3.41	5.30	3.86	7.22	1.86
	S	41.91	33.61	40.56	37.36	33.40	34.38	34.04
Pentlandite	At%							
	Fe	22.19	24.35	21.25	22.55	24.84	22.08	24.43
	Ni	20.04	25.90	21.25	21.81	24.87	23.93	26.12
	Cu	-	.01	.02	-	.02	-	.01
	Co	1.47	2.19	2.51	3.98	2.97	5.54	1.43
	S	56.31	47.54	54.98	51.64	47.29	48.45	48.01
Pyrrhotite	Wt%							
	Fe	53.53	59.42	55.26	57.17	60.39	58.11	58.90
	Ni	.17	.55	.28	.28	.68	.66	.37
	Cu	-	-	-	-	-	-	-
	Co	-	-	-	-	.03	.08	-
	S	46.31	40.02	44.46	42.55	38.90	41.15	40.73
Pyrrhotite	At%							
	Fe	39.84	45.83	43.56	43.46	46.88	44.54	45.24
	Ni	.12	.40	.20	.20	.51	.48	.27
	Cu	-	-	-	-	-	-	-
	Co	-	-	-	-	.02	.05	-
	S	60.04	53.76	56.34	56.34	52.59	54.92	54.49

cont'd...

./2

	8	9	10	11	12	13	14
Pentlandite Wt%							
Fe	31.04	31.17	30.25	31.90	33.42	38.97	39.25
Ni	34.80	34.63	35.29	35.39	31.13	25.44	25.20
Cu	.04	.04	-	-	.04	-	.01
Co	.62	.68	.56	.54	.59	.77	.71
S	33.50	33.49	33.90	32.17	34.81	34.82	34.82
Pentlandite At%							
Fe	25.21	25.32	24.52	26.13	26.90	31.29	31.51
Ni	26.89	26.76	27.20	27.57	23.83	19.43	19.24
Cu	.03	.03	-	-	.03	.59	-
Co	.48	.53	.43	.42	.45	.59	.54
S	47.40	47.37	47.85	45.89	48.80	48.70	48.69
Pyrrhotite Wt%							
Fe	59.03	59.48	57.91	61.11	59.16	62.24	62.28
Ni	.40	.52	1.26	.68	.22	.01	.01
Cu	-	.18	-	-	.01	-	-
Co	.01	-	-	-	-	-	-
S	40.56	39.82	40.82	38.20	40.60	37.75	37.71
Pyrrhotite At%							
Fe	45.38	45.93	44.47	47.63	45.48	48.67	48.67
Ni	.29	.38	.92	.51	.16	-	-
Cu	-	.12	-	-	.01	-	-
Co	.01	-	-	-	-	-	-
S	54.32	53.96	54.60	51.86	54.35	51.32	51.32

cont'd...

./3

	15	16	17	18	19	20	21
Pentlandite Wt%							
Fe	29.76	34.78	35.06	29.85	28.13	40.22	N.A.
Ni	33.16	30.37	26.71	33.25	32.90	25.00	
Cu	-	-	.03	-	-	.08	
Co	1.78	1.43	1.29	2.06	4.32	.82	
S	35.29	33.42	36.92	34.83	34.66	33.88	
Pentlandite At%							
Fe	23.91	28.23	27.82	24.05	22.71	32.47	N.A.
Ni	25.34	23.44	20.17	25.49	25.26	19.20	
Cu	-	-	.02	-	-	.06	
Co	1.36	1.10	.97	1.57	3.30	.63	
S	49.39	47.23	51.03	48.89	48.73	47.64	
Pyrrhotite Wt%							
Fe	58.20	63.70	59.50	59.05	57.91	62.54	59.19
Ni	.41	-	.01	.46	.55	-	.40
Cu	-	-	.03	-	-	-	-
Co	-	-	-	.02	.02	-	.07
S	41.39	36.29	40.46	40.47	41.52	37.46	40.33
Pyrrhotite At%							
Fe	44.54	50.19	45.76	45.43	44.28	48.94	45.57
Ni	.30	-	.01	.34	.40	-	.30
Cu	-	-	.02	-	-	-	-
Co	-	-	-	.01	.02	-	.05
S	55.16	49.81	54.24	54.22	55.30	51.05	54.08

cont'd...

./4

		22	23	24	25	26	27	28	29
Pentlandite	Wt%								
	Fe	28.89	31.35	30.06	28.39	31.11	27.60	30.49	30.06
	Ni	33.04	32.58	33.29	34.34	33.74	30.90	35.14	34.84
	Cu	-	-	.01	-	-	.04	.06	.08
	Co	3.78	1.87	1.86	3.00	.53	5.85	.29	.43
	S	34.29	34.21	34.79	34.27	34.62	35.61	34.03	34.59
Pentlandite	At%								
	Fe	23.27	25.34	24.22	22.97	25.09	22.15	24.68	24.25
	Ni	25.43	25.05	25.52	26.43	25.88	23.59	27.06	26.74
	Cu	-	-	.01	-	-	-	.04	.06
	Co	2.90	1.43	1.42	2.30	.40	4.45	.22	.33
	S	48.31	48.17	48.83	48.30	48.63	49.78	47.99	48.62
Pyrrhotite	Wt%								
	Fe	58.36	59.94	58.89	57.84	59.25	58.34	59.05	57.40
	Ni	.66	.35	.42	1.05	.81	.56	.60	.57
	Cu	-	-	-	-	-	.12	-	.02
	Co	-	-	-	-	-	.06	-	-
	S	40.97	39.70	40.69	41.11	39.94	40.92	40.34	42.01
Pyrrhotite	At%								
	Fe	44.77	46.31	45.25	44.34	45.72	44.71	45.46	43.77
	Ni	.48	.26	.31	.76	.59	.41	.44	.41
	Cu	-	-	-	-	-	.08	-	.01
	Co	-	-	-	-	-	.05	-	-
	S	54.75	53.43	54.44	54.89	53.69	54.69	54.09	55.80

Appendix 6

Universal Stage Composition Determinations

Sample No.	O/pxn (En)	C/pxn (Ca:Mg:Fe)	Olivine (Fo)
26A	82	46:44:10	-
28A-2	80	45:45:10	-
30A-1	82	44:48:8	-
32A-1	83	45:45:10	-
34A-1	82	44:46:10	-
36A-3	80	44:47:9	-
41A-1	82	-	-
42A-1	82	43:52:5	-
43A-1	84	44:48:8	-
44A	82	44:48:8	-
46A-1	84	-	-
47A-1	86	45:45:10	86
76A-1	-	42:53:5	87
78A-1	88	42:47:11	86
82A-1	81	44:50:6	80
85A	87	-	87
87A	84	-	79
89A	87	-	87
90A-1	87	-	85
92A-1	92	-	87
104A	86	45:43:12	85
106A	86	-	80
108A	84	45:45:10	-
114A	86	-	87
120A	82	-	-
121A	82	-	-
126A-1	-	-	-
130A-1	81	45:45:10	-
131A-2	82	44:48:8	-
132A	81	-	79
135A-1	82	-	-
138A-2	85	-	87
140A	87	-	80
156A-1	82	44:46:10	-
159A	82	-	-
160A-2	84	-	87
162A	86	-	-